

1225-0767(ISSN Print)
2287-6715(ISSN Online)
한국연구재단 우수등재학술지

한국해양공학회지

제34권 제1호 (통권 제152호)

2020년 2월

Journal of Ocean Engineering
and Technology



Vol. 34, No. 1 (Serial Number 152)
February 2020

사단법인 한국해양공학회

The Korean Society of Ocean Engineers

<http://www.joet.org>

한국해양공학회 Journal of Ocean Engineering and Technology

편집위원회

위원장

정준모 인하대학교

편집이사

김준영 한국해양대학교
신성원 한양대학교
안석환 중원대학교
이우동 경상대학교
최형식 한국해양대학교

편집위원

강대순 (주)지오시스템리서치
강희진 한국해양과학기술원
구원철 인하대학교
권순철 부산대학교
김국현 동명대학교
김연중 인제대학교
김영훈 경남대학교
김윤해 한국해양대학교
김진환 카이스트
김현식 동명대학교
남보우 서울대학교
류용욱 전남대학교
박승민 (주)헤인이엔씨
박종천 부산대학교
백광준 인하대학교
송창용 목포대학교
윤현규 창원대학교
이강수 한국해양과학기술원
이종현 제주대학교
이탁기 경상대학교
임영섭 서울대학교
정동호 한국해양과학기술원
정세민 조선대학교
조규성 동명대학교
최성웅 경상대학교
하태민 강원대학교
홍성남 경상대학교

국제논문 편집위원

Ahmet Ergin, Istanbul Technical University
Atilla Incecik, University of Strathclyde
Gökhan Tansel Tayyar, Istanbul Technical University
Hooi-Siang Kang, Universiti Teknologi Malaysia
Moo Hyun Kim, Texas A&M University
Norimi Mizutani, Nagoya University
Do Kyun Kim, Newcastle University
Taeseong Kim, Loughborough University

연구윤리위원회

위원장

서성부 동의대학교

운영분과 및 심의 교육·분과 위원

김진환 KAIST
류용욱 전남대학교
정한구 군산대학교

Editorial Boards

Editor-in-Chief

Joonmo Choung, Inha University, Korea

Manuscript Editors

Joon-Young Kim, Korea Maritime and Ocean University, Korea
Sungwon Shin, Hanyang University, Korea
Seokhwan Ahn, Jungwon University, Korea
Woo Dong Lee, Gyeongsang National University, Korea
Hyeungsik Choi, Korea Maritime and Ocean University, Korea

Editorial Board Members

TaeSoon Kang, GeoSystem Research Corp., Korea
Hee Jin Kang, KRISO, Korea
Weoncheol Koo, Inha University, Korea
Soonchul Kwon, Pusan National University, Korea
Kookhyun Kim, Tongmyong University, Korea
Yeon-Joong Kim, Inje University, Korea
Younghun Kim, Kyungnam University, Korea
Yun Hae Kim, Korea Maritime and Ocean University, Korea
Jinwhan Kim, KAIST, Korea
Hyun-Sik Kim, Chonnam National University, Korea
Bo Woo Nam, Seoul National University, Korea
Yong Uk Ryu, Pukyong National University, Korea
Seung Min Park, Hyein Engineering & Construction, Co. LTD, Korea
Jong Chun Park, Pusan National University, Korea
Kwang-Jun Paik, Inha University, Korea
Chang Yong Song, Mokpo National University, Korea
Hyeon Kyu Yoon, Changwon National University, Korea
Kangsu Lee, KRISO, Korea
Chong Hyun Lee, Jeju National University, Korea
Tak Kee Lee, Gyeongsang National University, Korea
Youngsub Lim, Seoul National University, Korea
Dongho Jung, KRISO, Korea
Se-Min Jeong, Chosun University, Korea
Gyusung Cho, Tongmyong University, Korea
Sung-Woong Choi, Gyeongsang National University, Korea
Taemin Ha, Kangwon National University, Korea
Sungnam Hong, Gyeongsang National University, Korea

International Advisory Editorial Board Members

Ahmet Ergin, Istanbul Technical University, Turkey
Atilla Incecik, University of Strathclyde, UK
Gökhan Tansel Tayyar, Istanbul Technical University, Turkey
Hooi-Siang Kang, Universiti Teknologi Malaysia, Malaysia
Moo Hyun Kim, Texas A&M University, USA
Norimi Mizutani, Nagoya University, Japan
Do Kyun Kim, Newcastle University, UK
Taeseong Kim, Loughborough University, UK

Research and Ethics Boards

Chief

Sung-Bu Suh, Dongeui University, Korea

Management and Deliberative and Education Department

Jinwhan Kim, KAIST, Korea
Yong Uk Ryu, Chonnam National University, Korea
Han Koo Jeong, Kunsan National University, Korea

AIMS and SCOPE

Journal of Ocean Engineering and Technology (JOET) is a medium for the publication of original research and development work in the field of ocean engineering. JOET covers the entire range of issues and technologies related to the following topics:

Marine hydro-mechanics including: Design of marine structures; Resistance and propulsion; Seakeeping and maneuvering; Experimental and computational fluid dynamics; Ocean wave mechanics; Thermodynamics and heat transfer; Hydraulics and pneumatics;

Marine structure-mechanics including: Structural strength; Fatigue strength; Optimization and reliability; Arctic technology and extreme mechanics; Noise, vibration, and acoustics; Plasticity engineering; Concrete engineering;

Coastal civil engineering including: Coastal structure engineering; Port and harbor structure engineering; Soil engineering; Drilling and exploration; Hydraulics of estuary; Seismic engineering; Coastal disaster prevention engineering;

Marine material engineering including: Metallic material engineering; Organic material engineering; Ceramics; Composite material engineering; Materials evaluation engineering; Surface engineering; Tribology;

Information technology and convergence fields including: Design for safety; IT-based design; IT-based production engineering; Welding mechanics; Design of underwater vehicle; Offshore energy system design; Environment and system evaluation; Control engineering; GPS and GIS; Inspection and sensor; Port and logistics; Leisure boat and deep sea water; Offshore process systems engineering;

Conference papers, research papers, diploma papers and academic articles can be submitted. All of the manuscripts are peer-reviewed.

GENERAL INFORMATION

“Journal of Ocean Engineering and Technology” is the official journal by “The Korean Society of Ocean Engineers”. The ISO abbreviation is “J. Ocean Eng. Technol.” and acronym is “JOET”. It was launched in 1987. It contains original research articles, case reports, brief communications and reviews on technical issues. It is published bimonthly in February, April, June, August, October, and December each year. Supplement numbers are published at times. All of the manuscripts are peer-reviewed.

Full text is freely available from <http://www.joet.org> and <http://www.ksoe.or.kr> without signing in. This journal was supported by the Korean Federation of Science and Technology Societies(KOFST) grant funded by the Korean government. Total or a part of the articles in this journal are abstracted in NRF (National Research Foundation Fund of Korea), Google Scholar, DOAJ(Directory of Open Access Journals), and KCI (Korean Citation Index).

Manuscript should be submitted via the online manuscript website <http://www.joet.org> Other correspondences can be sent via an email to the Editor in Chief.

Correspondence concerning business matters should be addressed to Secretary-Treasurer of KSOE, Heejin Lee, President O/T room No.1302, 13, Jungang-daero 180beon-gil, Dong-gu (48821), Busan, Korea (Tel: +82 51 759 0656, e-mail: ksoehj@ksoe.or.kr).

A subscription to the journal can be obtained by sending your order to or e-mailing to Secretary-Treasurer of KSOE. The annual charge for subscription is 100,000KRW or equivalent.

This is an open access article distributed under the terms of the creative commons attribution non-commercial license(<http://creativecommons.org/licenses/by-nc/4.0>) which permits unrestricted non-commercial use, distribution, and reproduction in any medium, provided the original work is properly cited.

© 2020 by The Korean Society of Ocean Engineers (KSOE) / ISSN(print) 1225-0767 / ISSN(online) 2287-6715

© It is identical to Creative Commons Non-Commercial Licenses.

This paper meets the requirements of KS X ISO 9706, ISO 9706-1994, and ANSI/NISO Z39.48-1992 (Permanence of Paper)

Printed on February 29, 2020 by Hanrimwon Co., Ltd., Seoul, Korea.

CONTENTS

Volume 34, Number 1

February, 2020

<Original Research Articles>

- A Feasibility Review for an Uneven Baseline Basis Minimal Ballast Ship
Hee Jin Kang, Kwang-Soo Kim, Jin Choi, Yeong-Yeon Lee, Haeseong Ahn and Geun-Tae Yim 1
- Study on Stopping Ability of a Ship Equipped with Azimuth Propeller
Jong-Yong Park, Pilgun Oh, Taejin Kim and Jun-Ho Lee 13
- Optimal Shape and Boil-Off Gas Generation of Fuel Tank for LNG Fueled Tugboat
Jung-Woog Kim, Jin-yeong Jeong and Dae-Jun Chang 19
- Extreme Value Analysis of Metocean Data for Barents Sea
Sung Boo Park, Seong Yun Shin, Da Gyun Shin, Kwang Hyo Jung, Yong Ho Choi,
Jaeyong Lee and Seung Jae Lee 26
- Estimation of Buckling and Ultimate Collapse Behaviour of Stiffened Curved Plates under Compressive Load
Joo-Shin Park, Yeon-Chul Ha and Jung-Kwan Seo 37
- Algorithm to Estimate Oil Spill Area Using Digital Properties of Image
Hye-Jin Jang and Jong-Ho Nam 46

A Feasibility Review for an Uneven Baseline Basis Minimal Ballast Ship

Hee Jin Kang¹, Kwang-Soo Kim^{1,3}, Jin Choi²,
 Yeong-Yeon Lee¹, Haeseong Ahn¹ and Geun-Tae Yim²

¹Principal Researcher, Advanced Ship Research Division, Korea Research Institute of Ships and Ocean Engineering (KRISO), Daejeon, Korea

²Senior Researcher, Autonomous Ship Research Department, Korea Research Institute of Ships and Ocean Engineering (KRISO), Daejeon, Korea

³Senior Director, Advanced Ship Research Division, Korea Research Institute of Ships and Ocean Engineering (KRISO), Daejeon, Korea

KEY WORDS: Uneven baseline, Ballast water management (BWM), Minimal ballast water ship (MIBS), Non ballast water ship (NOBS), ballast water treatment system (BWTS), Ship resistance performance

ABSTRACT: Although there are many kinds of advanced ballast water management systems, pioneering studies for ballast-water free ship and minimal ballast water ship concepts are in progress. In this study, the existing alternatives of ballast water are reviewed and a new design concept is studied on the basis of the existing bulk carrier hull form. To develop a new design alternative which has minimal ballast for ballast water discharge free operation, the new concept should have technical feasibilities that are related to the role of the ballast water, berth access, loading constraints, etc. For this purpose, a simplified systems engineering basis design approach is adopted using a business model as the system analysis and control tool. To check the performance feasibility of the new concept, ship resistance performance is reviewed based on a model scale ship resistance performance analysis.

Abbreviations

AUBAFLOW	automatic ballast flow	EARSM	explicit algebraic Reynolds stress model
BW	ballast water	EHP	effective horsepower
BWE	ballast water exchange	FOC	fuel oil consumption
BWM	ballast water management	IGES	initial graphics exchange specification
BWTS	ballast water treatment system	ISO/IEC	international organization for standardization/ international electro-technical commission
CFD	computational fluid dynamics	KPPs	key performance parameters
CSR-H	harmonized common structural rules	KB	vertical distance between the keel and the center of buoyancy
C_f	friction resistance coefficient	MIBS	minimal ballast water ship
C_p	prismatic coefficient	MOE	measure of effectiveness
C_m	total resistance coefficient of model-scale ship	MOP	measure of performance
C_{fm}	C_f of model-scale ship	NOBS	non-ballast water ship
C_{fs}	C_f of full-scale ship	RANS	Reynolds-averaged Navier-Stokes
C_r	residuary resistance coefficient	TA	trim aft
C_{ts}	total resistance coefficient of full-scale ship	TF	trim forward
D-1	regulation about ballast water exchange	T_m	mean draft at a midships
D-2	regulation about ballast water treatment	TPMs	technical Performance measures
DHP	delivery horsepower	WAVIS	wave and viscous flow (proprietary brands)
DISV	displacement volume	VLCC	very large crude oil carrier
DWT	deadweight tonnage	ULCC	ultra large crude oil carrier

Received 16 December 2019, revised 13 February 2020, accepted 14 February 2020

Corresponding author Hee Jin Kang: +82-42-866-3417, hjkang@kriso.re.kr

It is noted that this paper is revised edition based on proceedings of IMAM 2017 in Lisbon.

© 2020, The Korean Society of Ocean Engineers

This is an open access article distributed under the terms of the creative commons attribution non-commercial license (<http://creativecommons.org/licenses/by-nc/4.0>) which permits unrestricted non-commercial use, distribution, and reproduction in any medium, provided the original work is properly cited.

1. Introduction

Because the measures from the Ballast water management (BWM) convention are being enacted in order to reduce the environmental damage caused by the global movement of marine life in the ballast water of ships (Albert et al., 2013), the negative effect of treated ballast water on the marine environment is another urgent issue (Werschkun et al., 2014). Notably, research on non/minimal ballast water vessels is actively underway in response to the D-1 or D-2 discharge standards of the convention. When considering the role of ballast water, as shown in Table 1, the ballast water contributes to the ship's stability via proper maintenance of the draft and the center of gravity of a ship during voyage. Another aim of the ballast water is to maintain the appropriate immersion depth of the propeller for propulsion efficiency.

Table 1 Roles of the ballast water in a ship (Isbester, 2010)

Maintain the stability of the ship
Trim and heel control
Secure immersion depth of the propeller
Reduction of slamming
Reduction of the bending moment of the ship
Relieve the shear force of the ship

Ballast water is also used to adjust the trim and heel of a ship. The bending moment and shear force can also be adjusted by the ballast water.

Depending on the ship types and routes, generally, 30% to 40% of the deadweight tonnage (DWT) is used as ballast water (Kerr, 1994). Many pioneering studies have been conducted to meet the D-1 or D-2 discharge standards of the BWM convention without needing to discharge the environmentally harmful ballast water. Table 2 shows alternatives for the BWM methods (GEF, U. and IMO, G.P., 2011).

Among the various alternatives, in the case of 'no or minimal discharge' alternatives, the minimal ballast water ship (MIBS) and non-ballast water ship (NOBS) (Shingo, 2014) of a 'storm ballast' are considered to be practically applicable alternatives. Though there are some constraints for berthing and loading, in 2018, a NOBS concept basis ballast water-free '7,500 cubic meter liquefied natural gas (LNG) bunkering vessel' was launched for commercial purposes (<https://pulsenews.co.kr>). For the 'continuous flow' type alternatives, 'The Variable Buoyancy Ship Concept' of 'longitudinal trunks' is remarkable. For the trim and heel control, the concept has been shown to adequately control the trim and draft (Parsons and Kotinis, 2011a; Parsons and Kotinis, 2011b). In this study, a new design concept for 'no or minimal discharge' alternatives is studied while considering the ship's size and operational conditions.

Table 2 Alternatives for the BWM methods [derived and edited from GEF, U. and IMO, G. P. 2011]

Alternative methods	Features	Benefits	Penalties	Suitable Ship type/s
No ballast water				
· Zero ballast	(a) Novel hull design (b) Use of 'solid ballast TEUs'	Avoids all cost associated BWM	Higher hull build/ operating cost	(a) Ro-ro pax, car, container, high volume cargo ships (b) Existing box ships
No or minimal discharge				
· Storm ballast (must meet D-2)	Wide beam V-hull design	Avoids cost of large BWTS	Higher building cost, berth access or loading constraints due to wider beam	New dry bulk carriers
· Internal ballast (must meet D-2)	Fresh water shifted from tank to tank	Avoids all cost of BWTS	Reduces cargo capacity, air-draught, tank survey/inspection	Existing and new container ships, ro-ro pax, liners, livestock carriers
· Portable water (must meet D-2)	Only drinking water is added to clean tank/s	Avoids costs and loss of space for BWTS	Cost of potable water production/purchase	Super yachts, cruise liners, some livestock carriers, pax and military vessels
Continuous flow				
· Longitudinal trunks (meets D-1 and may equivalent to D-2)	Replaces ballast tanks with buoyancy trunks	Avoids costs of large BWTS and propeller efficiency gain/s	Higher build costs, risk of biota/sediment accumulation prevent	New Seaway-size and other large bulk carriers
· Ship buoyancy control (meets D-1 and may equivalent to D-2)	Multiple valves convert each BW tank into a free flooding buoyancy compartment	Avoids costs of BWE pumping and very large BWTS	Costs of multiple valves and control systems, valve servicing, coating and cleaning, slight increase to hull drag	Existing and new cargo ships
· AUBAFLOW (exceeds D-1)				Existing and new VLCCs + ULCCs
· Loop ballast exchange (above D-1 and may approach D-2)				
· Dyna ballast (exceeds D-1)	Enhanced bluewater BWE pumping	Avoids costs of BWTS	Any sediment/biota accumulating in a low-flow zone	Most types of existing and new cargo ships

2. Feasibility Study

To design a new minimal ballast vessel, a ship must be designed that has the functions of ballast water without or with the minimum use of ballast. The perspectives of performance, ship stability, resistance, trim and heel controllability, berth access and loading constraints should be considered. Technical complexity and cost related matters are also considered to ensure technical and economic feasibility.

To compensate for the existing BWM alternatives' penalties, an appropriate approach and design process are required. In a systems engineering process, it is essential to identify, validate, and verify the various constraints of shipbuilding and operation in the design phase for the development of minimal ballast water vessel. Generally, the systems engineering basis design process involves a "system analysis and control tool", which allows for the effective management of various design entities from various viewpoints, including technical and economic feasibility (Leonard, 1999; Kang et al., 2016). In this study, the business model was used as a system analysis and control tool, which was suggested by Kang et al. (2016). The business model consists of six elements: the design of a new concept for a minimal

ballast vessel (Task); the required value of the enhanced berth access and loading capability compared to the existing 'MIBS' (Value); the expected revenue of the designed concept, such as a decrease in the ecosystem disturbance (meeting D-2) and the reasonable hull build cost (Revenue); the available and considered infrastructure, such as port facilities, ships in operation, rules and regulations, ship yards (Infra); the channels to enable the design concepts, such as technical and economic feasibilities (Channel); and the stakeholders of the task, including ship owners, ship builders, port authorities, classification societies, and fishing industries (Stakeholder). The factors considered in this study are shown in Table 3.

By adopting a business model for the systems analysis and a control tool for the design process, the ISO/IEC 15288-based 'Vee' design process was adopted and modified, as shown in Fig. 1. In the early phase of the design process, the measure of effectiveness (MOE), key performance parameters (KPPs), measure of performance (MOP) and technical performance measures (TPMs) should be identified in order to validate and verify the feasibility of the design results in the early phase of the design process. During the design process, all the design aspects should be analyzed and determined within the boundaries of

Table 3 Business model for a new non / minimal ballast ship design

Task	Minimal ballast operation of a ship
Value	Enhanced berth access and loading capability compare to existing 'MIBS'
Revenue	Decrease in ecosystem disturbance (meeting D-2), a reasonable hull build cost
Infra	Port facilities, ships in operation, rules and regulations, shipyards
Channel	Technical and economic feasibility
Stakeholder	Ship owners, ship builders, port authorities, classification societies, fishing industries

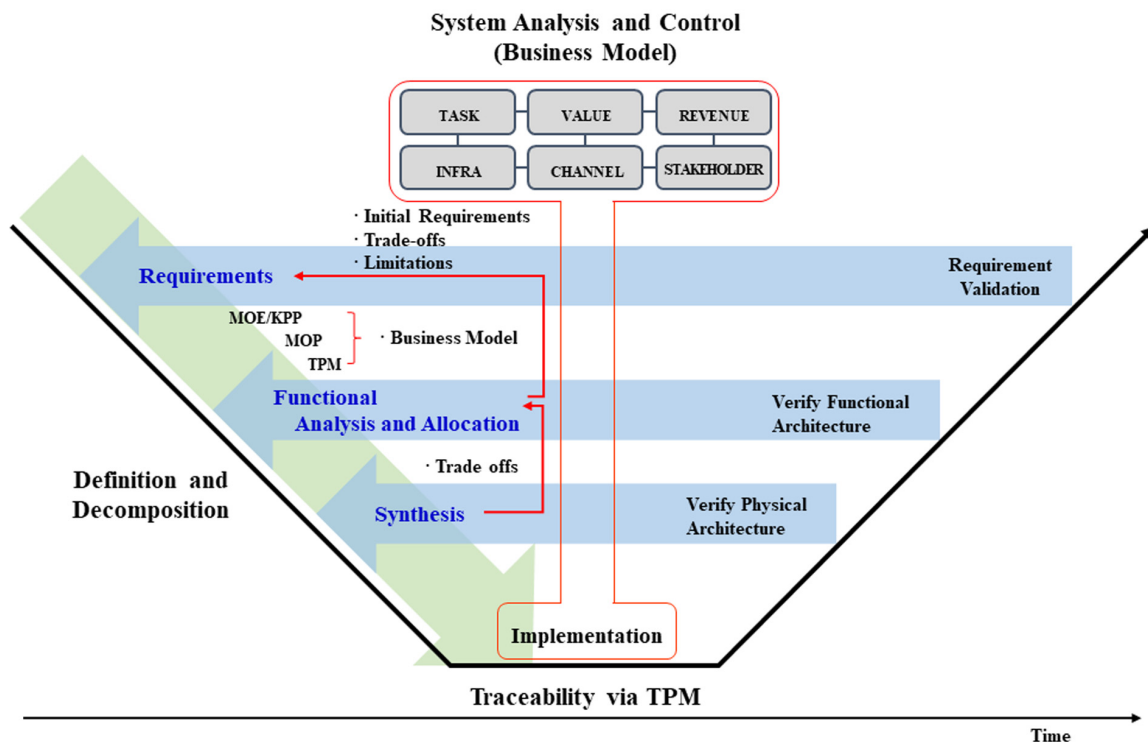


Fig. 1 Design process for a new minimal ballast ship design [derived and edited from (Kang et al., 2016)]

the defined business model.

2.1 Requirement analysis

To achieve this goal, eight requirements were derived, as shown in Table 4. R1 to R7 are the general requirements for a non/minimal ballast water ship. The new design should meet the requirements at the same level as the previous alternatives. R8 is the requirements to overcome the existing difficulties of a ‘storm ballast’ of the ‘no or minimal discharge’ alternatives.

R1 is a requirement related to the stability of a ship. When changing the existing hull form, such as the MIBS, it is difficult to achieve the same stability as that of the existing ship. In such cases, the placement of the keel or stabilizer should be reviewed in terms of the dynamic behavior, propulsion power of the ship, and cost. R2 is a requirement for the trim and heel control, considering the weight distribution of cargo. R3 stipulates the immersion depth required for securing the self-propulsion capability of a ship. R4 is a requirement related to the operation cost of the ship. R5 states the condition for bow slamming reduction, which should be considered together with R3 to ensure the proper immersion depth of the bow. R6 and R7 are requirements for managing the load applied to the ship according to the cargo weight distribution and the arrangement of the ballast of the ship. R8 requires that the designed concept should be able to utilize the existing port facilities. From the results of the analysis of the requirements, the TPMs are generated and shown in Table 5. The TPM is generated from each essential requirement for a minimal ballast ship, and the MOP is measured after all TPMs are satisfied. Then, the MOE / KPP can be evaluated as a considerable design result.

2.2 Functional analysis and allocation

Each requirement should be functionalized for the new minimal ballast ship design. To functionalize the requirements R1–R5 in Table 4, technologies pertaining to fluid performance are required. R6 and R7 are the requirements related to the structural strength, and R8 requires the ship be able to be adapted to existing harbor facilities. The functions to accommodate each requirement are listed in Table 6, including all the identified requirements.

2.3 Synthesis

In the synthesis process, the design alternatives shall be generated to implement the functions in Table 6 within the boundaries of the business model. To implement F1 and F4, any requirements for new rules and regulations should be minimized. In addition, the existing rules and regulations for ship stability and structural strength must be satisfied. For F2, a minimum level of the propeller immersion depth and bow draft must be achieved. For F3, any type of external attachment should be avoided to ensure the appropriate ship resistance performance. For F4 and F5, changes in the draft, beam, and bilge radius of the existing ship should be limited to ensure the berth access and usability of cargo loading facilities. The adjustment of the baselines of the bow and stern of a ship can be used to meet the functional requirements. However, when considering the required couplings and machinery systems among the bow, stern, and cargo hold parts of the ship for adjusting the baseline, the design concept shown in Fig. 2 does not meet the ‘revenue’ of the business model.

Since it is practically impossible for an adjustable hull form to meet the requirements of Table 4 and the business model of Table 3, to build

Table 4 Redefined requirements for the new non/minimal ballast ship design

R1	Maintain the stability of the ship	R5	Reduction of slamming
R2	Trim and heel control	R6	Reduction of the bending moment of the ship
R3	Secure immersion depth of the propeller	R7	Relief of the sheer force of the ship
R4	Ensure the ship resistance performance	R8	Harbor operability (berth access / loading constraints)

Table 5 Criteria, thresholds and indicators for TPMs

Type	Criterion	Threshold
TPM1	Ship stability	Meet the rules and regulations
TPM2	Trim and heel control	Same as original hull form
TPM3	Resistance performance	Minimum increase in EHP
TPM4	Structural strength	Meet the related CSR-H**
TPM5	Harbor operability	Berth access/loading constraints

** CSR-H: Harmonized Common Structural Rules

Table 6 Function list for new non/minimal ballast ship design

F1	Function to maintain ship stability	TPM1	R1
F2	Trim and heel control function	TPM2	R2, R3, R5
F3	Function to maintain resistance performance	TPM3	R4
F4	Function to sustain the structural strength of the ship	TPM4	R6, R7
F5	Function for berth access and usability for loading facilities	TPM5	R8

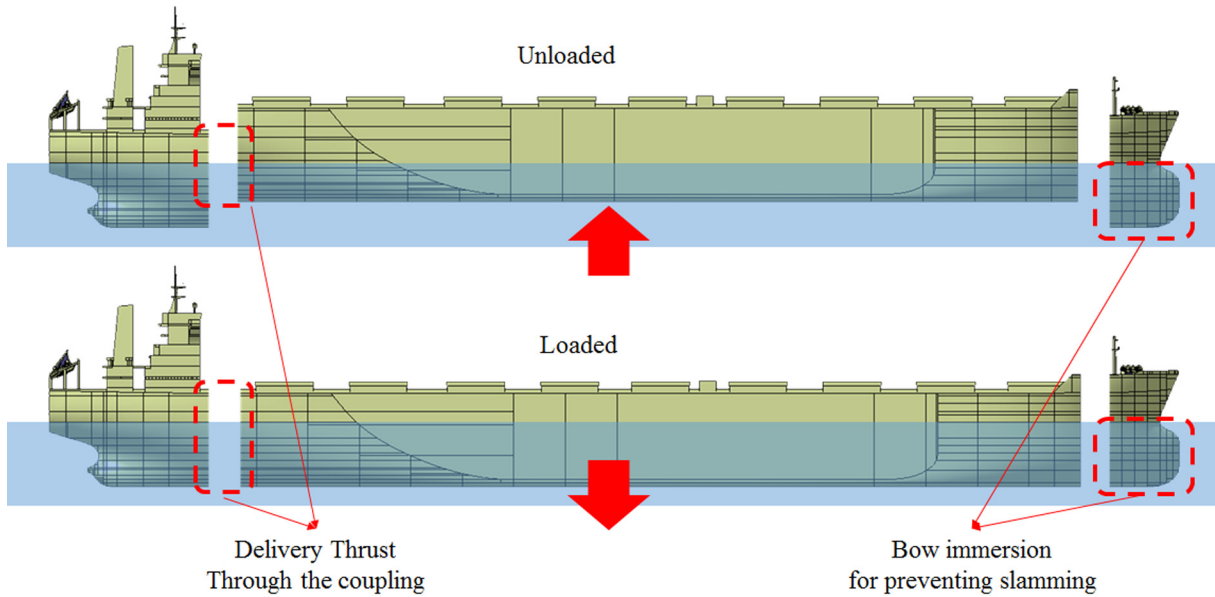


Fig. 2 An initial concept of the adjustable bow, stern and cargo hold baselines for non/minimal ballast operation

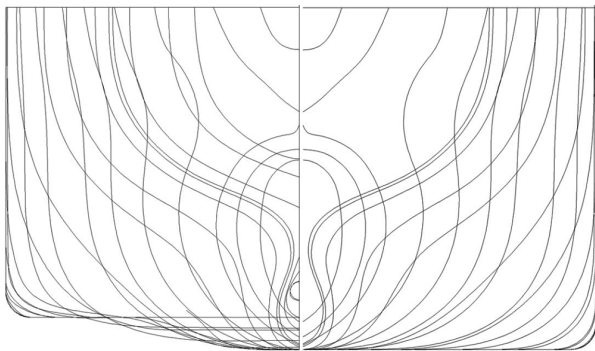


Fig. 3 Body plan, modified (left side) and original (right side) hull form

a reasonable design alternative for the functions in Table 6, a fixed type uneven baseline hull form (modified) has been generated on the basis of an existing 176K bulk carrier hull form (original). Fig. 3 shows the body plan of an uneven baseline minimal ballast bulk carrier.

From the Fig. 3, the suggested ‘modified’ hull form has uneven baselines of the bow, stern, and cargo holds. These differences should be addressed because an uneven baseline can affect the ship’s resistance performance. In addition, an uneven baseline interferes with

the fluid flow and affects the seakeeping ability for F1. Furthermore, measures should be taken to secure the longitudinal strength under repetitive hogging and sagging conditions. To reduce the adverse effects of the shear force and bending moment on the structural strength of the hull, the heel trim must be carefully weighed and controlled during the cargo loading process. For F1 and F4, a center-line bottom keel-based structural reinforcement can be used. While a fin-stabilizer for F1 has no effect on the normal concept of the static stability of a ship, it has a positive effect on the dynamic stability. Since the fin is usually not considered for a large ship, the cost effectiveness and possible capacity of the fin should be considered before implementation. To obtain the proper immersion depth of the propeller of the designed ship, a reduction of the propeller diameter can be considered by changing from a single-screw to twin-screw propulsion with an uneven baseline. In addition, for non-ballast exchange operation in certain loading conditions, a permanent ballast system will be required for F2 and F5. In this case, the operation of the permanent ballast should take the water depth and loading condition control ability of the port into account. The design should also consider the amount of required permanent ballasts for securing the appropriate immersion depth and a safe return voyage with empty cargo holds. By increasing the baseline of the cargo holds,

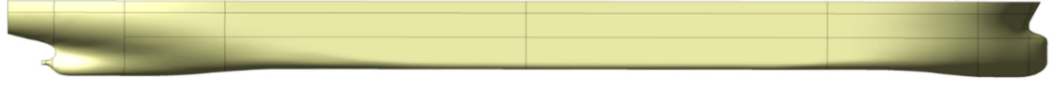
Table 7 Initial dimensions of the designed ship

	Original	Modified
Length (p.p.)	282.00 m	282.00 m
Breadth (mld)	45.00 m	45.00 m
Draught laden (Draught ballast TA)	17.70 m (7.70 m)	17.70 m (6.70 m)
Trim	-0.175 m	-0.176 m
Baseline of cargo holds	-	2.45 m elevated
GM (metacentric height)	4.88 m	6.84 m
Deadweight	168,310 t	127,935 t

Table 8 List of developments for a new non/minimal ballast ship design

S1	Uneven baseline of cargo holds	F2 and F5
S2	Permanent ballast system only for loading and unloading	F4
S3	Bottom keel system	F1 and F3

Table 9 Geometry and principal particulars of the model ship for CFD

Original				
Modified				
Condition	Original	Modified	Original	Modified
T_m (m)	17.7	17.7	0.5429	0.5429
S (m ²)	19,981	19,113	18.8015	17.9843
Design speed	15 kt (7.717 m/s)		1.3515 (m/s)	

※ T_m (Draft of the ship), S (Area of wetted surface)

the wetted surface area is decreased slightly, which can contribute to the ship's resistance performance. However, since the uneven baseline may have a negative effect on the ship resistance performance, the feasibility of design alternatives for F3 should be carefully examined. For F4, in the hull form modification process the applicability of the hull form to the existing rules and regulations is considered.

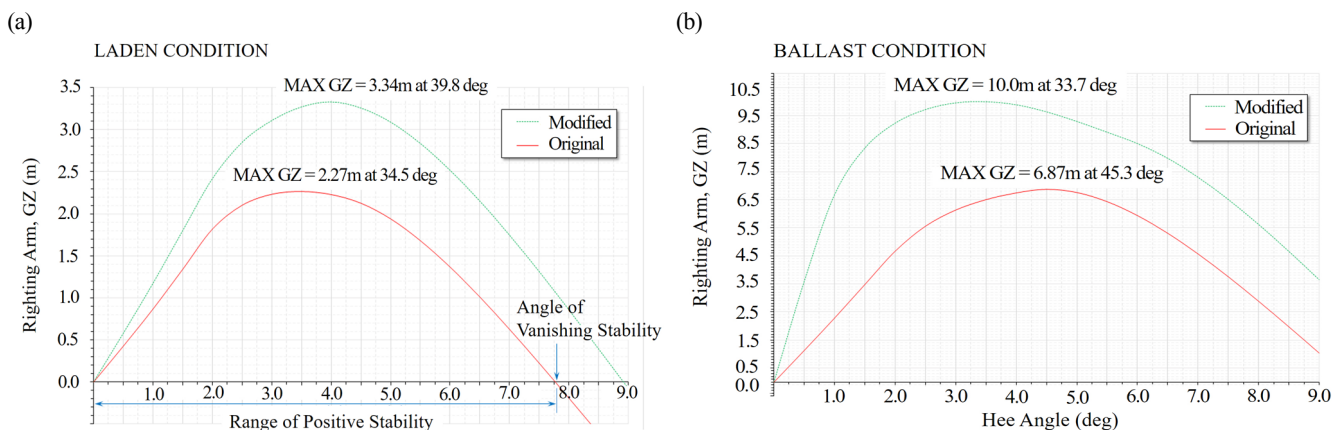
The provisional specifications of the designed ship are described in Table 7. From the hull form modification of the existing 176K bulk carrier, the wetted surface is reduced by approximately 4.4% compared to those of the original hull form under full loaded conditions. Under ballasting conditions, the required fixed ballast was estimated at approximately 42,000 t for a 7.5 m TA.

The synthesis results of reviewing the technical alternatives for the required functions are summarized in Table 8. The conceptually designed ship was reconfigured from the existing 176K bulk carrier. The tanks for the ballast are minimized and the auxiliaries and superstructure have been relocated for the initial trim and heel conditions. For S1, the uneven baseline of the cargo holds, consideration should be given to the influence of these differences on

the ship's resistance performance, structural safety, and workability at shipyards. For S2, the amount of permanent ballast should be minimized to consider the controllability of the loading weight distribution. Finally, for S3 the bottom keel should be properly configured to prevent it from detaching from the baseline of the bow and stern.

3. Ship Resistance Performance basis Feasibility Evaluation

The ship resistance performance affects the operating cost, and especially the fuel oil consumption. For this reason, the ship resistance performance should be determined in the early design phase. Although the model ship basin test is recommended, for a fast and effective evaluation in this study, a computational fluid dynamics (CFD)-based evaluation was adopted with the model ship basin test results and the sea trial data of an existing 176K bulk carrier. Thus, when the evaluation results have economic feasibility, the model ship-based test will be adopted in the next study. For the model scale CFD simulation,

**Fig. 4** GZ curves of the original and the modified hull form, (a) Laden condition (b) Ballast condition

a hull model is generated, as described in Table 9.

Regarding the ship's stability performance, the designed uneven baseline hull form has a larger righting arm compared to the original hull form, as shown in Fig. 4.

For the model scale CFD simulations, the Reynolds-averaged Navier-Stokes (RANS) equation-based Wave and viscous flow (WAVIS) software which KRISO (Korea Research Institute of Ships and Ocean Engineering) developed and widely used in Korean ship yards was used. As shown in Table 10, understanding the simulation of the flow around the ship helps in generating an accurate grid arrangement. The grid includes the free surface area with a total of 3.6M grid points for the half domain, which is equivalent to the medium size grid in a previous study (Kim et al., 2011). Starting from the initial graphics exchange specification (IGES) description of the

'original' and 'modified' hull forms, the commercial program GRIDGEN (Pointwise, Inc.) was used to generate the H-O type multiblock structured grid systems. In the CFD simulation in this study, the free surface was captured using the level-set method, while for the turbulence closure, the Explicit algebraic reynolds stress model (EARSIM) was used with Launder and Spalding's wall function. The details of the numerical methods used can be found in Kim et al. (2011), Kim et al. (2014).

From the numerical resistance test, as shown in Table 11, the effective horsepower (EHP) was predicted to increase from 1.5 to 2.0%, depending on the speed of the bulk carrier, compared to the existing 176K bulk carrier. From the information on the differences between the predicted EHP and the actual instrumented delivery horsepower (DHP) of the existing 176K bulk carrier, the DHP of the

Table 10 Grid information and distribution

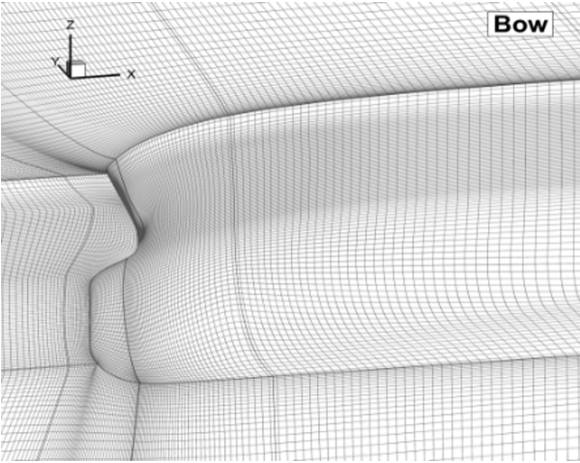
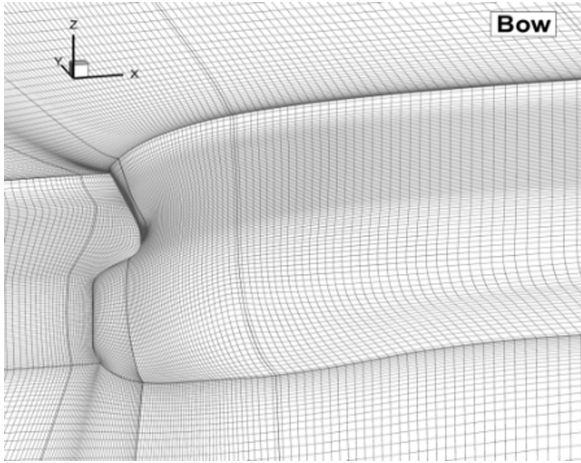
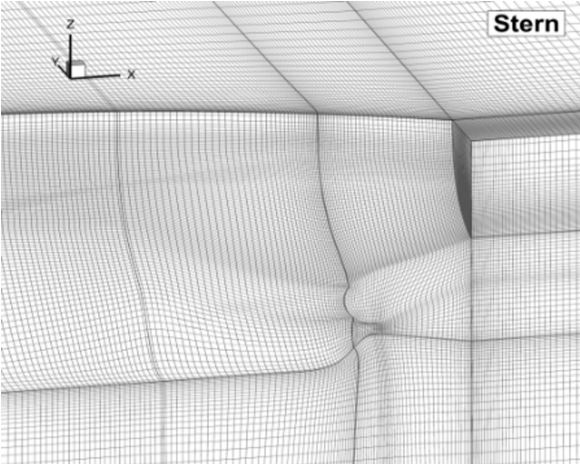
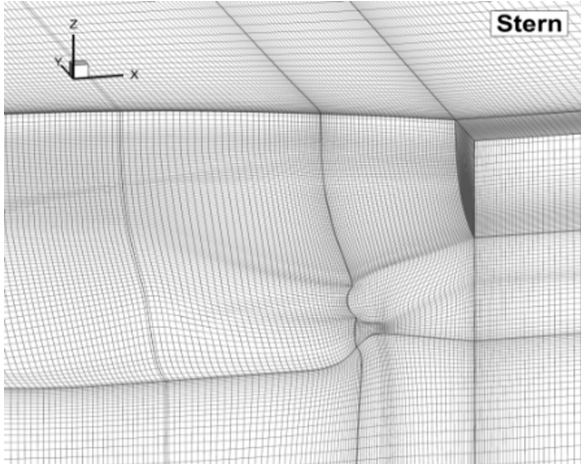
Grid information	
Number of Grid points (half)	3.6M
Number of grid block	13
Average y^+	~ 80
Half domain size $[x, y, z]$	$[-1.5 L \sim 2.5 L, 0 L \sim 1.0 L, -1.0 L \sim 0.03 L]$
Grid distribution	
Original (bow)	Modified (bow)
	
Original (stern)	Modified (stern)
	

Table 11 Numerical resistance test results

	V/s		Fn	Re	CFD (model scale)			ITTC		Cr	Cts	Full scale prediction	
	kt	m/s			Cf	Cp	Ctm	Cfm	Cfs			R (kN)	EHP (kW)
Original	12	6.173	0.1174	9.55E+06	2.98151	0.60113	3.58264	3.02422	1.40958	0.55842	1.96800	768.7	4745.3
	13	6.688	0.1272	1.03E+07	2.94135	0.59370	3.53505	2.98244	1.39624	0.55261	1.94885	893.3	5974.5
	14	7.202	0.1369	1.11E+07	2.9053	0.59787	3.50317	2.94452	1.38406	0.55865	1.94271	1032.8	7438.5
	15	7.717	0.1467	1.19E+07	2.86288	0.61369	3.47657	2.90987	1.37286	0.56670	1.93956	1183.7	9134.1
Modified	12	6.173	0.1174	9.55E+06	2.97653	0.73649	3.71303	3.02422	1.40958	0.68881	2.09839	784.4	4842.0
	13	6.688	0.1272	1.03E+07	2.92307	0.73461	3.65768	2.98244	1.39624	0.67524	2.07148	908.7	6077.3
	14	7.202	0.1369	1.11E+07	2.87961	0.74548	3.62509	2.94452	1.38406	0.68057	2.06463	1050.4	7565.3
	15	7.717	0.1467	1.19E+07	2.8348	0.75967	3.59447	2.90987	1.37286	0.68460	2.05746	1201.6	9272.6

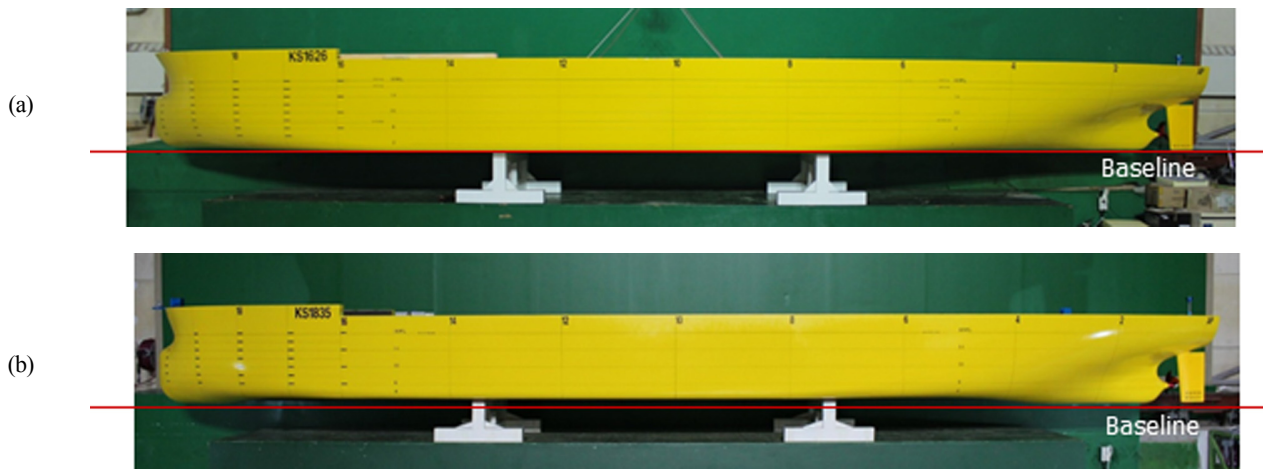
※ V/s : Velocity of the ship, CFD: Computational fluid dynamics, ITTC: The International Towing Tank Conference, Cf : friction resistance coefficient, Cp : prismatic coefficient, Ctm : total resistance coefficient of model-scale ship, Cfm : Cf of model-scale ship, Cfs : Cf of full-scale ship, Cr : residuary resistance coefficient, Cts : total resistance coefficient of full-scale ship, R : Resistance, EHP : Effective horse power

designed ship was estimated to have the same ratio for predicting fuel oil consumption as that of the designed ship at the actual scale.

For more detailed ship resistance performance comparison, model ship basin test has adopted. Fig. 5 shows model ships and Table 12 shows basin test results at same draft (17.7 m) conditions. From the test, EHP increased 5.25% and BHP (Breake horse power) increased 6.55% on average from 12 kt (6.173 m/s) to 15 kt (7.717 m/s) compare

to ‘Original’ hull form.

Empirically, losses in the cargo capacity can be compensated with an enlarged freeboard by considering the bulk general cargo loading condition. Assuming that the modified and original hull form has same cargo amount, the ‘Original’ hull form’s draft can be reduced to 15.89 m when the draft of ‘Modified’ hull form fixed to 17.70 m. At this time, the BHP gap between ‘Modified’ and ‘Original’ hull form

**Fig. 5** Model ships, (a) original and (b) modified hull form**Table 12** Model ship basin resistance test results at same draft condition

	V/s		PE (kW)	PB (kW)	RPM (1/s)	BHP increase	RPM increase	EHP increase
	kt	m/s						
Original	12	6.173	4391.0	6430.0	69.49	-	-	-
	13	6.688	5528.0	8074.0	75.15	-	-	-
	14	7.202	6871.0	10019.0	80.88	-	-	-
	15	7.717	8538.0	12462.0	86.97	-	-	-
Modified	12	6.173	4601.8	6832.0	70.62	6.3%	1.6%	4.8%
	13	6.688	5819.8	8609.0	76.43	6.6%	1.7%	5.3%
	14	7.202	7261.8	10716.0	82.32	7.0%	1.8%	5.7%
	15	7.717	8981.0	13248.0	88.36	6.3%	1.6%	5.2%

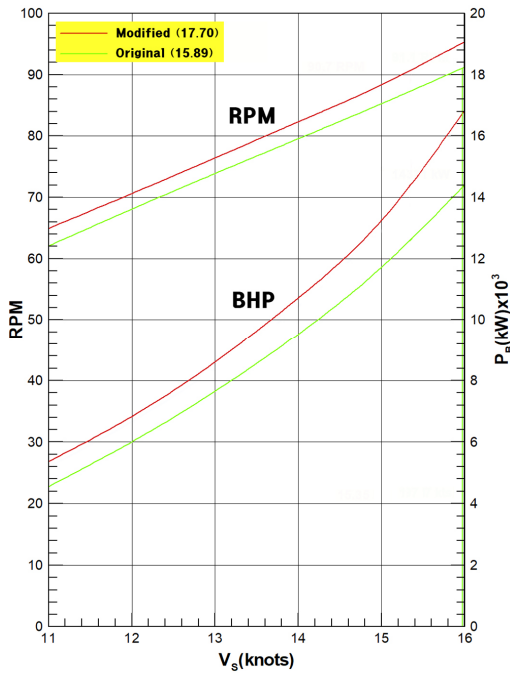


Fig. 6 BHP and RPM, (a) original and (b) modified hull form

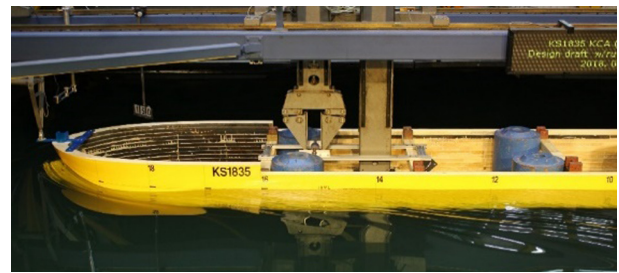
increases more than 12.5% as shown in Fig. 6. Fig. 7 shows model ship basin test pictures, conditions and nominal velocity contour at propeller plane at same displacement condition and Fig. 6 shows RPM and BHP of ‘Modified’ and ‘Original’ hull forms.

To compensate loses in ship resistance performance of ‘modified’ hull form, flow stress intensive parts of hull geometry as shown in Fig. 8 shall be improved. Moreover, enlarged beam width can be considered to increase cargo loading capacity of ‘modified’ hull form.

Regarding the sea keeping ability, the characteristics of the ship motion in sea waves are important. As shown in Fig. 9, compared to the original hull form, although the modified hull form shows lack of sea keeping performance in heave and roll motion, the pitch motion characteristics of the ‘modified’ hull form do not significantly differ from those of the original hull form. To analyze ship behavior characteristics, SMTP (Ship motion total package), which is the KRISO’s in-house simulation tool (new version of SURVSHIP (Survivability of ship)) has used (Lee, 2015). In the simulation, 0.02 second time step has applied. Figure 6 shows ship behavior characteristics in the regular wave with beam-sea (entrance angle of 90 degree) condition. Due to uneven baseline, suggested hull form shows



(a)



(b)

TF (m)	TA (m)	Tm (m)	KB (m)	Lcb (%)	DISV (m ³)
17.612	17.788	17.700	10.181	2.81	169,593

TF (m)	TA (m)	Tm (m)	KB (m)	Lcb (%)	DISV (m ³)
15.890	15.890	15.890	8.244	3.56	169,593

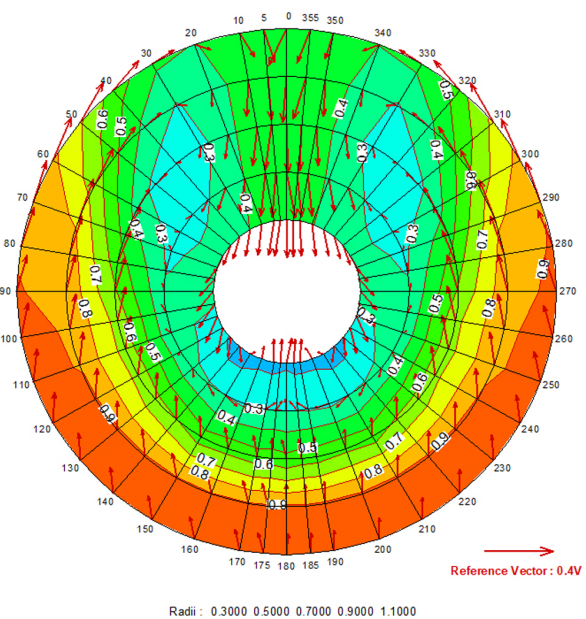
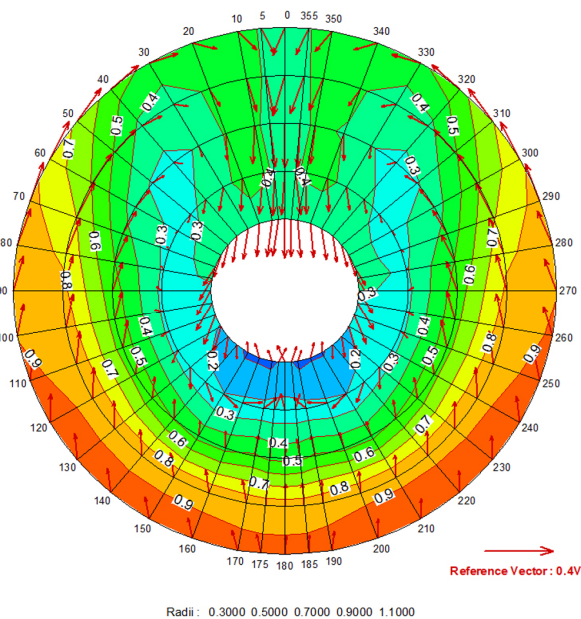


Fig. 7 Model ship basin tests (above) and nominal velocity contour at propeller plane (below), (a) original and (b) modified hull form at same displacement condition

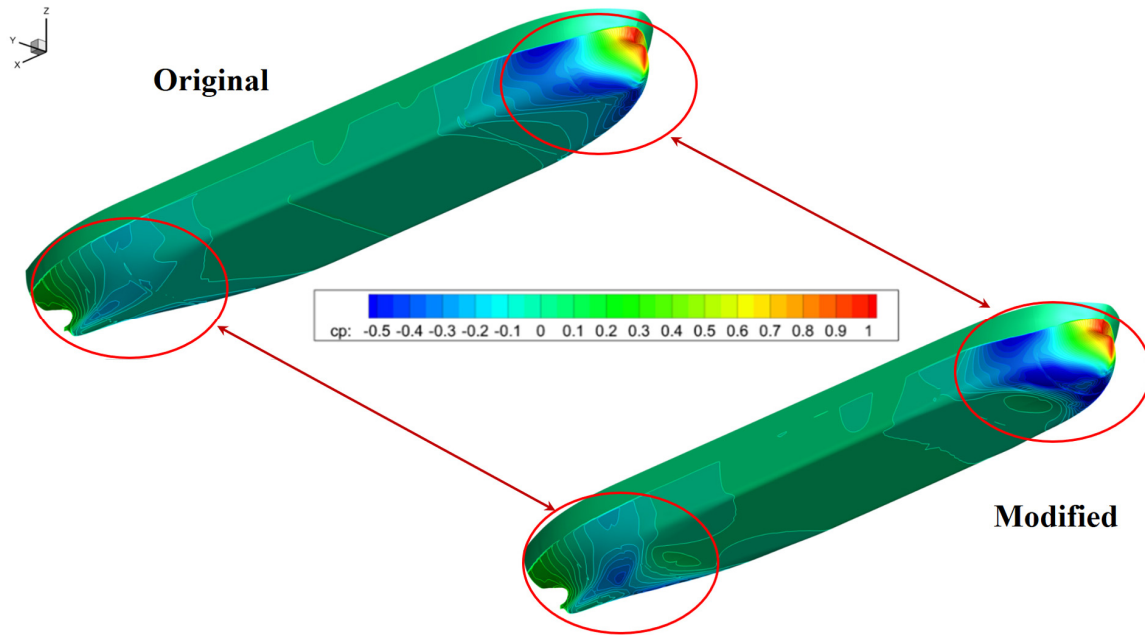


Fig. 8 Comparison of the pressure distribution between the original (above) and the modified (below) hull form

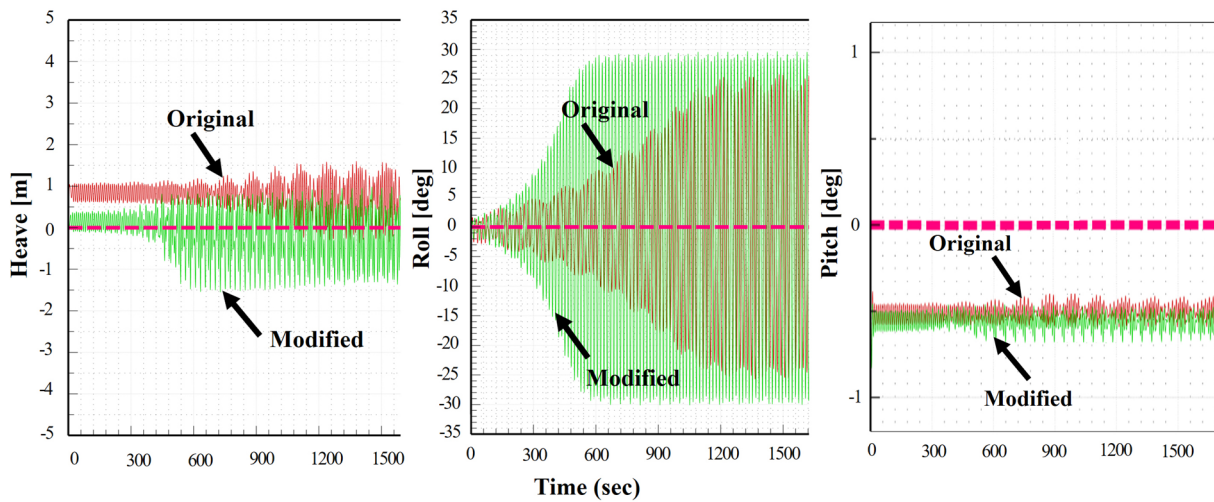


Fig. 9 Sample of the designed ship's motion analysis results in waves under fully loaded conditions (wave height: 2 m, beam sea condition)

lack of seakeeping ability especially in heave and roll motions. In case of Heave motion, it is estimated that waves between bow and stern uneven baseline enlarges ship motion compare to 'original' hull form. For roll motion, it is estimated that shorten immersion depth of 'modified' hull form enlarges initial roll motion.

To compensate for the losses in the ship motion under waves, relationship between the geometry of mid-ship section and roll damping will be considered (Park et al., 2019). If the propeller diameter is decreased to accommodate for the adjusted ship speed and the engine performance, then the elevating height of the baseline of the cargo holds can be decreased to secure the proper cargo capacity, ship resistance, and seakeeping performance. When considering only the mid-ship section of the suggested uneven baseline minimal ballast bulk carrier, a decrease in the depth of the cargo holds will lead to a

decrease in the ultimate bending moment capacity. To compensate for the decreased ultimate bending moment capacity, the weight of the ship's structure can be increased. For this reason, in order to convince the technical feasibility of the suggested uneven baseline minimal ballast bulk carrier, the structural design evaluation under different sea states should be adopted in the next study.

4. Conclusion

To design a new minimal ballast ship which operate certain amount of permanent ballast for ballast-water free operation, the existing alternatives for ballast water were reviewed. To overcome the lack of berth access and loading constraints of the MIBS / NOBS 'storm ballast', the conceptually an uneven baseline basis 'no or minimal

discharge' alternative so called 'modified' hull form suggested. To generate the 'modified' concept, a simplified systems engineering-based design approach was adopted. By examining the roles of the ballast water and existing alternatives, seven general requirements for a new minimal ballast ship and one specific requirement for overcoming the penalties of a 'storm ballast' were identified. Then, five functional requirements were generated for the uneven baseline minimal ballast vessel. As suggested, the concept has wide and parallel sides compared to the existing V-hull design of a 'storm ballast', so the lack of berth access capability can be compensated theoretically. As for loading constraints, the smaller beam size of the suggested concept compare to exiting MIBS / NOBS concept can be helpful in compensating for the load constraints. However, during the model ship basin test, under the same draft conditions, the EHP of 'modified' increased 5.25% and BHP increased 6.55% on average compare to 'original' hull form. Given the loss in cargo loading capacity, the suggested 'modified' hull form's economic feasibility is assessed at an awkward level. So, resistance performance at same displacement condition has also tested via model ship basin test. From the basin test, more than 12.5 loss in BHP has convinced. From this review result, losses in the cargo capacity and ship resistance performance shall be consider concurrently in the design phase to have technical and economic feasibility. By optimizing the geometry and dimension of the 'modified' hull form, a certain amount of loss in resistance performance and cargo capacity shall be compensated in the next study. Although the suggested uneven baseline basis 'modified' hull form has many rooms for commercializing, the suggested design, evaluation process and methodologies can be adapted to generate various attempts at developing non/minimal ballast ships to keep the healthy ocean environment from organisms of different ecosystems or a large amount of sterile sea water.

Acknowledgements

The initial concept of an 'uneven baseline minimal ballast water bulk carrier' was introduced as a proceeding at the 17th International Congress on Maritime Transportation and Harvesting of Sea Resources (IMAM) (Kang et al., 2017) and concretized in this study. This research was supported by a grant from the National R&D Project of KRISO research project PES3000.

References

- Albert, R.J., Lishman, J.M., & Saxena, J.R. (2013). Ballast Water Regulations and the Move Toward Concentration Based Numeric Discharge Limits. *Ecological Applications*, 23(2), 289-300. <https://doi.org/10.1890/12-0669.1>
- GEF, U., & IMO, G.P. (2011). GESAMP. Establishing Equivalency in the Performance Testing and Compliance Monitoring of Emerging Alternative Ballast Water Management Systems (EABWMS), A Technical Review.
- Isbester, J. (2010). *Bulk Carrier Practice*. Nautical Institute.
- Kang, H.J., Yang, Y.-S., Ki, M.S., Shin, M.S., Choi, J., Cha, J.H., & Lee, D. (2016). A Concept Study for Cost Effective NGH Mid-stream Supply Chain Establishing Strategies. *Ocean Engineering*, 113, 162-173. <https://doi.org/10.1016/j.oceaneng.2015.12.052>
- Kang, H.J., Choi, J., Ahn, H.-S., & Kim, K.-S. (2017). Systems Engineering-basis Feasibility Study for Development of Ballast Water-Free Vessel. *Proceedings of IMAM 2017, Maritime Transportation and Harvesting of Sea Resources*. Lisbon, Portugal.
- Kerr, S. (1994). *Ballast Water Ports and Shipping Study (No. 5)*. AGPS.
- Kim, J., Park, I.R., Kim, K.S., Van, S.H., & Kim, Y.C. (2011). Development of Numerical Method for the Evaluation of Ship Resistance and Self-Propulsion Performances. *Journal of the Society of Naval Architects of Korea*, 48(2), 147-157. <https://doi.org/10.3744/SNAK.2011.48.2.147>
- Kim, Y.C., Kim, K.S., & Kim, J. (2014). Numerical Prediction of Ship Hydrodynamic Performances using Explicit Algebraic Reynolds Stress Turbulence Model. *Journal of the Society of Naval Architects of Korea*, 51(1), 67-77. <https://doi.org/10.3744/SNAK.2014.51.1.67>
- Lee, G.J. (2015). Dynamic Orifice Flow Model and Compartment Models for Flooding Simulation of a Damaged Ship. *Ocean Engineering Journal*, 109, 635-653. <https://doi.org/10.1016/j.oceaneng.2015.09.051>
- Leonard, J. (1999). *Systems Engineering Fundamentals*. Defense Ssystems Management Coll Fort Belvoir VA.
- Parsons, M.G., & Kotinis, M. (2011a). Refinement of the Ballast-Free Ship Concept, Department of Naval Architecture and Marine Engineering, University of Michigan.
- Parsons, M.G., & Kotinis, M. (2011b). Trim and Draft Control Capability of the Variable Buoyancy Ship. *Journal of Ship Production and Design*, 27(3), 118-126.
- Park, B., Jung, D.W., Jung, J., Park, I., Cho, S.K., & Sung, H.G. (2019). Experimental Study on Estimation of Roll Damping for Various Mid-ship Sections. *Journal of Ocean Engineering Technology*, 33(4), 322-329. <https://doi.org/10.26748/KSOE.2019.004>
- Shingo, S. (2014). Preliminary Hull Form Planning for Non-Ballast Water Ship and Minimal Ballast Water Ship (1st Report)-Simplified Estimation Method of Propulsive Performance. *Journal of the Japan Society of Naval Architects and Ocean Engineers*, 20, 21-26. <https://doi.org/10.2534/jjasnaoe.20.21>
- Werschkun, B., Banerji, S., Basurko, O.C., David, M., Fuhr, F., Gollasch, S., ... Kehrner, A. (2014). Emerging Risks from Ballast Water Treatment: The Run-up to the International Ballast Water Management Convention. *Chemosphere*, 112, 256-266. <https://doi.org/10.1016/j.chemosphere.2014.03.135>

Author ORCIDs and Contributions

Author name	ORCID	Contributions
Kang, Hee Jin	0000-0002-8241-3751	①④⑤
Kim, Kwang-Soo	0000-0001-7548-7157	③
Choi, Jin	0000-0001-9842-2049	③
Lee, Yeong-Yeon	0000-0002-0408-6222	②
Ahn, Haeseong	0000-0001-6330-3744	⑤
Yim, Geun-Tae	0000-0002-5382-8931	②

- ① Conceived of the presented idea or developed the theory
- ② Carried out the experiment or collected the data
- ③ Performed the analytic calculations or numerical simulations
- ④ Wrote the manuscript
- ⑤ Supervised the findings of this study

Study on Stopping Ability of a Ship Equipped with Azimuth Propeller

Jong-Yong Park¹, Pilgun Oh², Taejin Kim³ and Jun-Ho Lee⁴

¹Assistant Professor, Department of Naval Architecture and Marine System Engineering, Pukyong National University, Busan, Korea

²Assistant Professor, Department of Graphic Art Information Engineering, Pukyong National University, Busan, Korea

³Assistant Professor, Department of Oceanography, Pukyong National University, Busan, Korea

⁴Assistant Professor, Training Ship NARA, Pukyong National University, Busan, Korea

KEY WORDS: Stopping ability, Azimuth propeller, Research vessel NARA, Full scale maneuvering trial, Track reach

ABSTRACT: An azimuth propeller can generate thrust in all directions by rotating its housing with an electric motor. An azimuth propeller can be operated using several methods to stop a ship. This study aims to derive an efficient method to stop a ship safely using an azimuth propeller through full-scale maneuvering trials with the research vessel "NARA" of Pukyong National University in 4.63 m/s (9 kts). Five methods with different azimuth propeller operations were tested to stop the ship. The test results confirmed that the simultaneous use of the thrust and the hydrodynamic force acting on the strut is the most effective method to stop the ship.

1. Introduction

An azimuth propeller refers to a propeller capable of generating thrust in all directions by rotating its housing through an electric motor. It is used for offshore specialized vessels because it improves berthing and maneuvering performances in the port, and it enables dynamic positioning. A maritime autonomous surface ship, which has recently attracted attention, is likely to be equipped with a bow thruster and an azimuth propeller, rather than a general propulsion and steering gear system, to implement automatic berthing and un-berthing. Therefore, continuous studies will be necessary for the maneuvering performance of ships equipped with an azimuth propeller.

The maneuvering performance of ships are primarily categorized into turning, course changing, and stopping abilities. As a ship is typically equipped with two or more azimuth propellers, various methods can be used to manipulate the propellers for turning and course changing, as well as for stopping a ship. According to ship captains and maritime pilots, ships equipped with azimuth propellers can reduce the track reach by 50% or more at the time of emergency stop compared with ships equipped with general single-shaft propellers, depending on the stopping method (Nowicki, 2014). Previous studies on the stopping ability of ships have focused primarily on methods using maneuvering mathematical models

(Nakato et al., 1976; Yoshimura, 1994). Recent studies have investigated methods for estimating the stopping ability of full-scale ships using the free-running model test or computational fluid dynamics (Ueno et al., 2017; Sun et al., 2018). However, few studies have reviewed methods for improving the stopping ability of ships through full-scale maneuvering trials using azimuth propellers.

This study aims to derive an effective method to safely stop a ship through a full-scale maneuvering trial using azimuth propellers. The full-scale maneuvering was performed using the research vessel "NARA" of Pukyong National University. Five different approaches were tested to stop ships by varying the operation of azimuth propellers. Using the test results, the track reach of the ship was analyzed to determine the most effective method.

2. Preparation of Full-Scale Maneuvering Trial

2.1 Test vessel and azimuth propeller

This study was conducted using the research vessel NARA of Pukyong National University. The general arrangement and specifications of NARA are shown in Fig. 1 and Table 1, respectively.

NARA was equipped with two Rolls-Royce US 155 contra-rotating propellers (CRPs), which were azimuth propellers equipped with a pair of CRPs. The appearance and specifications of the azimuth propeller of NARA are shown in Fig. 2 and Table 2, respectively.

Received 23 November 2019, revised 30 January 2020, accepted 6 February 2020

Corresponding author Jun-Ho Lee: +82-51-629-5995, leejh@pknu.ac.kr

© 2020, The Korean Society of Ocean Engineers

This is an open access article distributed under the terms of the creative commons attribution non-commercial license (<http://creativecommons.org/licenses/by-nc/4.0>) which permits unrestricted non-commercial use, distribution, and reproduction in any medium, provided the original work is properly cited.

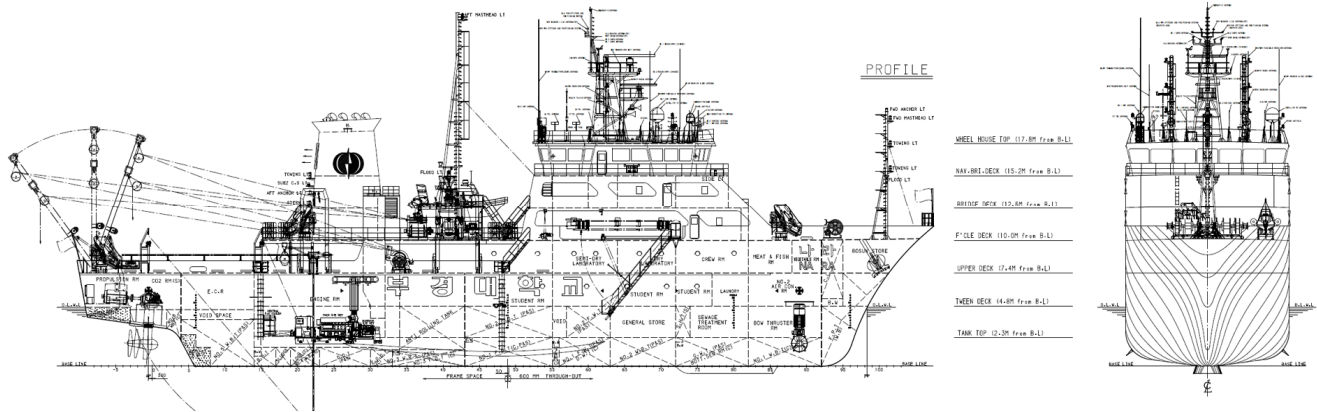


Fig. 1 General arrangement of NARA

Table 1 Principal dimensions of NARA

Item	Value
Length overall, LOA	70.7 m
Length between perpendicular, LBP	59.7 m
Breadth	13.5 m
Draft	4.7 m
Displacement	1,494 t
Metacentric height, GM	0.6 m
Designed speed	7.1 m/s (13.8 kt)

Table 2 Azimuth thruster units of NARA

Item	Value
Max. power on the input shaft	1,100 kW
Main engine nominal speed	0-1200 rpm
Max. allowable torque on the input shaft	8.75 kN·m
Gear reduction ratio in unit	5.311:1
Propeller type	Contra-Rotating propellers (CRP), Monoblock, Fixed pitch
Propeller diameter	2200 mm / 1950 (front / aft propeller)
Number of propeller blades	4 / 5 (front / aft propeller)
Propeller revolution speed	0-226 rpm
Stem length	3,620 mm
Steering speed	3 rpm



Fig. 2 Azimuth propeller of NARA

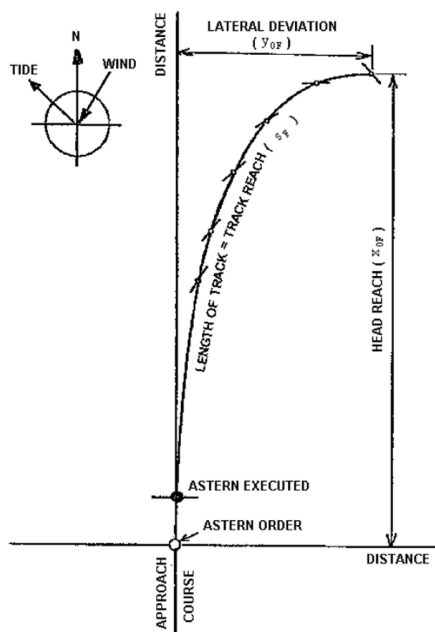
2.2 Test methods

The International Maritime Organization enacted and legislated steering performance standards (maneuverability resolution) in 1994, providing the minimum maneuvering performance required for ships. Crash astern and stopping inertia tests were performed to identify the stopping ability, and the crash astern test was conducted for test-driving commercial vessels. The crash astern test method is as follows. The propeller is windmilled by discontinuing fuel supply to the engine of the ship moving forward at a certain speed, and the engine rotation is reversed to stop the ship when the engine reaches approximately 20% of the rotational speed at the maximum continuous rate. The data to be derived from the crash astern test are defined in Fig. 3, including the track reach, head reach, and lateral deviation during the stop (ITTC, 2017).

The stopping process of a ship, as previously described, is a general method applicable to all types of vessels. For ships equipped with azimuth propellers, additional ship stopping methods exist. The first method is to stop a ship by rotating an azimuth propeller by 180° to change the thrust direction when the angle of the azimuth propeller in the moving-forward situation is defined as 0°. Although this method

Table 3 Case description of the stopping procedure (Nowicki, 2014)

Case	Description
1	Inertia stopping (propellers windmilling) with the azimuth angle of deflection 90° outward
2	Stopping with the azimuth angle of deflection 90° outwards. Propellers revolutions not changed.
3	Stopping by turning azimuth around (180°). When turning the azimuth, the number of propeller revolutions decreased, and the propeller revolutions returned.
4	Stopping by changing the propeller direction of revolution. The astern number of propeller revolutions is the same as that ahead.
5	Stopping by indirect maneuver: deflection of azimuths by 30° outward, with simultaneous reversing of propellers. The astern number of propeller revolutions is the same as that ahead.

**Fig. 3** Definitions used in stopping trials (ITTC, 2017)

improves the stopping ability in comparison with the case of using reverse propulsion, an excessive load can be applied to the propeller blades when rotating the azimuth propeller. The second method is to simultaneously apply the reverse propulsion and rotate the azimuth propeller at a certain angle to additionally use the hydrodynamic force acting on the housing and strut to stop a ship. The rotation of the azimuth propeller at a certain angle results in the generation of lift and drag owing to the angle of attack on the propeller housing and the strut having a shape similar to the blade surface, which can be used to stop the ship. In this study, the five methods used by Nowicki (2014) were tested to stop the ship. Table 3 describes the applied stopping procedures.

3. Results of Full-Scale Maneuvering Trial

The full-scale maneuvering trial was conducted on April 23, 2019, near Mijo-myeon in the Southern coast (near latitude: 34.72°, longitude: 128.11°). During the trial, the average wind speed and wind direction in this region were 6.5 m/s, and 15.8°, respectively, and no current was measured. The initial speed was set at 4.63 m/s (9 kts),

which was approximately 65% of NARA's service speed. According to the provisions of the International Maritime Organization (IMO, 2002), a stopping test must be conducted at a speed equivalent to 90% of the service speed; however, our test was conducted at 4.63 m/s (9 kts) owing to severe hull vibrations at that speed. The measurement period of the test data was 1 Hz. The position information of this vessel were measured by latitude and longitude coordinates, but they were converted into the Universal Transverse Mercator coordinates in this study. The measured velocity was the ground speed, but environmental disturbances such as wind and current in this region prevented the vessel from stopping accurately based on the ground speed. Hence, the track reach, lateral deviation, and time to dead were derived assuming that the vessel stopped when the vessel speed reached 0.46 m/s (0.9 kts) or less, which was 10% of the initial speed. Figs. 4 to 8 show the graphs of the test results by each stopping method. The left-side graph shows the vessel speed and track reach, and the right-side graph indicates the trajectory of the ship.

Table 4 shows a summary of the track reach, lateral deviation, and time to dead for each stopping method.

In Cases 1 and 2, which stop the ship by rotating the azimuth propeller 90° outward, the hydrodynamic force acting on the strut and the housing were used to stop the ship. In Case 3, which stops the ship by rotating the azimuth propeller 180°, and in Case 4, which stops the ship by reverse propulsion, the thrust of the propeller was used directly to stop the ship. In Case 5, which stops the ship by rotating the azimuth propeller 30° outward while reversing the propellers, both the hydrodynamic force acting on the strut and the housing as well as the thrust of the propeller were used to stop the ship. The difference between Cases 1 and 2 is the propeller rotation. The acceleration of the fluid due to propeller rotation was added to the movement speed of the hull, thereby forming an angle of attack in the propeller housing and the strut. The difference in the angle of attack of the propeller housing and the strut between Cases 1 and 2 changed the hydrodynamic force in the ship's stopping direction, resulting in a difference in the track reach. The comparison of the results from Cases 3 and 4 reveals that the method of stopping the ship using reverse propulsion reduces the track reach by 21% compared to that of rotating the azimuth propeller by 180°. This difference is considered to be caused by the difference in the time required for the thrust of the propeller to act in the stopping direction of the ship. As the steering speed of the azimuth propeller

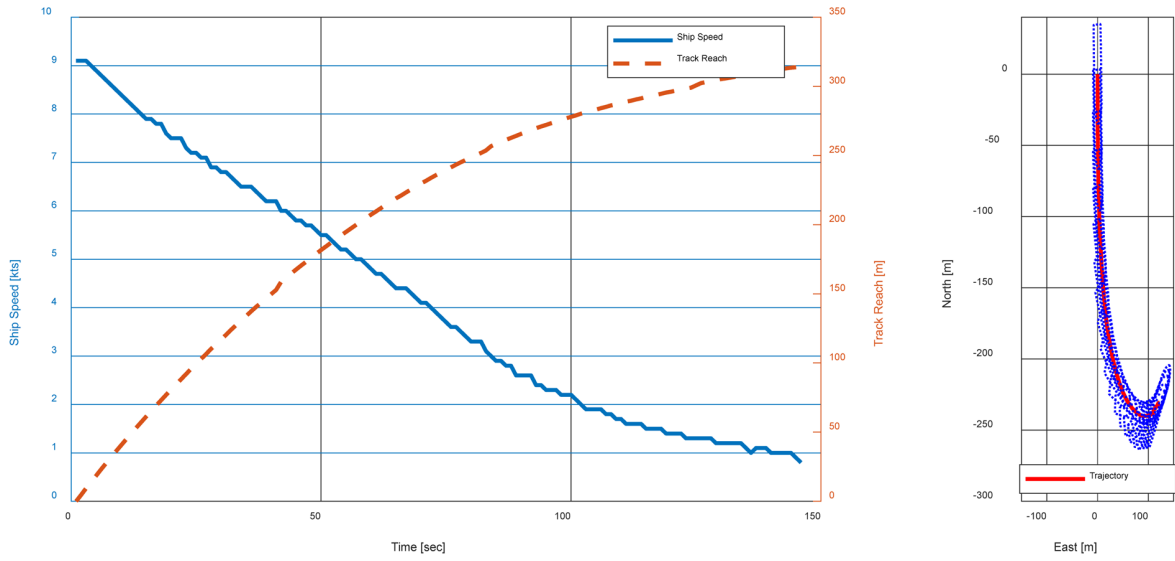


Fig. 4 Stopping test results for 1st stopping mode

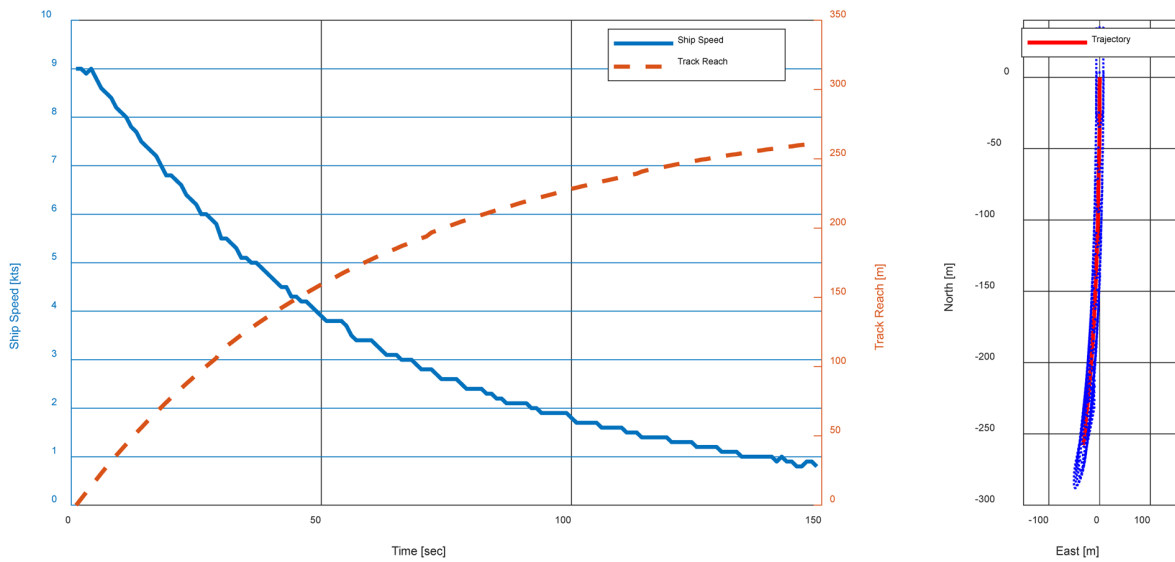


Fig. 5 Stopping test results for 2nd stopping mode

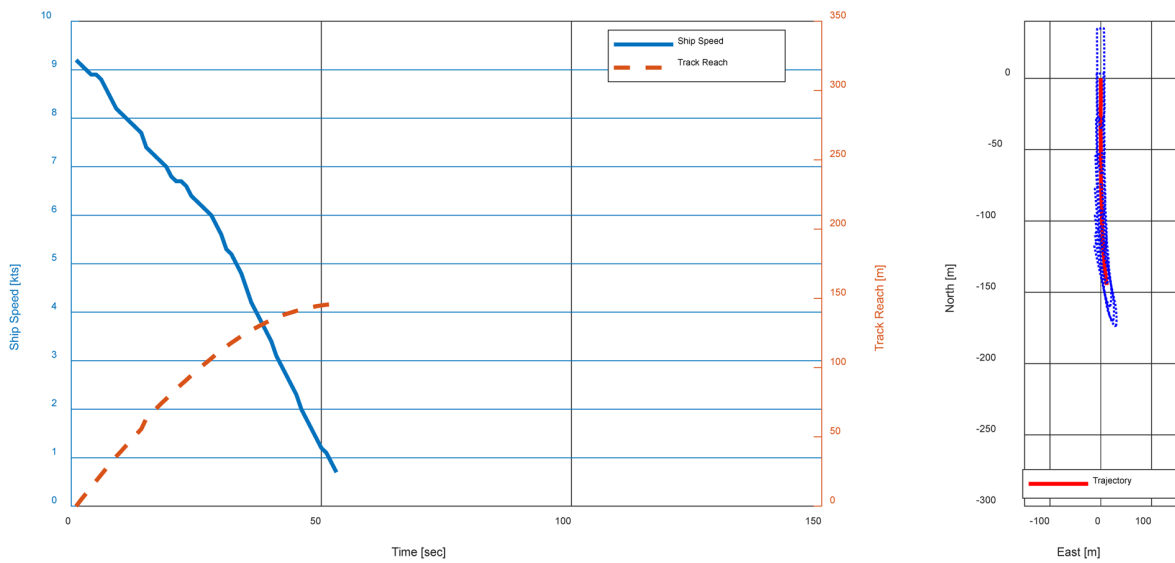


Fig. 6 Stopping test results for 3rd stopping mode

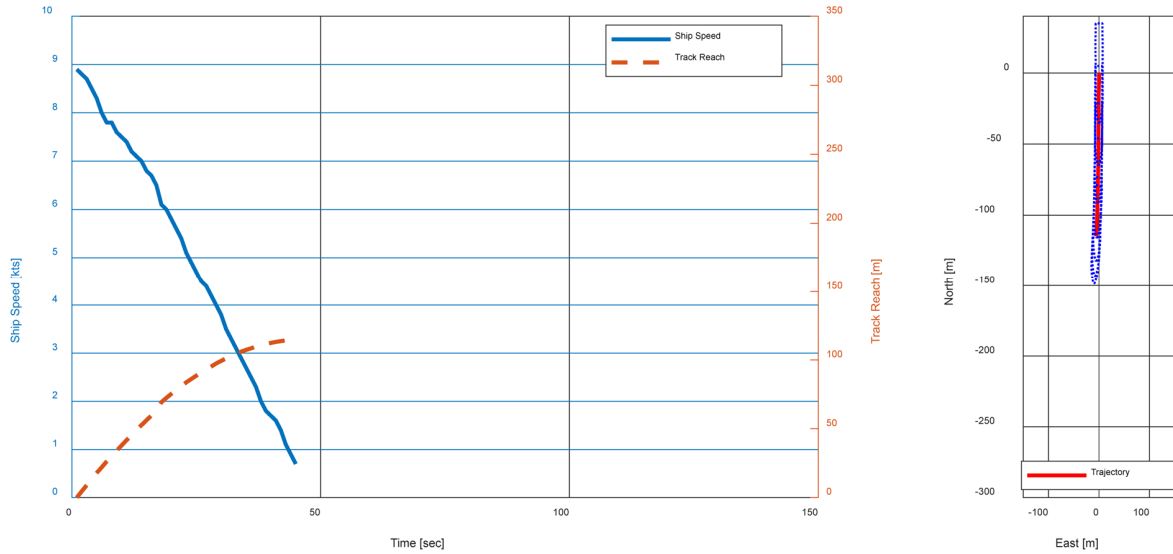


Fig. 7 Stopping test results for 4th stopping mode

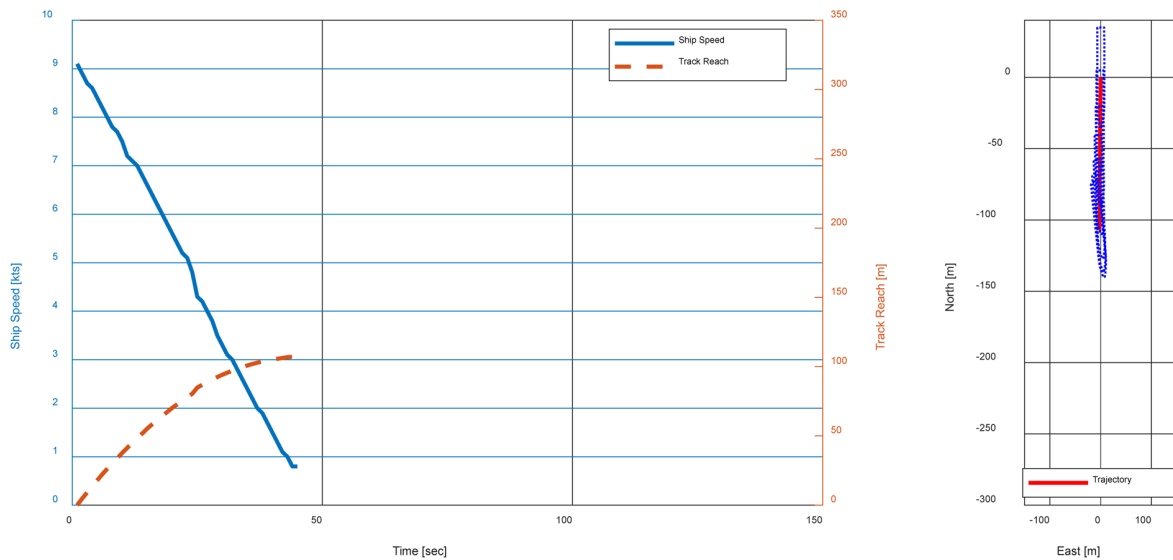


Fig. 8 Stopping test results for 5th stopping mode

Table 4 Stopping test results

Case	Track reach, <i>TR</i>		Head reach, <i>HR</i>		Lateral deviation, <i>LD</i>		Time to dead, <i>TD</i> (s)
	(m)	(LBP)	(m)	(LBP)	(m)	(LBP)	
1	313.84	5.26	230.83	3.87	121.58	2.04	155
2	260.88	4.37	257.75	4.32	32.65	0.55	157
3	145.80	2.44	144.83	2.43	11.85	0.20	61
4	114.70	1.92	114.74	1.92	5.59	0.09	56
5	107.15	1.79	106.99	1.79	3.54	0.06	56

was 3 rpm according to the specifications listed in Table 2, approximately 10 s was required to rotate the azimuth propeller by 180°. In Case 3, reverse propulsion began after the rotation of the azimuth propeller was completed. Fig. 6 shows that the speed reduction rate increased after approximately 25 s. Meanwhile, because the reverse propulsion in Case 4 began immediately after a deceleration in rotation when the stopping test was initiated, the thrust generation time

could be shortened in the stopping direction of the ship, in comparison to Case 3. Furthermore, in both methods, the slipstream of the propeller was directed to the stern, which affected the pressure distribution on the stern and hence the resistance acting on the hull. The propeller in Case 3 was located closer to the hull than compared with Case 4, which could affect the increase in distance traveled by the ship before stopping. The results of Case 5 show that this method is the most effective for

stopping the ship among all the methods. Rotating the azimuth propeller by 30° reduces the thrust in the stopping direction by approximately 13%, but the thrust of the propeller housing and strut due to the angle of attack acts additionally in the direction opposite to the traveling direction of the ship. The overall results confirmed that the methods of Cases 3, 4, and 5, which directly used the thrust of the propeller to stop, was more effective in stopping ships compared to the methods of Cases 1 and 2, which used the hydrodynamic force acting on the propeller housing and the strut to stop the ship.

4. Conclusion

To determine the efficient operation method of azimuth propellers to stop a ship, a full-scale maneuvering trial was conducted using the research vessel NARA of Pukyong National University. First, the method of directly using the thrust of azimuth propellers to stop the ship was more effective than the stopping method using the hydrodynamic force of the propeller housing and strut. Next, the method of stopping the ship using reverse propulsion was more effective than rotating the azimuth propeller by 180°. Subsequently, the method of simultaneously using the thrust of the azimuth propeller, the hydrodynamic force of the propeller housing, and the strut was the most effective in stopping the ship.

The limitations of this study are as follows. First, the conclusions of this study might not be applicable to all ship speeds. The change in ship speed varied the change in the angle of attack between the propeller housing and the strut, which could yield different test results. Next, the operation angle of 30° for the azimuth propeller, which was applied in Case 5, could not be guaranteed to be optimal for stopping the ship. The method in Case 5 might yield different results depending on the operation angle of the azimuth propeller because it simultaneously used the thrust of the propeller and the two thrusts acting on the adjuncts. Therefore, further studies are required to systematically conduct tests for each speed and operation angle of the azimuth propeller and to derive the optimal method for stopping ships by summarizing the results in a lookup table.

Acknowledgements

This study was funded by the National University Promotion Program for Pukyong National University in 2019.

References

Nowicki, J. (2014). Stopping of Ships Equipped with Azipods. *International Journal on Marine Navigation and Safety of Sea Transportation*, 8(3), 373-376. <https://doi.org/10.12716/1001.08.03.07>

ITTC. (2017). Full Scale Manoeuvring Trials. ITTC Recommended Procedures and Guidelines, Revision 02, 7.5-04-02-01.

IMO. (2002). Standards for Ship Manoeuvrability. Resolution MSC, 137(76), MSC 76/23/Add.1-Annex 6.

Sun, C., Wang, J., & Wan, D. (2018). Numerical Simulations of Ship Stopping Maneuver With Reversing Propeller. In *The Thirteenth ISOPE Pacific/Asia Offshore Mechanics Symposium*, Jeju, Korea, ISOPE-P-18-005.

Ueno, M., Suzuki, R., & Tsukada, Y. (2017). Estimation of Stopping Ability of Full-scale Ship using Free-running Model. *Ocean Engineering*, 130, 260-273. <https://doi.org/10.1016/j.oceaneng.2016.12.001>

Yoshimura, Y. (1994). Studies on the stopping ability of a manoeuvring standard. *Journal of the Society of Naval Architects of Japan*, 176, 259-265.

Nakato, M., Kose, K., Teramoto, S., & Simamune, S. (1976). Experimental study on accelerating and decelerating ship motions. *Journal of the Society of Naval Architects of Japan*, 140, 77-84.

Author ORCIDs and Contributions

Author name	ORCID	Contributions
Park, Jong-Yong	0000-0002-5200-6012	③④⑤
Oh, Pilgun	0000-0001-8601-8380	⑤
Kim, Taejin	0000-0001-8222-8647	⑤
Lee, Jun-Ho	0000-0002-3747-167X	①②

- ① Conceived of the presented idea or developed the theory
- ② Carried out the experiment or collected the data
- ③ Performed the analytic calculations or numerical simulations
- ④ Wrote the manuscript
- ⑤ Supervised the findings of this study

Optimal Shape and Boil-Off Gas Generation of Fuel Tank for LNG Fueled Tugboat

Jung-Woog Kim¹, Jin-yeong Jeong² and Dae-Jun Chang³

¹Master Student, Department of Mechanical Engineering, Korea Advanced Institute of Science and Technology, Daejeon, Korea

²Ph.D. Candidate, Department of Mechanical Engineering, Korea Advanced Institute of Science and Technology, Daejeon, Korea

³Associate Professor, Department of Mechanical Engineering, Korea Advanced Institute of Science and Technology, Daejeon, Korea

KEY WORDS: LNG fuel tank, LNG fuel tank, Tugboat, Boil-off gas (BOG)

ABSTRACT: This paper proposes the optimal shape of an LNG fuel tank with a lattice pressure vessel (LPV) design for a tugboat. The LPV is a Type C tank with a design philosophy of “design by analysis,” which facilitates greater variability of shape compared with other traditional Type C tanks. Further, compared with conventional cylindrical fuel tanks, the LPV provides better volumetric efficiency. Considering the shape of a fuel tank room, a trapezoidal shape of the LPV is concluded as the most optimal design. This study performs two major analyses of the LPV: structural and heat transfer analyses. First, a design procedure of the LPV based on structural analyses is elaborated. The finite element method is used for the analyses. Furthermore, the results guarantee that the maximum stresses by applied loads do not exceed an allowable stress limitation. Second, the heat transfer analysis of the LPV is conducted. LNG boil-off gas generation is analyzed based on various insulation materials and the degree of vacuum.

1. Introduction

Owing to pollutants emitted from ships, global warming and environmental pollution are becoming serious problems in the field of world maritime transport. Existing ship fuels include heavy fuel oil (HFO), which is heavy oil, and marine diesel oil (MDO) and marine gas oil (MGO), which are a mixture of heavy oil and diesel; environmental pollutants are discharged from these fuels. Pollutants in the main emission gases include sulfur oxides (SO_x), nitrogenoxides (NO_x), and carbondioxide (CO₂).

The International Maritime Organization (IMO) introduced regulations to limit emissions from ships. According to the SO_x regulation, the sulfur content in fuels used in an emission control area (ECA) is limited to 0.5% as of 2020, and according to the NO_x regulation, it should satisfy the “Tier II” level in general waters and “Tier III” in the ECA as of 2016. In addition, regulations on CO₂ emissions have been gradually applied by introducing the energy efficiency design index (EEDI). The EEDI refers to the amount of CO₂ (gCO₂/t·mile) generated by a new ship that carries one ton of cargo for one mile. The EEDI has been proposed by the IMO’s Marine Environmental Protection Committee (MEPC) and requires a 10% reduction in CO₂ emissions at each phase as of 2008 (Ivica and Ante, 2015). In the MEPC 72nd conference in May 2018, it was proposed to

advance to Phase II (20% CO₂ reduction) in 2020 and to Phase III (30% CO₂ reduction) in 2025. Furthermore, it was proposed to advance to Phase IV (40% CO₂ reduction) in 2030 instead of 2040 (IMO, 2018).

Therefore, liquefied natural gas (LNG), which is an eco-friendly fuel, is known to be a promising alternative fuel suitable for reducing the emissions of SO_x, NO_x, and CO₂, which are pollutants emitted from ships. According to Alternative Fuels Insight (AFI) provided by DNV-GL, there are 170 LNG-operated ships and 147 LNG-propelled ships as of October 2019, and 55 more ships will be built by 2020 (DNV-GL, 2019).

Starting in September 2020, the five largest ports in Korea will be designated as ECAs. Accordingly, domestic coastal ships are also built as LNG-propelled ships, and tugboats, which account for a large proportion, will have to use the LNG fuel. Furthermore, because tugboats push and pull large ships, these boats require high power for the total weight than other coastal ships (Kifune and Nishio, 2015). This indicates that tugboats require a high-power engine and a large LNG fuel tank. As the hull is limited in space, a fuel tank suitable to the shape of a tugboat and having a high volume efficiency is required.

The pressurized fuel tank does not affect the gas fuel supply, and it can withstand the maximum design pressure even if the internal pressure of the tank increases due to boil-off gas (BOG). Therefore,

Received 19 November 2019, revised 3 February 2020, accepted 14 February 2020

Corresponding author Daejun Chang: +82-42-350-1514, djchang@kaist.ac.kr

© 2020, The Korean Society of Ocean Engineers

This is an open access article distributed under the terms of the creative commons attribution non-commercial license (<http://creativecommons.org/licenses/by-nc/4.0>) which permits unrestricted non-commercial use, distribution, and reproduction in any medium, provided the original work is properly cited.

BOG treatment equipment is not required. However, because the existing Type C fuel tank is a cylinder-type, and thus, its aspect ratio is fixed, it is difficult to design a free shape. Furthermore, it can only contain a small amount of LNG fuel due to its round shape (Ahn et al., 2017). A lattice pressure vessel (LPV) can be designed freely and can increase the volume ratio and volume efficiency compared with the conventional cylindrical fuel tank. In addition, the aspect ratio is not limited, allowing fuel tank designs of any size (Lee et al., 2017).

The BOG generation from an LNG fuel tank is related to the surface area according to the size of the fuel tank and insulation performance. Due to the heat inflow generated by the temperature difference between the outside temperature and the inside of the tank, the LNG, whose temperature is -163°C at atmospheric pressure, is vaporized to generate the BOG. Therefore, a double structure should be used for the fuel tank to maintain the vacuum and the heat insulating material so that the heat inflow is minimized. This method and application have been applied in LNG storage systems, and the thermal conductivity (k_e) and the heat flux (q) according to the vacuum level have been verified through experiments with various insulation materials (Fesmire, 2015).

In this study, the optimum shape of the fuel tank for an LNG-fueled tugboat is designed and an LPV, which can improve the storage efficiency of the LNG, is proposed. Furthermore, by applying various insulation materials in the proposed fuel tank, the BOG generation analysis is conducted to predict the minimum BOG generation inside a fuel tank suitable for a tugboat.

2. Optimum Shape Design of LNG Fuel Tank of Tugboat

2.1 LNG fuel tank space in tugboat

The fuel tank in ships using natural gas as fuel should be installed so that it can be protected from the risk of collision or stranding. The fuel tank designed in this study and its location were also determined based on this criterion. A detailed criterion is as follows. On the side of the fuel tank, the distance measured vertically from the side of the ship at the level of the summer load should be greater than the smaller value between $B/5$ and 11.5 m. For the lower surface, the distance from the side of the ship to the tank should be greater than the smaller value between $B/15$ and 2 m, where B is the maximum width of the ship (IGF CODE, 2015).

Fig. 1 shows the modeling of the 3.7 MW (5,000 hp) LNG-fueled tugboat and the floor plan inside the bow. The bow part of the tugboat is allocated for the LNG fuel tank and fuel supply system. As the width becomes narrower according to the linearity of the bow, the right side of the fuel tank should be designed in a proper shape to maximize the space. Therefore, the fuel tank is designed in a trapezoidal shape, and the space of the opposite fuel supply system is designed according to the volume and weight of the fuel tank. The detailed design process is addressed in Section 2.2. If a cylindrical fuel tank is installed in this space, the streamlined shape in the space will not be efficiently used.

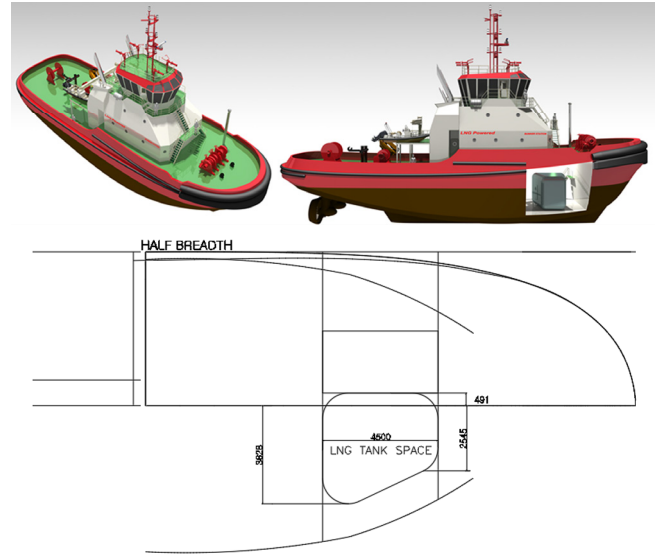


Fig. 1 Drawing of fuel tank room in the tugboat

This directly affects the capacity of the fuel tank and reduces the amount of available LNG. Consequently, the LNG bunkering cycle is shortened, and the BOG generated during fueling leads to inefficient operation of the tugboat.

Unlike conventional cylindrical tanks, the LPV used in this study has a free shape. As the aspect ratio is not determined, the LPV can be designed to fit the space of the fuel tank room. Comparing the volume efficiency ratio between the cylinder tank and the LPV, the maximum volume efficiency ratio of the cylinder is 78.5%, whereas the ideal ratio of the LPV is 100% (Ahn et al., 2017). In addition, as the LPV is a pressure tank, BOG treatment equipment is not required, and thus, it is possible to maximize the fuel tank space.

For the fuel tank of the tugboat, a trapezoidal LPV was designed based on the characteristics of the space with a side of a streamlined shape. Therefore, considering the characteristics of the fuel tank space, the difference between the cylindrical tank and the LPV is evident. As shown in Fig. 2, when the cylindrical tank is used in the fuel tank space, the volume would be 17 m^3 even if the cylinders are simply stacked. In contrast, for the LPV designed in this study, the volume is 37.5 m^3 because it can utilize most of the fuel tank space. In other words, the LPV is approximately 55% more space-efficient than

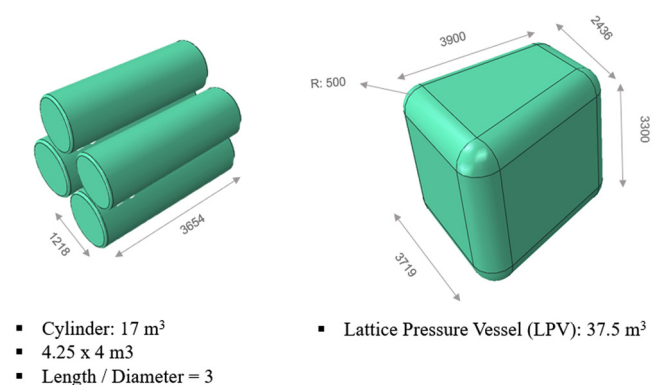


Fig. 2 Comparison of cylinder tanks and LPV in the fuel tank room

cylinder tanks. In addition, the maintenance of the cylindrical tank is complicated because each tank is equipped with pipes and safety valves for fuel movement, whereas the maintenance of the LPV is relatively simple because it is equipped with fewer pipes and safety valves. Therefore, the LPV will incur lower maintenance cost.

2.2 Lattice pressure vessel shape design

The LPV is designed based on IGF code, IGC code, and ASME BPV code. The regulations specify the design by analysis requirements, fracture mechanics, and criteria for non-cylindrical tanks (IGF, 2015; IGC, 2014; ASME, 2013).

Based on the above regulations, the LPV is designed through Abaqus, a finite element analysis program. The design procedure of the LPV by finite element analysis is shown in Fig. 3. First, elements in the LPV are created and combined. The material is then selected, and boundary conditions and loads are applied. Finally, the analysis is conducted, and the design is repeated until the result satisfies the design criteria.

The accept criteria in Fig. 3 follow the Annex of the IGF Code, “Standard for the use of limit state methodologies in the design of fuel containment systems of novel configuration.” The IGF code requires three-dimensional finite element analysis, hydrodynamic analysis, buckling, fatigue, and crack propagation analysis. The analysis conducted in this study focuses on the allowable stress that does not cause plastic deformation. Specific criteria are as follows.

$$\sigma_m \leq f \quad (1)$$

$$\sigma_L \leq 1.5f \quad (2)$$

$$\sigma_b \leq 1.5F \quad (3)$$

$$\sigma_L + \sigma_b \leq 1.5F \quad (4)$$

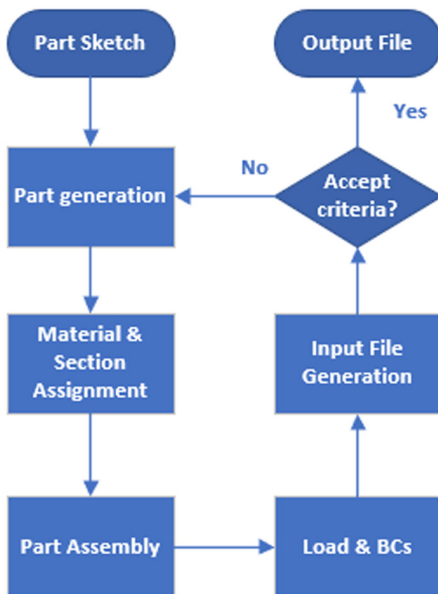


Fig. 3 Design procedure of LPV

$$\sigma_m + \sigma_b \leq 1.5F \quad (5)$$

$$\sigma_m + \sigma_b + \sigma_g \leq 3.0F \quad (6)$$

$$\sigma_L + \sigma_b + \sigma_g \leq 3.0F \quad (7)$$

where

σ_m = primary general membrane stress

σ_L = primary local membrane stress

σ_b = primary bending stress

σ_g = secondary stress

$$f = \frac{\sigma_Y}{\gamma_{s1} \gamma_m \gamma_c}$$

$$F = \frac{\sigma_Y}{\gamma_{s2} \gamma_m \gamma_c}$$

$$\gamma_{s1} = 0.76 \times \frac{1.6}{\kappa_1}$$

$$\gamma_{s2} = 0.76 \times \frac{1.5}{\kappa_2}$$

$$\kappa_1 = \min\left(\frac{\sigma_{UTS}}{\sigma_Y} \times \frac{1.6}{3.5}, 1\right)$$

$$\kappa_2 = \min\left(\frac{\sigma_{UTS}}{\sigma_Y} \times \frac{1.5}{3}, 1\right)$$

$$f = \frac{\sigma_Y}{\gamma_{s1} \times 1.2 \times 1.03} \text{ for stainless steel}$$

$$F = \frac{\sigma_Y}{\gamma_{s2} \times 1.2 \times 1.03} \text{ for stainless steel}$$

σ_{UTS} = ultimate tensile strength

σ_Y = yield strength

Primary general membrane stress indicates the stress generated on the plate due to internal pressure, and primary local membrane stress indicates the stress generated on the joint. The membrane stress is analyzed to have the same value in the plate thickness direction. Primary bending stress is the stress that fluctuates along the thickness direction. Primary bending stress is the stress that changes along the thickness direction. In designing the LPV, the accept criteria for primary stress generation should be satisfied so that structurally proven designs can be obtained. The accept criteria were determined by applying safety factors such as material factor and consequence factor to ultimate tensile strength and yield strength.

Therefore, the design pressure, weight, and gravity of the LNG were considered as the main load conditions in the LPV designed in this study. In addition, for the design criteria, the allowable stress was used. As the design pressure, 1 MPa, which is the maximum allowable relief valve setting specified in the IGF code, was used.

3. Analysis of BOG Generation by Insulation

3.1 Insulation Information

Various insulation materials are used in the LNG fuel tank.

Table 1 Insulation properties (Tseng et al., 1997; Fesmire, 2015)

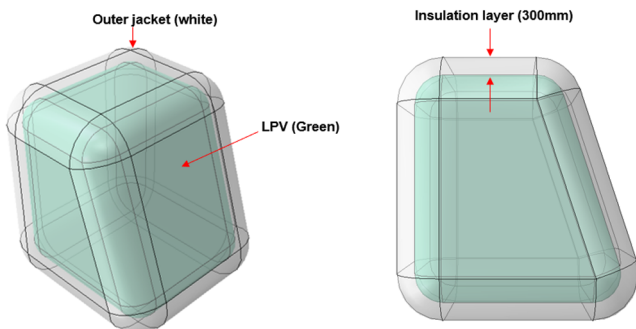
Items	Unit	Aerogel blanket	Perlite powder	Glass bubble	Polyurethane foam
Thermal conductivity (101.3 kPa)	W/m·K	0.011	0.035	0.025	0.023
Thermal conductivity (0.013 kPa)	W/m·K	0.003	0.004	0.002	0.009
Thickness	m	0.300	0.300	0.300	0.300

Currently, polyurethane foam, perlite powder, glass bubble, and aerogel blanket are widely used for cryogenic insulation. In addition, to minimize the heat inflow generated by the temperature difference between the inside and outside, the vacuum level in the insulation is increased and the insulation is used in the LNG fuel tank. This is a test-proven method, and in 2015, perlite powder, glass bubble, aerogel blanket, multi-layer insulation, fiberglass, and layered composite insulation (LCI) were applied to a cryogenic liquid storage container and the heat conduction effect according to the vacuum level was tested (Fesmire, 2015). In the case of polyurethane foam, there was a case where the thermal insulation performance was tested not only in the LNG industry but also in the liquid hydrogen temperature range. In this case, the thermal insulation performance was tested under vacuum as well as atmospheric pressure (Tseng et al., 1997). Therefore, this study analyzed the amount of BOG generated from the fuel tank according to various insulators. Aerosol, perlite powder, glass bubble, and polyurethane foam were used as insulation materials. Each insulation material was analyzed in atmospheric pressure and vacuum. The insulation properties are shown in Table 1.

3.2 BOG generation analysis

Fig. 4 shows a tugboat LNG fuel tank with an insulation layer and outer jacket. The LPV, which is a fuel tank, is protected by a uniform insulating layer and outer jacket to reduce heat inflow. The information about the fuel tank with the insulation layer is summarized in Table 2.

The amount of BOG generated is calculated using external temperature, LNG temperature, density, and phase change heat. The relevant information is summarized in Table 3. In this study, it is

**Fig. 4** LPV with insulation system**Table 2** LPV insulation system specification

LPV volume (m ³)	Surface area (m ²)	Liquid level (%)
37.5	79.8	90

Table 3 BOG calculation parameters

Ambient temperature (K)	LNG temperature (K)	LNG density (kg/m ³)	Heat of vaporization (kJ/kg)
318.15	111.15	450	664.7

assumed that heat transfer by convection and radiation has no effect considering that the insulation layer has sufficient thickness. In other words, the amount of BOG generated was analyzed by considering the heat transfer by conduction alone. It was assumed that the LNG level is 90%, the temperature gradient in the tank would be negligible, and the outside temperature would be 45°C. The equation of state for the thermodynamic properties of the LNG used in the calculation is the Peng-Robinson equation. Based on this information, the derivation process of the amount of the generated BOG is given in Eqs. (8)-(11). The thermal resistance in the one-dimensional conduction heat transfer can be derived using Eq. (8). Assuming that all sides of the LPV are planar, the thermal resistance (t) can be determined from the insulation thickness (k), thermal conductivity (A), and cross-sectional area (R). Eq. (9) helps calculate the heat intrusion (q). Dividing the thermal resistance (T_{amb}) obtained from Eq. (8) by the difference between the external temperature (R) and the temperature of the LNG (T_{LNG}) results in thermal intrusion (q). The equation for calculating the BOG, or the LNG evaporating due to heat intrusion (q), is shown in Eq. (10). The BOG calculated using Eq. (10) is the amount of the LNG that evaporates during a day and is calculated by the ratio of the heat intrusion (q) and the latent heat of evaporation of the LNG (h_{fg}). Finally, to calculate the boil-off rate (BOR), the BOG relative to the amount of the LNG in the fuel tank should be calculated using Eq. (11). The LNG in the fuel tank is obtained by multiplying the density of the LNG (ρ_{LNG}), the volume of the fuel tank (V), and the liquid fraction (LLF).

$$R = \frac{t}{kA} \quad (8)$$

$$q = \frac{T_{amb} - T_{LNG}}{R} \div 1000 \quad (9)$$

$$BOG = \frac{q}{h_{fg}} \times 3600 \times 24 \quad (10)$$

$$BOR = \frac{BOG}{LLF \times \rho \times V} \times 100 \quad (11)$$

where

- t insulation thickness (m)
- k conductivity (W/m·K)

A	surface area (m ²)
R	thermal resistance (K/W)
T_{amb}	ambient temperature (K)
T_{LNG}	LNG temperature (K)
q	heat ingress (kW)
h_{fg}	heat of vaporization (kJ/kg)
LLF	liquid level fraction
ρ	density (kg/m ³)
V	volume (m ³)
BOG	boil off gas (kg/day)
BOR	boil off rate (%/day)

4. Results and Discussion

4.1 Shape design result of fuel tank

Fig. 5 shows the LPV designed in this study. The designed LPV is trapezoidal by considering the shape of the fuel tank space, and it is 3.3

m in height, 3.9 m in length, 3.7 m in the lower side and 2.4 m in the upper side, and the radius is 0.5 m. The component is composed of a 19-mm-thick outer surface and 15-mm-thick stiffener. Consequently, the volume and weight of the LPV were estimated to be 37.5 m³ and 25.37 ton, respectively. Table 4 shows the materials, density, physical properties, allowable stress, design pressure, and LNG density information in the design. The load conditions used in the design include internal pressure, the weight of the LNG, and gravity.

Fig. 6 shows the finite element analysis results of the LNG LPV. In the results, the von Mises stress indicates that the safety factor is applied to the combination of bending stress and membrane stress. Therefore, to satisfy the design specification presented in the IGF code conservatively, the von Mises stress must be within the allowable stress.

The LPV designed in this study has a maximum von Mises stress of 204.3 MPa and does not exceed 205 MPa, the allowable stress of SUS304. In conclusion, the combination of bending stress and

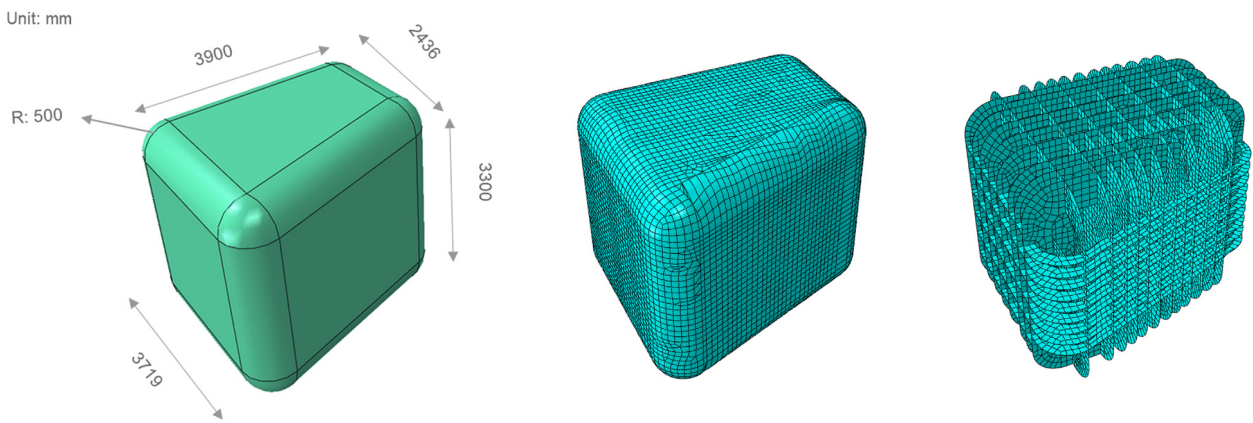


Fig. 5 Designed LPV

Table 4 Properties used in LPV

Material	Density (kg/m ³)	Poisson's ratio	Young's modulus (MPa)	Allowable stress (MPa)	Design pressure (MPa)	LNG density (kg/m ³)
SUS304	8030	0.31	195	205	1	500

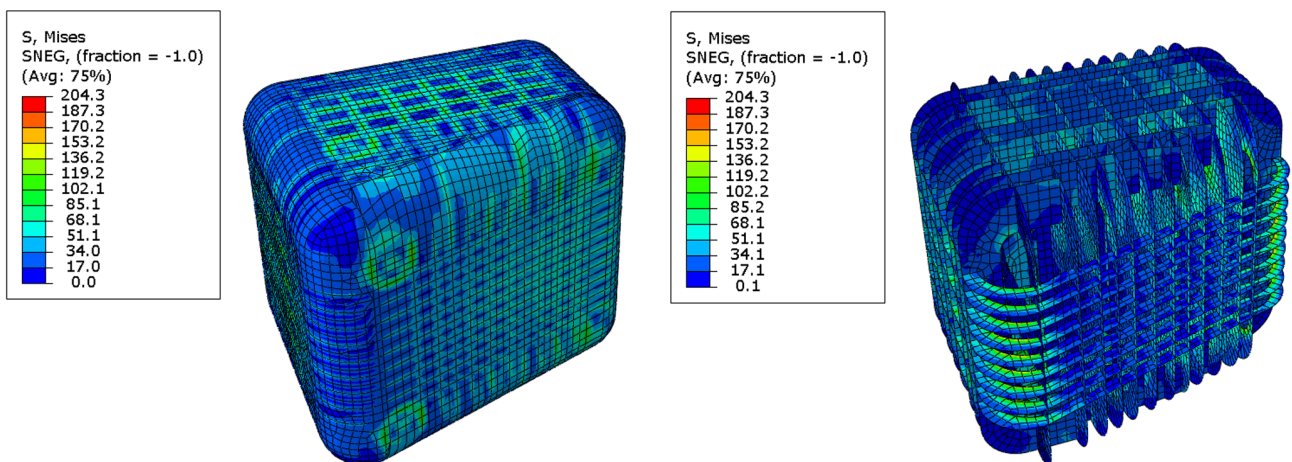


Fig. 6 Analysis result of LPV (von Mises stress)

membrane stress caused by internal pressure, the weight of the LNG, and gravity is considered to satisfy the allowable stress. Thus, the structural design of the LPV having the design pressure of 1 MPa is completed.

4.2 BOG generation result

The results of the amount of BOG generated with various insulators at atmospheric pressure are summarized in Table 5. BOR is 0.518 %/day for aerosol, which has the lowest thermal conductivity, and 1.649 %/day for perlite powder, which has the highest thermal conductivity. Table 6 shows the results of the amount of BOG generated when vacuum is applied to various insulations. In the vacuum state, as the thermal conductivity is lower than that at atmospheric pressure, the BOR is also low. The BOR is approximately 0.094 %/day for the glass bubble with the lowest thermal conductivity and 0.424 %/day for polyurethane foam with the highest thermal conductivity.

The results of the amount of BOG generated according to the vacuum level and insulation material can be used for the tugboat operation plan. If the tugboat fuel supply cycle is established, a target BOR will be designed, which leads to the degree of a vacuum and selection of the insulation layer. As a future study, if the target BOR of the tugboat fuel tank is determined, it will be possible to select the optimum insulation condition and set the operation strategy of the tugboat through economic evaluation according to various insulation materials and vacuum level.

Table 5 BOG calculation result (101.3 kPa)

Items	Unit	Aerogel blanket	Perlite powder	Glass bubble	Polyurethane foam
Thermal conductivity	W/m·K	0.011	0.035	0.025	0.023
Thickness	m	0.300	0.300	0.300	0.300
Thermal resistance	K/W	0.342	0.107	0.150	0.163
Heat ingress	kW	0.606	1.927	1.377	1.266
BOG	kg/day	78.729	250.500	178.929	164.614
BOR	%/day	0.518	1.649	1.178	1.084

Table 6 BOG calculation result (0.013 kPa)

Items	Unit	Aerogel blanket	Perlite powder	Glass bubble	Polyurethane foam
Thermal conductivity	W/m·K	0.003	0.004	0.002	0.009
Thickness	m	0.300	0.300	0.300	0.300
Thermal resistance	K/W	1.253	0.940	1.880	0.418
Heat ingress	kW	0.165	0.220	0.110	0.496
BOG	kg/day	21.471	28.629	14.314	64.414
BOR	%/day	0.141	0.189	0.094	0.424

5. Conclusion

In this study, the optimum shape of a fuel tank for an LNG-fueled tugboat was designed and an LPV was proposed to improve the volume efficiency. In addition, the minimum amount of BOG generated was estimated according to the heat inflow by applying various insulation materials to the proposed fuel tank.

The optimum shape for the 3.7 MW (5,000 hp) tugboat is a trapezoid with a volume of 37.5 m³ and a fuel tank is designed with rounded corners to minimize surface area. The surface area of the fuel tank was 79.8 m² when the LPV was applied, and the volume efficiency in the same fuel tank space was increased by 55% compared with that of the cylindrical pressure vessel. The finite element analysis considering the fuel tank internal pressure, weight of the LNG, and gravity resulted in a von Mises stress of 204.3 MPa, which is within the allowable stress and thus confirmed the safety of the design.

Various insulation materials were applied to the fuel tank to calculate the amount of BOG generated. Consequently, the glass bubble generated the smallest amount of BOG with 14.3 kg/day at 0.013 kPa and polyurethane foam generated the highest amount of BOG with 64.4 kg/day. Similarly, from the BOR calculation results, it was observed that polyurethane foam showed the highest value of 0.42 %/day, whereas perlite powder and aerosol insulation showed a similar amount of generated BOG.

The use of high-performance insulation minimizes the amount of BOG generated, which eliminates the need for BOG treatment equipment and increases the safety of the fuel tank. However, from an economic point of view, the initial investment cost of the fuel tank can be increased. Therefore, research on the optimum insulation material and insulation condition is necessary.

Acknowledgment

This study was funded by the Ministry of Oceans and Fisheries and supported by the Marine Industry Growth Technology Development Project by the Marine Fisheries Research and Development Institute (Development of an eco-friendly 3.7 MW (5,000 hp) LNG fuel tugboat (project number: 20190170)).

References

- Ahn, J.K., Choi, Y.S., Jo, C.H., Cho, Y.H., Chang, D.J., Chung, H., ... & Bergan. (2017). Design of a Prismatic Pressure Vessel with Internal X-beam Structures for Application in Ships. *Ships and Offshore Structures*, 12(6), 781-792. <https://doi.org/10.1080/17445302.2016.1247487>
- ASME. (2013). BPV Code Section VIII Division 2: Alternative Rules - Design and Fabrication of Pressure Vessels.
- DNV-GL. (2019). Alternative Fuels Insight Platform (AFI). Retrieved November 2019 from <https://store.veracity.com/da10a663-a409-4764-be66-e7a55401275a>

- Fesmire, J.E. (2015). Standardization in Cryogenic Insulation Systems Testing and Performance Data. *Physics Procedia*, 67, 1089-1097. <https://doi.org/10.1016/j.phpro.2015.06.205>
- IGC. (2014). International Code of Safety for Ships using Gases or Other Low-Flashpoint Fuels. Retrieved November 2019 from <http://www.imo.org/en/KnowledgeCentre/IndexofIMOR/esolutions/MSC%20Resolutions/MSC%20370%2093.pdf>
- IGF. (2015). International Code of Safety for Ships using Gases or Other Low-Flashpoint Fuels. Retrieved November 2019 from [http://www.imo.org/en/KnowledgeCentre/IndexofIMOR/esolutions/Maritime-Safety-Committee-\(MSC\)/Documents/MSC.391\(95\).pdf](http://www.imo.org/en/KnowledgeCentre/IndexofIMOR/esolutions/Maritime-Safety-Committee-(MSC)/Documents/MSC.391(95).pdf)
- International Maritime Organization (IMO). (2018). Report on the Marine Environment Protection Committee on Its Seventy-second Session. Marine Environment Protection Committee (MEPC) 72th Session, Retrieved November 2019 from http://www.crs.hr/Portals/0/docs/eng/imo_iacs_eu/imo/mepc_reports/MEPC%2072%20-%20Report.pdf?ver2018-06-29-140230-617
- Ivica A., & Ante S. (2015). Influence of the Required EEDI Reduction Factor on the CO₂ Emission from Bulk Carriers. *Energy Policy*. 84, 107-116. <https://doi.org/10.1016/j.enpol.2015.04.031>
- Kifune, H., & Nishio, T. (2015). A Study of Fuel Consumption Model Using Tugboat's Propulsion System. *Journal of the Japan Institute of Marine Engineering*, 50(4), 527-534. <https://doi.org/10.5988/jime.50.527>
- Lee, J.M., Choi, Y.S., Jo, C.H., & Chang, D.J. (2017). Design of a Prismatic Pressure Vessel: an Engineering Solution for Non-stiffened-type Vessels. *Ocean Engineering*, 142, 639-649. <https://doi.org/10.1016/j.oceaneng.2017.07.039>
- Tseng, C.J., Yamaguchi, M., & Ohmori, T. (1997). Thermal Conductivity of Polyurethane Foams from Room Temperature to 20 K. *Cryogenics*, 37(6), 305-312. [https://doi.org/10.1016/S0011-2275\(97\)00023-4](https://doi.org/10.1016/S0011-2275(97)00023-4)

Author ORCIDs and Contributions

Author name	ORCID	Contributions
Kim, Jung-Woog	0000-0001-6565-7001	①②③④
Jeong, Jin-yeong	0000-0002-7645-6579	①②④
Chang, Dae-Jun	0000-0001-7094-8874	①⑤

- ① Conceived of the presented idea or developed the theory
- ② Carried out the experiment or collected the data
- ③ Performed the analytic calculations or numerical simulations
- ④ Wrote the manuscript
- ⑤ Supervised the findings of this study

Extreme Value Analysis of Metocean Data for Barents Sea

Sung Boo Park¹, Seong Yun Shin¹, Da Gyun Shin¹, Kwang Hyo Jung²,
Yong Ho Choi³, Jaeyong Lee⁴ and Seung Jae Lee⁵

¹Graduate student, Department of Naval Architecture and Ocean Engineering, Pusan National University, Busan, Korea

²Professor, Department of Naval Architecture and Ocean Engineering, Pusan National University, Busan, Korea

³Principal Researcher, Ship and Offshore Research Center, Samsung Heavy Industries, Co. Ltd, Daejeon, Korea

⁴Professor, Department of Naval Architecture and Ocean Engineering, Dong-Eui University, Busan, Korea

⁵Professor, Division of Naval Architecture and Ocean Systems Engineering, Korea Maritime and Ocean University, Busan, Korea

KEY WORDS: Extreme value analysis, Metocean data, Significant wave height, Spectral peak wave period, I-FORM, Gumbel distribution, Weibull distribution, Log-normal distribution

ABSTRACT: An extreme value analysis of metocean data which include wave, wind, and current data is a prerequisite for the operation and survival of offshore structures. The purpose of this study was to provide information about the return wave, wind, and current values for the Barents Sea using extreme value analysis. Hindcast datasets of the Global Reanalysis of Ocean Waves 2012 (GROW2012) for a waves, winds and currents were obtained from the Oceanweather Inc. The Gumbel distribution, 2 and 3 parameters Weibull distributions and log-normal distribution were used for the extreme value analysis. The least square method was used to estimate the parameters for the extreme value distribution. The return values, including the significant wave height, spectral peak wave period, wind speed and current speed at surface, were calculated and it will be utilized to design offshore structures to be operated in the Barents Sea.

1. Introduction

According to the National Oceanic and Atmospheric Administration (NOAA), the Earth's average temperature is increasing annually as global warming continues, and the temperature of the Arctic region is increasing twice as fast as those of other regions (NOAA, 2018). With Arctic glaciers melting owing to global warming, the importance of developing marine resources buried in the Arctic is emerging. According to the United States Geological Survey, undiscovered recoverable resources in the Arctic region include approximately 90 billion barrels (Bbbl) of oil, 1,669 trillion cubic feet (Tcf) of gas, and 44 Bbbl of natural gas liquid (Bird et al., 2008). It is estimated that 13% of the world's undiscovered oil volume and 30% of the world's undiscovered gas volume are buried in the Arctic region. In general, marine resources in the deep sea are developed by offshore structures, and it is important to collect and analyze the metocean data of sea areas where marine resources are buried for the operation and survival of offshore structures. Metocean data include wave, wind, current, water depth, tide, and soil conditions. To reflect metocean data in the design of offshore structures, extreme value analysis should be conducted (API, 2005). Metocean data can be collected from

measurement data of actual sea areas that use buoys or ships, hindcast data that estimate the desired data of the past through numerical methods based on past metocean data, and satellite data that use satellites. According to DNVGL (2015), for the design of offshore structures, the significant wave height (H_s) and spectral peak wave period (T_p) of 100-year return values should be used for waves, whereas the 100-year return value of the one-hour average wind speed at 10 m above the mean sea level (MSL) should be used for wind speed. For ocean currents, the 10-year return value of the current speed should be reflected in the design.

To derive return values through statistical methods, methods for selecting the collected data must be determined. Such methods can be primarily categorized into global and event models. Global models include the initial distribution and total sample methods that use the entire data statistically, and the event models include the peak over threshold method, which uses data above a certain threshold, and the annual maxim method, which uses only the annual maximum values (DNV, 2014).

Extreme value distributions (EVDs) used for extreme value analyses include the Gumbel, Frechet, Weibull, and log-normal distributions. Methods for estimating the parameters of EVDs include

Received 15 October 2019, revised 28 January 2020, accepted 14 February 2020

Corresponding author Kwang Hyo Jung; +82-51-510-2343, kjung@pusan.ac.kr

© 2020, The Korean Society of Ocean Engineers

This is an open access article distributed under the terms of the creative commons attribution non-commercial license (<http://creativecommons.org/licenses/by-nc/4.0>) which permits unrestricted non-commercial use, distribution, and reproduction in any medium, provided the original work is properly cited.

the method of moment, maximum likelihood estimation, and least-squares method (DNV, 2014). Jeong et al. (2004) conducted extreme value analyses using Weibull, Gumbel, Log-Pearson type-III, and log-normal distributions using the H_s data of approximately 20 years obtained from 67 ocean stations in South Korea. They provided design wave height information in the deep-sea for the return period of 50 years and suggested that Gumbel distribution was the most suitable method. In addition, they provided the extreme highest tide level information for each return period by conducting an extreme value analysis through generalized extreme value, Gumbel, and Weibull distributions using the extreme highest tide level data of 23 tide stations on the coast of South Korea, and they suggested that Gumbel distribution was the most suitable method (Jeong et al., 2008). Ko et al. (2014) developed a numerical wind speed model that numerically implemented typhoons for four locations on the west coast of the Korean Peninsula (Gunsan, Mokpo, Jeju, and Haemosu No. 1) and presented extreme wind speeds for the four locations by applying the Gumbel distribution and estimating parameters through the probability weighted moment method.

EVDs were applied to various metocean data. In the case of wave data, however, H_s and T_p were important design elements for the design of offshore structures. DNVGL (2017) and BV (2015) recommended the use of the inversed first order reliability method (I-FORM), which used the joint distribution of EVDs, to obtain the return values for H_s and T_p .

In this study, the metocean data (wave, wind, and current) of the Barents Sea in the Arctic region were collected. In addition, for the extreme value analysis of the wave data, return values were calculated using I-FORM, which used the joint distribution of the marginal probability distribution for H_s (Gumbel distribution and two- and three-parameter Weibull distributions) and the conditional probability distribution of T_p for the given H_s (log-normal distribution) (DNVGL, 2017; BV, 2015; Choi, 2016). For the wind and current speeds, which are single variables, extreme value analysis was conducted through the Gumbel distribution and two- and three-parameter Weibull distributions. The least-squares method was used for parameter estimation, and the Kolmogorov-Smirnov (K-S) test was applied as the goodness-of-fit test. Through these processes, the return values for H_s , T_p , wind speed, and current speed required for the design of offshore structures to be operated in the Barents Sea were derived.

2. Metocean Data Collection and Analysis

The project site (Fig. 1) is the Barents Sea of water depth 258 m (latitude: 73N and longitude: 44E), where gas fields were distributed around the site (Fig. 2). For the wave (H_s , T_p , and wave direction), wind (wind speed and wind direction), current (current speed and current direction), and an ice floe thickness data, the hindcast datasets of Global Reanalysis of Ocean Waves 2012 (GROW2012) from Oceanweather Inc. were purchased. In the hindcast datasets of GROW2012, wave and wind models provided by the General

Bathymetric Chart of the Oceans and Climate Forecast System Reanalysis were used to estimate the data for waves, wind, current, and ice floe (Oceanweather Inc.).

To conduct the extreme value analysis, the consistency, period, and validity of the collected data must be examined first (Van Os et al., 2011). Compared with the measurement data, the hindcast data have no possibility of missing data and generating outliers owing to typhoons or defects in the measuring equipment and can secure a data period irrespective of the installation time of the measuring equipment. The wave and wind data were recorded at one hour intervals for a decade from January 2007 to December 2016, and the current data were recorded in the water depth direction at one day intervals for two decades from January 1993 to December 2012. The ice floe thickness data during the same period as that of the current data were provided, but it was discovered that no ice existed in the project site.



Fig. 1 Project site in Barents Sea (Wikipedia, 2019)

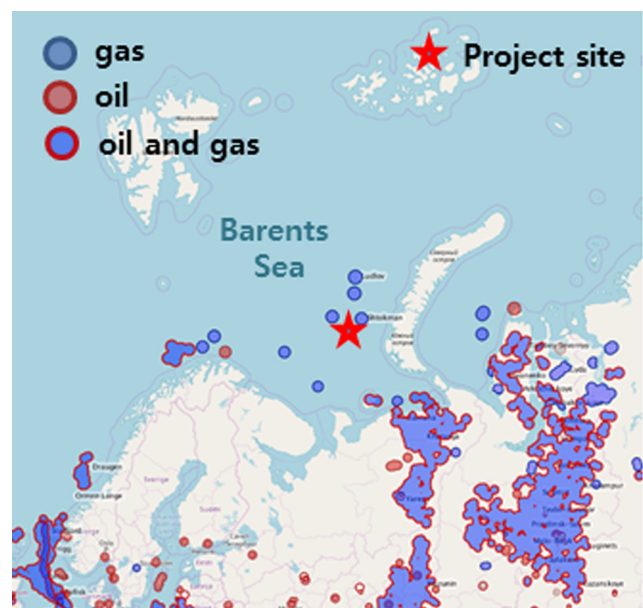


Fig. 2 Oil and gas filed in Barents Sea (WorldMap, n.d.)

Barents Sea		Spectral peak period(s)																								sum	
Significant wave height(m)	Range	0s<Tp<1	1s<Tp<2	2s<Tp<3	3s<Tp<4	4s<Tp<5	5s<Tp<6	6s<Tp<7	7s<Tp<8	8s<Tp<9	9s<Tp<10	10s<Tp<11	11s<Tp<12	12s<Tp<13	13s<Tp<14	14s<Tp<15	15s<Tp<16	16s<Tp<17	17s<Tp<18	18s<Tp<19	19s<Tp<20	20s<Tp<21	21s<Tp<22	22s<Tp<23	23s<Tp<24	24s<Tp<25	sum
	0s<Hs<1	0	0	0	337	2150	3111	874	334	338	561	582	365	211	156	128	43	21	14	13	0	0	0	0	0	0	0
1s<Hs<2	0	0	0	52	1465	7942	10279	5823	1642	1017	1297	1679	1431	1243	1039	479	204	161	51	30	21	13	2	2	0	35872	
2s<Hs<3	0	0	0	0	24	245	3871	8606	4271	1200	672	747	918	723	948	710	243	176	81	53	27	10	1	0	0	23526	
3s<Hs<4	0	0	0	0	0	7	80	1636	4850	2111	555	364	394	331	336	200	78	84	36	10	0	0	0	0	0	11072	
4s<Hs<5	0	0	0	0	0	0	3	25	920	2150	726	165	148	183	158	114	33	39	14	3	0	0	0	0	0	4681	
5s<Hs<6	0	0	0	0	0	0	0	0	6	488	1026	220	104	59	79	64	29	0	0	0	0	0	0	0	0	2075	
6s<Hs<7	0	0	0	0	0	0	0	0	0	12	264	231	67	51	71	16	0	0	0	0	0	0	0	0	0	712	
7s<Hs<8	0	0	0	0	0	0	0	0	0	3	40	119	30	25	26	18	0	0	0	0	0	0	0	0	0	261	
8s<Hs<9	0	0	0	0	0	0	0	0	0	0	0	0	101	39	18	0	2	1	0	0	0	0	0	0	0	161	
9s<Hs<10	0	0	0	0	0	0	0	0	0	0	0	0	14	28	8	1	0	7	0	0	0	0	0	0	0	58	
10s<Hs<11	0	0	0	0	0	0	0	0	0	0	0	0	0	0	8	6	0	2	0	0	0	0	0	0	0	16	
11s<Hs<12	0	0	0	0	0	0	0	0	0	0	0	0	0	0	0	0	0	0	0	0	0	0	0	0	0	0	
sum	0	0	0	389	3639	11305	15107	16424	12027	7542	5162	4005	3370	2805	2792	1646	618	474	195	96	48	23	3	2	0	87672	

Fig. 3 Wave scatter diagram with H_s and T_p

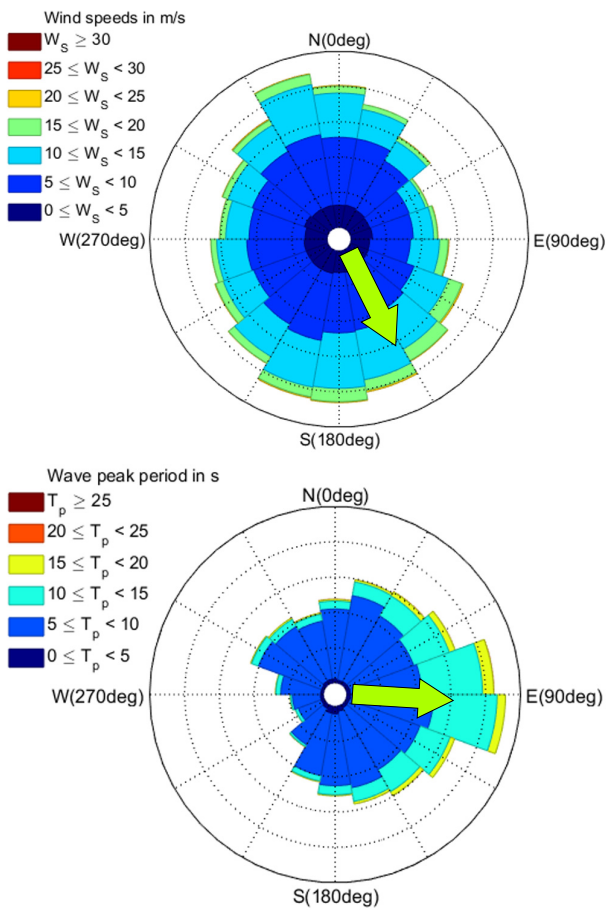


Fig. 4 Wave rose and wind rose

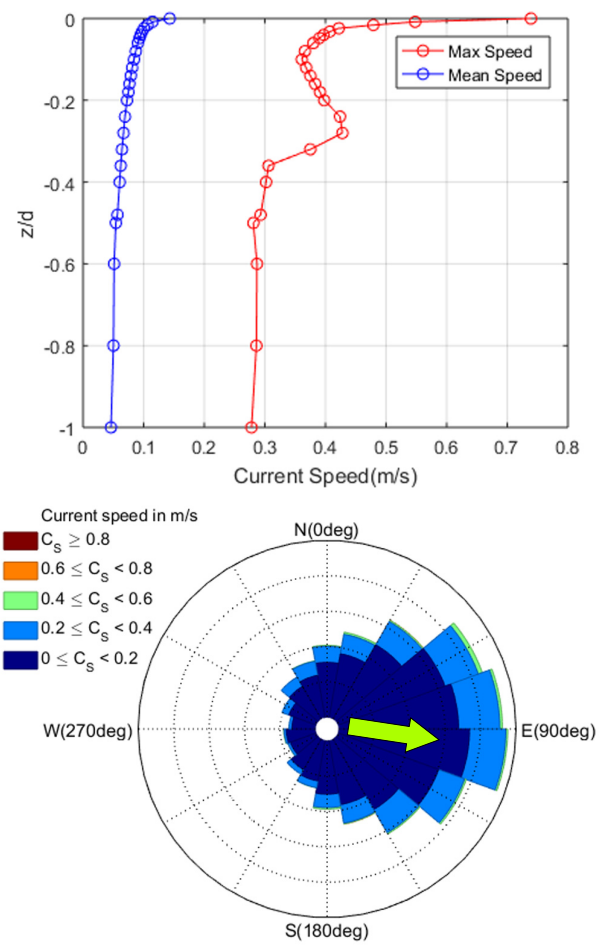


Fig. 5 Current profile and current rose at surface

The wave data showed the wave scatter diagram (WSD) for H_s and T_p ; the wave rose for the wave direction and T_p , and the wind data showed that the wind rose for the wind direction and wind speed (W_s) (Figs. 3 and 4). The current data represented the current increase for the current direction and current speed (C_s) at the surface and the current profile in the water depth direction (Fig. 5).

The WSD showed frequencies at 1 m intervals for H_s and at 1s intervals for T_p , and the total number of data was approximately 87,600. The wave conditions with the highest frequencies in the

project site were 1-2 m for H_s and 6-7 s for T_p . The wave, wind, and current directions could be confirmed through the rose diagrams, and the directions were categorized into east (90°), south (180°), and west (270°) in the clockwise direction from the north direction (0°). In the case of the hindcast data purchased from Oceanweather Inc., the wave and current directions were defined as the directions to which the wave and current were moving, while the wind direction was defined as the direction from which the wind was coming. The wave and wind directions with the highest frequencies were East and North-

Northwest (Fig. 4). Fig. 5 shows the current speed profile and direction in the water depth direction (z). The current speed profile was nondimensionalized with the water depth of the project site (d). The average and maximum current speeds were the fastest at the surface, and the dominant current direction at the surface was from the West to the East.

3. Extreme Value Analysis

For the extreme value analysis of metocean data, data collection, data selection, EVD selection, parameter estimation method selection, goodness-of-fit test, and return value derivation are required (Mathiesen et al., 1994). In this study, a global model that utilizes all of the collected metocean data was selected. In addition, the Gumbel distribution, two- and three-parameter Weibull distributions, and log-normal distribution were used as EVDs. The least-squares method was used to estimate the parameters of the EVDs. As the goodness-of-fit test, the K-S test that uses the maximum distance as a test statistic by comparing the cumulative distribution function (CDF) of metocean data with that of each EVD was used (Jeong et al., 2004; Jeong et al., 2008).

Eqs. (1)-(4) show the CDF of each EVD (Coles, 2001; Goda, 2000).

Gumbel distribution CDF:

$$F(H_s) = \exp\left\{-\exp\left[-\left(\frac{H_s - \gamma}{\alpha}\right)\right]\right\} \quad (1)$$

2-parameter Weibull distribution CDF:

$$F(H_s) = 1 - \exp\left[-\left(\frac{H_s}{\alpha}\right)^\beta\right] \quad (2)$$

3-parameter Weibull distribution CDF:

$$F(H_s) = 1 - \exp\left[-\left(\frac{H_s - \gamma}{\alpha}\right)^\beta\right] \quad (3)$$

H_s is the significant wave height; α , β , and γ are the scale parameter, shape parameter, and location parameter, respectively.

Log-normal distribution CDF:

$$F(T_p|H_s) = \frac{1}{2} \left[1 + \operatorname{erf}\left(\frac{\ln(T_p - \mu)}{\sqrt{2}\sigma}\right) \right] = \Phi\left(\frac{\ln(T_p - \mu)}{\sigma}\right) \quad (4)$$

T_p is the spectral peak wave period, and Φ is the CDF of the standard normal distribution (eq. (5)).

$$\Phi(x) = \frac{1}{\sqrt{2\pi}} \int_{-\infty}^x e^{-t^2} dt \quad (5)$$

μ of the log-normal distribution can be expressed with the average value of $\ln(T_p)$, as shown in Eq. (6); σ can be expressed with the standard deviation of $\ln(T_p)$, as shown in Eq. (7) (DNV, 2014).

$$\mu = E[\ln T_p] = a_0 + a_1 H_s^{a_2} \quad (6)$$

$$\sigma = \operatorname{std}[\ln T_p] = b_0 + b_1 e^{b_2 H_s} \quad (7)$$

To estimate the parameters and coefficients (a_0 , a_1 , a_2 , b_0 , b_1 and b_2) using the least-squares method, taking the log of both sides of each EVD, the log-normal distribution average equation, and the standard deviation equation followed by summarizing them into linear equations result in Eqs. (8)-(12).

Gumbel distribution:

$$-\ln[-\ln(F(H_s))] = \frac{1}{\alpha}(H_s - \gamma) \quad (8)$$

2-parameter Weibull distribution:

$$\ln[-\ln(F(H_s))] = \beta \ln(H_s) - \beta \ln \alpha \quad (9)$$

3-parameter Weibull distribution:

$$\ln[-\ln(F(H_s))] = \beta \ln(H_s - \gamma) - \beta \ln \alpha \quad (10)$$

Log-normal distribution (mean):

$$\ln(\mu - a_0) = \ln(a_1) + a_2 \ln(H_s) \quad (11)$$

Log-normal distribution(standard deviation):

$$\ln(\sigma - b_0) = \ln(b_1) + b_2 H_s \quad (12)$$

For Eqs. (8) and (9), the least-squares method can be used directly. For Eq. (10), however, the parameters for which the R^2 value was closest to 1 were estimated, while the value of γ was changed approximately 1,000 times within the range in which the value in the log was not negative. The R^2 value is the coefficient of determination that indicates the goodness-of-fit corresponding to the regression line. It approaches 1 as the samples used in statistical analysis exhibits smaller errors with the regression line.

Once the parameters are obtained through the least-squares method, the return values can be obtained using Eqs. (13)-(16).

Gumbel distribution:

$$H_s = -\alpha \ln[-\ln(F(H_s))] + \gamma \quad (13)$$

2-parameter Weibull distribution:

$$H_s = \alpha [-\ln(1 - F(H_s))]^{\frac{1}{\beta}} \quad (14)$$

3-parameter Weibull distribution:

$$H_s = \alpha [-\ln(1 - F(H_s))]^{\frac{1}{\beta}} + \gamma \quad (15)$$

Log-normal distribution CDF:

$$T_p = \exp\left[\sigma \Phi^{-1}\left(F_{T_p|H_s}(T_p)\right)\right] + \mu \quad (16)$$

After changing the variable from H_s to wind speed and current speed, their return values were derived using the same method as presented above.

3.1 Extreme value analysis on wave and results

H_s and T_p , which are wave data, can be expressed by the conditional modeling approach, and the joint probability distribution of the two variables can be expressed as the product of the marginal probability distribution of H_s and the conditional probability distribution of T_p for a given H_s (Orimolade et al., 2016; DNVGL, 2017).

In this study, the marginal probability distribution of H_s was assumed to be a Gumbel distribution and two- and three-parameter Weibull distributions using the WSD and the conditional probability distribution of T_p , as the given H_s was assumed to be a log-normal distribution to calculate return values using the I-FORM method. Extreme value analysis was conducted after transforming the EVDs from the probability distribution function form to the CDF form for the convenience of calculation. The I-FORM method was proposed by Winterstein et al. (1993), and the data of Haver and Nyhus (1986) were used for the parameter estimation equations of the EVDs used. In other words, the I-FORM method calculates the exceedance probability in advance and obtains the corresponding response rapidly.

The procedure of the I-FORM method is expressed in Eqs. (17)-(24) (Haver and Winterstein, 2009).

$$Q = 1 - F(H_s, T_p) = 1/N \quad (17)$$

Q is the exceedance probability. It is the reciprocal number of N , which is the total number of data.

$$F(H_s, T_p) = \int f(H_s, T_p) dH_s dT_p = F(H_s)F(T_p|H_s) \quad (18)$$

where $F(H_s)$ is the CDF of the marginal probability distribution, and $F(T_p|H_s)$ is the CDF of the conditional probability distribution

EVDs are moved to the space of the standard normal distributions of u_1 and u_2 .

$$\Phi(u_1) = F_{H_s}(H_s), \quad \Phi(u_2) = F_{T_p|H_s}(T_p) \quad (19)$$

A circle equation with a radius of B was introduced and represented by the relationship between the short-term period (T_{ss}) an return period (T_r).

$$\sqrt{u_1^2 + u_2^2} = B = \Phi^{-1}\left(1 - \frac{T_{ss}}{365 \times 24 \times T_r}\right) = \Phi^{-1}\left(1 - \frac{1}{N}\right) \quad (20)$$

where B is the reliability index. One hour was used for T_{ss} , T_r is the return period; 1, 10, and 100 years were used.

$$u_{1i} = Bs_i, \quad u_{2i} = \pm \sqrt{B^2 - u_{1i}^2} \quad (21)$$

s_i in Eq. (21) is a dummy index, i.e., a number in the section between -1.0 and 1.0 . Once B is determined H_s and T_p can be obtained using the inverse function of each EVD (Eqs. (22)-(24)).

$$H_{s_i} = F_{H_s}^{-1}(\Phi(u_{1i})) \quad (22)$$

$$\mu_i = a_0 + a_1 H_{s_i}^{a_2}, \quad \sigma_i = b_0 + b_1 e^{b_2 H_{s_i}} \quad (23)$$

$$T_{p_i}^{\pm} = F_{T_p|H_s}^{-1}(\Phi(\pm u_{2i})) \quad (24)$$

The parameters of each EVD were estimated using the least-squares method, and the goodness-of-fit was tested using the K-S test. The parameters for which the R^2 value was the highest were extracted using MATLAB software (Figs. 6-7). The R^2 value was 0.99, indicating that the numerical values agreed well with the actual values. The parameters were obtained using the slopes and y-intercept values (Tables 1-2).

To test the estimated parameters, the maximum distance difference between the CDF of the wave data and the CDF that included the parameters obtained by the least-squares method is shown in Fig. 8. Based on the result of the K-S test, a test statistic (D) value is presented. If this value is smaller than the threshold (D_{cri}) of 0.118 by the number of wave data at the significance level of 5%, then the null

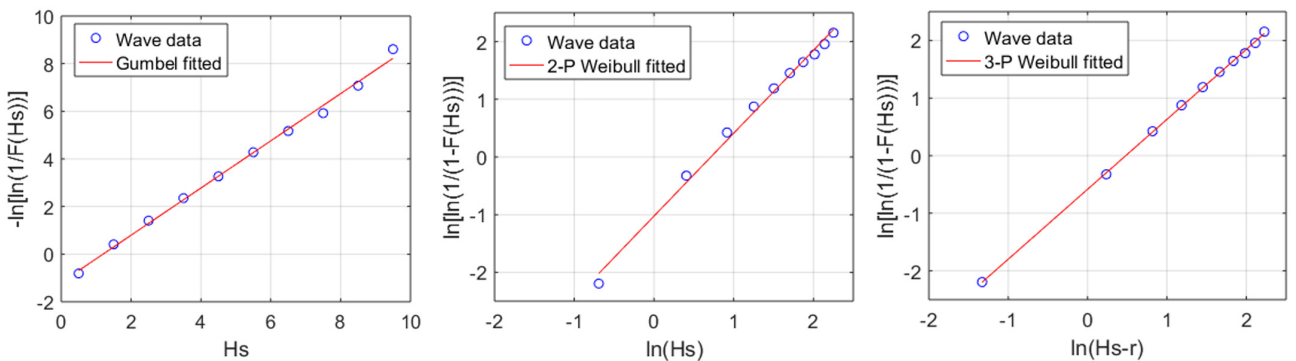


Fig. 6 Parameter estimation of extreme value distributions using least-squares method for significant wave height

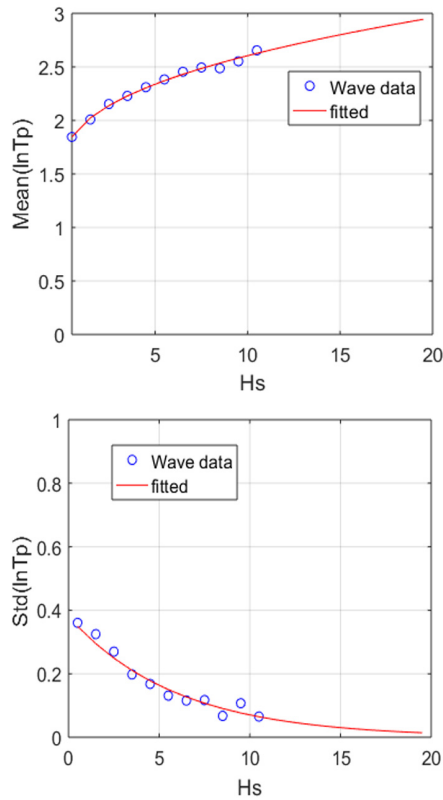


Fig. 7 Parameter estimation of log-normal distribution using least-squares method for spectral peak wave period

Table 1 Parameters of extreme value distributions for significant wave height

Parameter	Gumbel distribution	2-parameter Weibull distribution	3-parameter Weibull distribution
α (Scale)	1.009	2.014	1.616
β (Shape)	-	1.437	1.214
γ (Location)	1.198	0	0.235
R^2	0.996	0.994	0.999

Table 2 Parameters of log-normal distribution

Parameter (a)	Log-normal distribution	Parameter (b)	Log-normal distribution
a_0	1.533	b_0	0
a_1	0.415	b_1	0.380
a_2	0.412	b_2	-0.169
R^2	0.995	R^2	0.923

hypothesis that no difference exists between the two CDFs mentioned above can not be rejected (Kanji, 2006). In other words, it was discovered that the graphs of CDFs, including the parameters, agreed well with the actual data.

The contours for H_s and T_p were expressed using the I-FORM

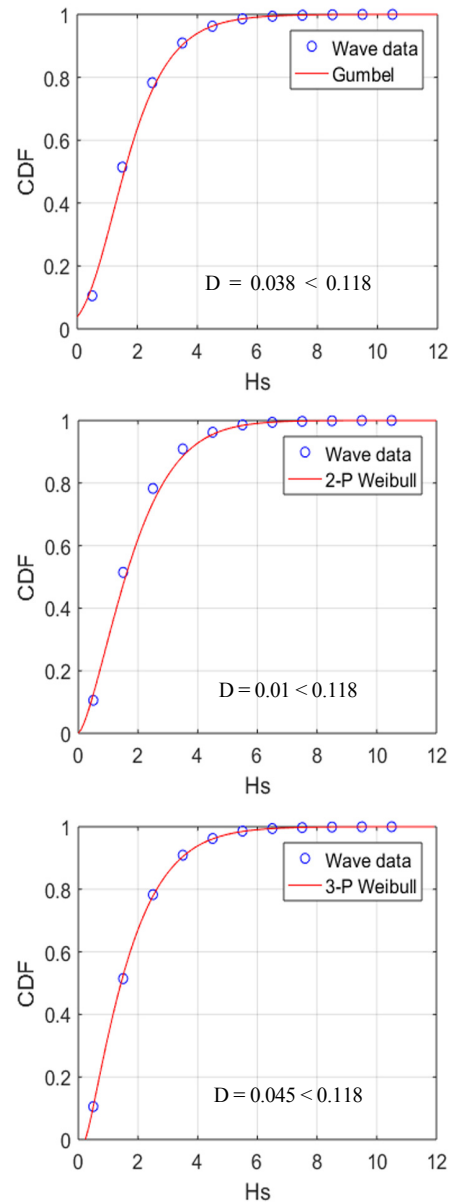


Fig. 8 Comparison between CDF of wave data and CDF of extreme value distribution

method of Eqs. (17)-(24), as shown in Fig. 9. The contours are shown for each return period (RP), and the return values corresponding to each return period are shown in Table 3.

When the 10-year hindcast data were compared with the 10-year return values, the highest prediction values could be obtained when the Gumbel distribution was assumed as the marginal probability distribution. The next highest values were derived by the three-parameter Weibull distribution, and two-parameter Weibull distribution exhibited the most similar results to those of the collected data. This was because the Gumbel distribution had a higher degree of scatter than the Weibull distribution. In addition, when the equations for obtaining the return values of the two- and three-parameter Weibull distributions were compared, it was discovered that different results were obtained depending on the value of the location parameter.

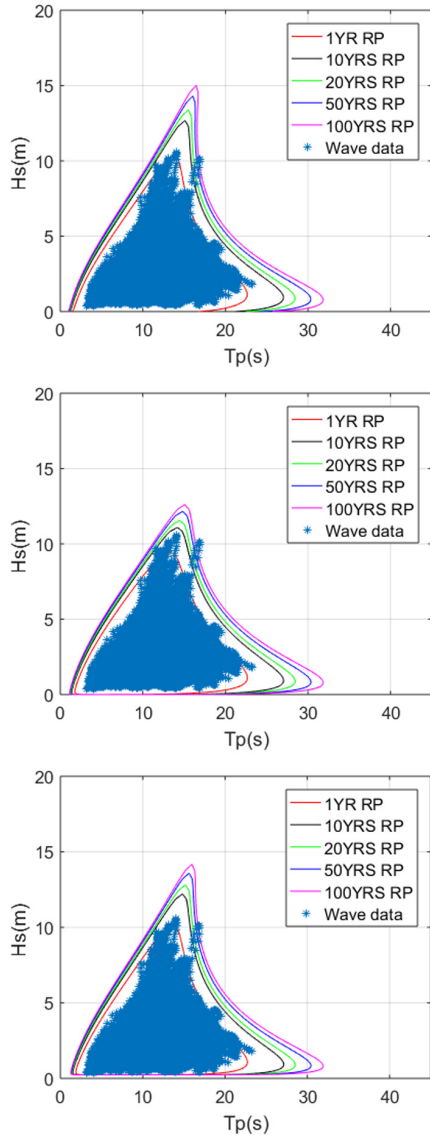


Fig. 9 Environmental contour for significant wave height and spectral peak wave period

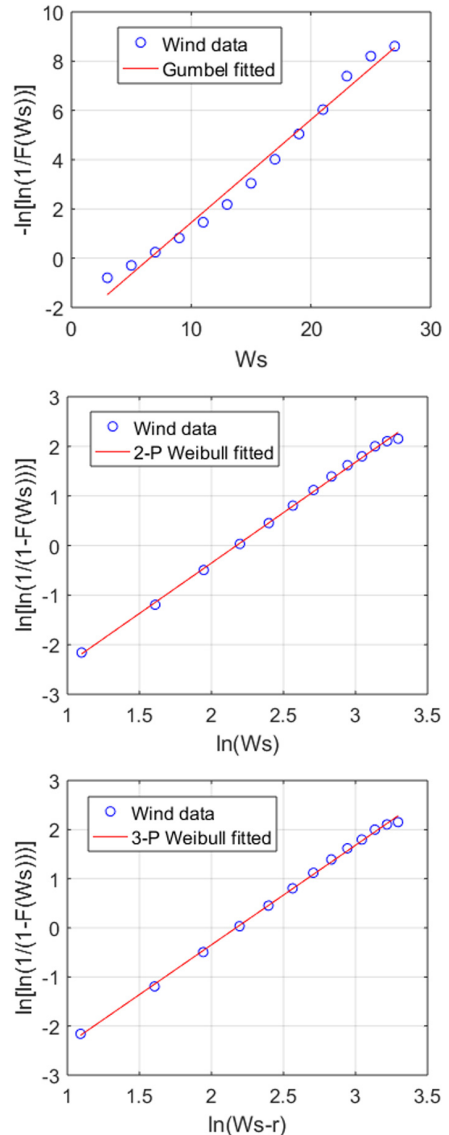


Fig. 10 Parameter estimation of extreme value distributions using least square method for wind speed

Table 3 Return value for wave (H_s , T_p)

Return period (yr, yrs)	Gumbel distribution		2-parameter Weibull distribution		3-parameter Weibull distribution	
	H_s (m)	T_p (s)	H_s (m)	T_p (s)	H_s (m)	T_p (s)
1	10.36	13.75	9.48	13.22	10.17	13.64
10	12.68	15.11	11.09	14.18	12.21	14.83
20	13.38	15.52	11.56	14.45	12.80	15.18
50	14.31	16.05	12.16	14.81	13.59	15.63
100	15.01	16.45	12.61	15.07	14.17	15.97

Table 4 Parameters of extreme value distribution for wind speed

Parameter	Gumbel distribution	2-parameter Weibull distribution	3-parameter Weibull distribution
α	2.392	8.790	8.763
β	-	2.033	2.028
γ	6.543	0	0.022
R^2	0.987	0.999	0.999

3.2 Extreme value analysis on wind and current and results

The wind speed (W_s) was distributed within the 0-27 m/s range and the total number of data was approximately 87,600. The CDF was obtained at 2 m/s intervals. The current speed (C_s) ranged from

0 to 70 cm/s and the total number of data was 7,200. The CDF was obtained at 5 cm/s intervals. To derive the return values for the W_s and C_s , which were single variables, the Gumbel distribution and two- and three-parameter Weibull distributions were used as EVDs, and the least-squares method was used for parameter estimation (Figs. 10 and 12). The parameters were obtained using the slopes and y-intercept values when the R^2 value was the highest (Tables 4 and 6). The K-S

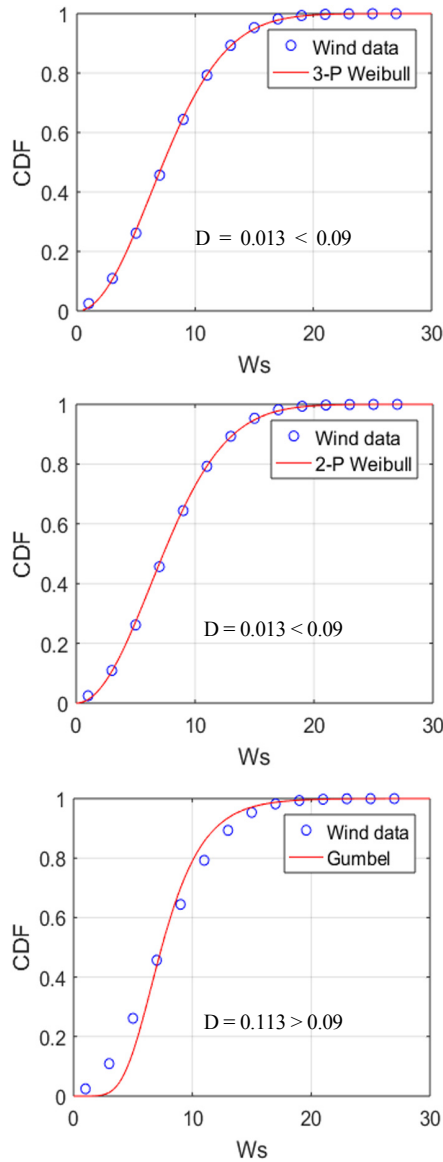


Fig. 11 Comparison between CDF of wind data and CDF of extreme value distributions

Table 5 Return value for wind speed

Return period (yr, yrs)	Gumbel distribution	2-parameter Weibull distribution	3-parameter Weibull distribution
	Wind speed (W_s) (m/s)		
1	28.26	26.01	26.03
10	33.77	29.07	29.10
20	35.43	29.93	29.96
50	37.62	31.03	31.06
100	39.28	31.83	31.86

test was used to test the parameters, and test statistic (D) values are presented as results (Figs. 11 and 13). If these values are smaller than the threshold (D_{cri}) of 0.09 by the number of wind and current data at

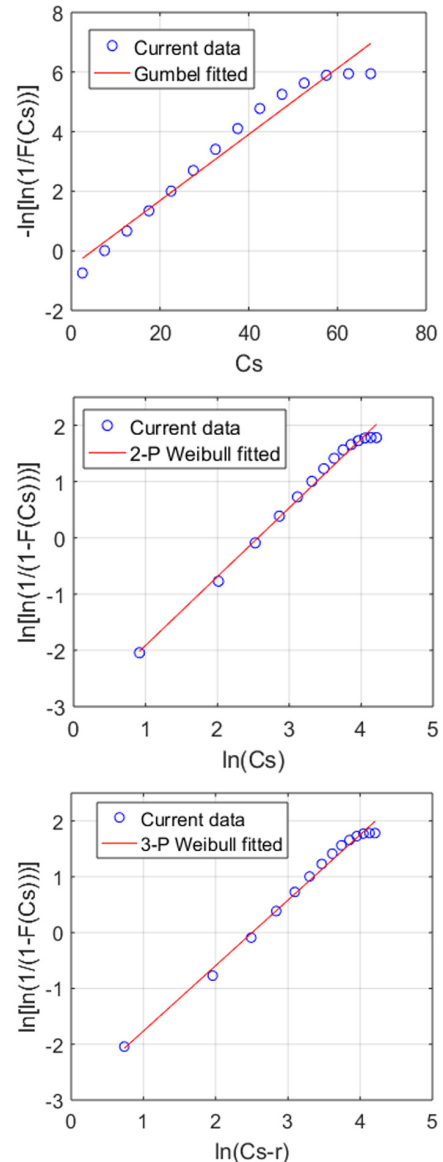


Fig. 12 Parameter estimation of extreme value distributions using least square method for current speed at surface

Table 6 Parameters of extreme value distribution for current speed at surface

Parameter	Gumbel distribution	2-parameter Weibull distribution	3-parameter Weibull distribution
α	9.010	12.986	12.235
β	-	1.224	1.173
γ	4.800	0	0.414
R^2	0.963	0.992	0.992

the significance level of 5%, then the null hypothesis cannot be rejected. In other words, it was discovered that the graphs of the CDFs, including the parameters, agreed well with the actual data. The return values for the W_s and C_s were calculated using a method similar to the analysis of the wave data (Tables 5 and 7).

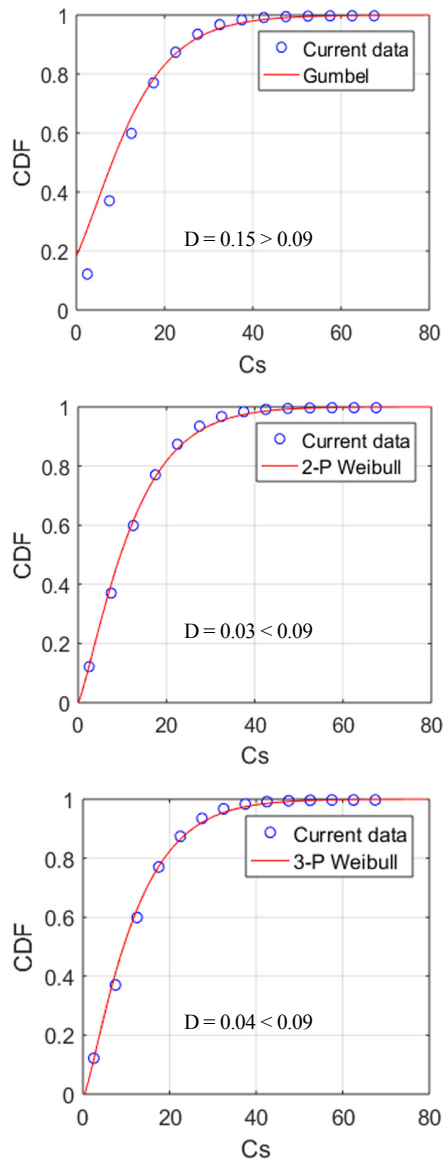


Fig. 13 Comparison between CDF of current data at surface and CDF of extreme value distributions

Table 7 Return value for current speed at surface

Return period (yr, yrs)	Gumbel distribution	2-parameter Weibull distribution	3-parameter Weibull distribution
	Current speed (C_s) (cm/s)		
1	57.95	55.38	56.01
10	78.70	72.49	74.05
20	84.95	77.46	79.32
50	93.20	83.92	86.20
100	99.45	88.73	91.35

As for the overall tendency of the return values for the W_s and C_s , the Gumbel distribution exhibited the highest prediction values, similarly to the results of the wave data, followed by the three- and

two-parameter Weibull distributions. When the maximum W_s and C_s of the 10-year hindcast data (27 m/s and 70 cm/s, respectively) were compared with the 10-year return values of the two-parameter Weibull distribution (29.07 m/s and 72.49 cm/s, respectively) large differences of 7.6% and 3.5% were discovered, respectively.

The prediction values of the Gumbel distribution were the highest because the null hypothesis was rejected as the test statistic was higher than the threshold in the K-S test results; hence, overestimated results were obtained. This was because the intervals determined to calculate the ranges and frequencies of the W_s and C_s were larger compared to the wave data; hence, errors were accumulated when the parameters were calculated using the least-squares method. The reclassification of data through the independent and identically distributed (IID) verification of changes in the intervals for extracting the frequencies of the W_s and C_s is expected to further improve the accuracy (Choi et al., 2019).

4. Conclusion

In this study, an extreme value analysis for the H_s , T_p , wind speed, and current speed was conducted using the hindcast metocean data of the Barents Sea in the Arctic region to derive return values required for the design of offshore structures. In the extreme value analysis for the H_s and T_p , the marginal probability distribution of the H_s was assumed to be a Gumbel distribution and two- and three-parameter Weibull distributions, and the conditional probability distribution of the T_p for the given H_s was assumed to be a log-normal distribution to calculate return values using the I-FORM method. For the W_s and C_s , which were single variables, return values were calculated through the Gumbel distribution and two- and three-parameter Weibull distributions. The parameters were estimated using the least-squares method and tested through the K-S test.

The return values for the H_s , T_p , and wind speed for the 100-year return period and those for current speed for the 10-year return period, which are required for the design of general offshore structures were summarized (as shown in Table 8). As the degree of scatter of metocean data increased, the differences in return values between the Gumbel and Weibull distributions increased. The Weibull distribution should be used for widely distributed metocean data, such as wind speed and current speed data.

The results of this study can be used as the metocean data design values of offshore structures to be installed in the Barents Sea;

Table 8 Extreme value for metocean data with

Metocean data	Return period	Return value
Wave	H_s (m)	12.61 ~ 15.01
	T_p (s)	15.07 ~ 16.45
Wind speed (m/s)	100 (yrs)	31.83 ~ 39.28
Current speed at surface (cm/s)	10 (yrs)	72.49 ~ 78.70

furthermore, they can be utilized as basic data for offshore structure motion and mooring analyses, structural analyses, and air gap calculations. In the future, the method of estimating parameters will be extended from the least-squares method to the moment area and maximum likelihood methods. In addition, in the case of widely distributed metocean data, such as W_s and C_s data, they will be reclassified through an IID verification to select appropriate intervals.

Acknowledgement

This work was supported by the Technology Innovation Programs of “Development of Arctic Ocean-Based Floating Offshore Structure Geometry Capable of Year-Round Operation Under ARC7 Condition by Applying Position Maintenance and Mooring Systems (Project No.: 10063405),” “Construction of Equipment for Assessing the Performance of Hydrogen Fuel Cell ESS Systems for MW-Class Vessels and Test Method Development (Project No.: 20006636),” and the “South Korea-U.K. Offshore Plant Global Professional Training Program (Project No.: 0001288),” which were funded by the Ministry of Trade, Industry, and Energy of the Republic of Korea.

References

- API (American Petroleum Institute). (2005). Design and Analysis of Station keeping Systems for Floating Structures. API RP-2SK 3rd Edition.
- Bird, K.J., Charpentier, R.R., Gautier, D.L., Houseknecht, D.W., Klett, T.R., Pitman, J.K., ... Wandrey, C.R. (2008). Circum-Arctic Resource Appraisal: Estimates of Undiscovered Oil and Gas North of the Arctic Circle (No. 2008-3049). US Geological Survey. <https://doi.org/10.3133/fs20083049>
- BV (Bureau Veritas). (2015). Classification of Mooring Systems for Permanent and Mobile Offshore Units. BV Rule Note NR 493 DT R03 E.
- Choi, Y.H. (2016). Extreme Value Analysis of Environmental Data. Proceedings of the Fall Conference of the Korean Society of Ocean Engineers, Busan, Korea, 181-186.
- Choi, Y.H., Yeon, S.M., Kim, H., & Lee, D. (2019). Extreme Value Analysis of Statistically Independent Stochastic Variables. Journal of Ocean Engineering and Technology, 33(3), 222-228. <https://doi.org/10.26748/KSOE.2018.093>
- Coles, S. (2001). An Introduction to Statistical Modeling of Extreme Values. Springer Texts in Statistics, London: Springer. <https://doi.org/10.1007/978-1-4471-3675-0>
- DNVGL. (2017). Environmental Conditions and Environmental Loads. DNV-RP-C205.
- DNVGL (Det Norske Veritas and Germanischer Lloyd). (2015). Position Mooring. DNV-OS-E301.
- DNV (Det Norske Veritas). (2014). Environmental Conditions and Environmental Loads. DNV-RP-C205.
- Goda, Y. (2000). Random Seas and Design of Maritime Structures (2nd ed.). Singapore: World Scientific Publishing Company.
- Haver, S., & Nyhus, K.A. (1986). A Wave Climate Description for Long Term Response Calculations. Proceedings of 5th International OMAE Symposium, Tokyo, 4, 27-34.
- Haver, S., & Winterstein, S.R. (2009). Environmental Contour Lines: A Method for Estimating Long Term Extremes by a Short Term Analysis. Transactions of the Society of Naval Architects and Marine Engineers, 116, 116-127.
- Jeong, S.T., Kim, J.D., Ko, D.H., & Yoon, G.L. (2008). Parameter Estimation and Analysis of Extreme Highest Tide Level in Marginal Seas around Korea. Journal of Korean Society of Coastal and Ocean Engineers, 20(5), 482-490.
- Jeong, S.T., Kim, J.D., & Cho, H.Y. (2004). Characteristics on the Extreme Value Distributions of Deepwater Design Wave Heights off the Korean Coast. Journal of Korean Society of Coastal and Ocean Engineers, 16(3), 130-141.
- Kanji, G.K. (2006). 100 Statistical Tests. SAGE.
- Ko, D.H., Jeong, S.T., Cho, H.Y., & Kang, K.S. (2014). Extreme Offshore Wind Estimation using Typhoon Simulation. Journal of Korean Society of Coastal and Ocean Engineers, 26(1), 16-24. <https://doi.org/10.9765/KSCOE.2014.26.1.16>
- Mathiesen, M., Goda, Y., Hawkes, P.J., Mansard, E., Martín, M.J., Peltier, E., ... Van Vledder, G. (1994). Recommended Practice for Extreme Wave Analysis. Journal of hydraulic Research, 32(6), 803-814. <https://doi.org/10.1080/002216894.09498691>
- National Oceanic and Atmospheric Administration (NOAA). (2018). Arctic Report Card 2018.
- Orimolade, A.P., Haver, S., & Gudmestad, O.T. (2016). Estimation of Extreme Significant Wave Heights and the Associated Uncertainties: A Case Study using NORA10 Hindcast Data for the Barents Sea. Marine Structures, 49, 1-17. <https://doi.org/10.1016/j.marstruc.2016.05.004>
- Van Os, J., Caires, S., & Van Gent, M. (2011). Guidelines for Metocean Data Analysis. Proceedings of the 21st International Offshore and Polar Engineering Conference, International Society of Offshore and Polar Engineers.
- Winterstein, S.R., Ude, T.C., Cornell, C.A., Bjerager, P., & Haver, S. (1993). Environmental Parameters for Extreme Response: Inverse FORM with Omission Factors. Proceedings of the 6th International Conference on Structural Safety and Reliability (ICOSSAR-93), Innsbruck, Austria, 551-557.
- Wikipedia. (2019). Barents Sea. Retrieved August 2019 from https://en.wikipedia.org/wiki/Barents_Sea
- WorldMap. (n.d.). Oil & Gas Map. Retrieved August 2019 from <https://worldmap.harvard.edu/maps/6718>

Author ORCIDs and Contributions

Author name	ORCID	Contributions
Park, Sung Boo	0000-0001-9587-2183	①②③④
Shin, Seong Yun	0000-0001-6665-9092	③
Shin, Da Gyun	0000-0002-3976-1961	②
Jung, Kwang Hyo	0000-0002-8229-6655	⑤
Choi, Yong Ho	0000-0002-6653-5476	③
Lee, Jae Yong	0000-0002-4469-7765	②
Lee, Seung Jae	0000-0001-8992-6915	②

- ① Conceived of the presented idea or developed the theory
- ② Carried out the experiment or collected the data
- ③ Performed the analytic calculations or numerical simulations
- ④ Wrote the manuscript
- ⑤ Supervised the findings of this study

Estimation of Buckling and Ultimate Collapse Behaviour of Stiffened Curved Plates under Compressive Load

Joo-Shin Park¹, Yeon-Chul Ha² and Jung-Kwan Seo³

¹Pro., Ship and Offshore Research Institute, Samsung Heavy Industry Co. Ltd., Geoje, Korea

²Associate Professor, The Korea Ship and Offshore Research Institute, Pusan National University, Busan, Korea

³Professor, The Korea Ship and Offshore Research Institute, Pusan National University, Busan, Korea

KEY WORDS: Stiffened curved plate, Buckling, Ultimate collapse mode, Compressive load, Curvature

ABSTRACT: Unstiffened and stiffened cylindrically curved plates are often used in ship structures. For example, they can be found on a deck with a camber, a side shell at the fore and aft parts, and the circular bilge part of a ship structure. It is believed that such cylindrically curved plates can be fundamentally modelled using a portion of a circular cylinder. From estimations using cylindrically curved plate models, it is known that the curvature generally increases the buckling strength compared to a flat plate under axial compression. The existence of curvature is also expected to increase both the ultimate and buckling strengths. In the present study, a series of finite element analyses were conducted on stiffened curved plates with several varying parameters such as the curvature, panel slenderness ratio, and web height and type of stiffener applied. The results of numerical calculations on stiffened and unstiffened curved plates were examined to clarify the influences of such parameters on the characteristics of their buckling/plastic collapse behavior and strength under an axial compression.

1. Introduction

Cylindrically curved structural plates are widely used as element members of various structural systems such as oil and gas storages for ships and offshore structures, cooling towers, and hull shell plating structures. Ship structures typically have welded plates, and design methods related to the use of flat plates as longitudinal and transverse strength members have been remarkably developed, many of which have become well established (Paik, 2018). However, as compared with a flat plate, as shown in Fig. 1, a curved plate has limited use as a structural member in deck plating cambers, side shell plating, fore and aft parts, and circular bilge parts, or for buckling strength evaluations, and is designed by taking into account only the curvature effect for a simple flat plate (Park and Seo, 2019).

Therefore, to apply a curved plate, a structural design reflecting the lightweight and high-speed characteristics of a ship structure will require a clear understanding of the precise non-linear material and geometric structural behaviors under various load conditions. In terms of the structural strength, a hull should maintain sufficient strength under longitudinal bending moments caused by its self-loading, weight, and external force distribution. In this case, the most important aspect is the compressive strength of the stiffened plates on the deck and at the bottom

of the ship. In particular, it is essential to examine the ultimate compressive strength in terms of the safety of the hull girder structure. The buckling and plasticity of a stiffened plate structure with an increasing in-plane compressive load, along with a complex nonlinear behavior occurring until the ultimate strength is reached, need to be investigated. Previous studies related to this issue were reviewed for a typical stiffened curved plate applied in a bilge structure.



Fig. 1 Cylindrically local curved plate and stiffened curved

Received 9 December 2019, revised 27 December 2019, accepted 14 February 2020

Corresponding author Jung-Kwan Seo: +82-51-510-2415, seojk@pusan.ac.kr

© 2020, The Korean Society of Ocean Engineers

This is an open access article distributed under the terms of the creative commons attribution non-commercial license (<http://creativecommons.org/licenses/by-nc/4.0>) which permits unrestricted non-commercial use, distribution, and reproduction in any medium, provided the original work is properly cited.

A study on the buckling and plastic collapse using a nonlinear numerical analysis of the development of an ultimate strength prediction equation for unstiffened curved plates used in ships was conducted, and the ultimate strength for the buckling mode and the initial deflection effect through an eigenvalue analysis for a change in curvature during elastic buckling under a compressive load was also investigated (Park et al., 2008; Kim et al., 2014). In addition, empirical equations on the aspect ratio and curvature effects have been proposed for various combined loads such as transverse compressive, shear, and longitudinal compressive loads (Kwen et al., 2004).

For stiffened curved plates, an analysis of the stiffener and curvature effect of container ships using a commercial finite element analysis (Oh et al., 2011), an empirical equation (Seo et al., 2016), an ultimate strength behavior analysis for compressive and hydrostatic loads with the initial deflection, and the residual stress based on a numerical analysis was conducted (Park et al., 2005). Cho et al. (2007) analyzed the curvature effect on the compressive load through an ultimate strength test and a numerical analysis for six stiffened curved plates.

Most recently, the quantitative curvature factor based on the curvature of stiffened curved plates was developed through an extensive numerical analysis on the curvature, slenderness ratio, aspect ratio, web height, and initial deflection effects of stiffeners for stiffened curved plates used on container ships (Park and Seo, 2019). Studies on the collapse behavior characteristics of curved plate members related to container ships on a large-scale have recently been conducted.

However, previous studies on the quantification and analysis of collapse mode patterns of stiffened curved plates have been limited. In the case of a flat stiffened plate structure, the characteristics of each of the six collapse modes have been clearly distinguished both theoretically and analytically, through which, the minimum value of the collapse modes has been identified as the ultimate strength (Paik, 2018). By contrast, in the case of stiffened curved plates, previous studies were mainly carried out through a numerical analysis of the buckling and ultimate strength according to the curvature and stiffener.

Therefore, in this study, for a clear identification of the collapse pattern of the stiffened curved plates, buckling and elasto-plastic collapse behaviors according to the change in the type of stiffener (flat bar, angle bar, tee bar), curvature (flank angle, θ), and panel slenderness ratio (slenderness ratio, β) used in a ship were analyzed in detail to quantitatively analyze the collapse mode.

2. Numerical Analysis of Stiffened Curved Plate

2.1 Analysis Model Selection

To characterize the collapse mode of the curved plate for the curved plates used in a ship bilge and for various ship types, in this study, a container ship designed with the largest bilge curvature was selected and the analysis model shown in Fig. 2 was applied.

The selected stiffened curved plate has a continuous stiffened plate structure and consists of various types of surrounding members

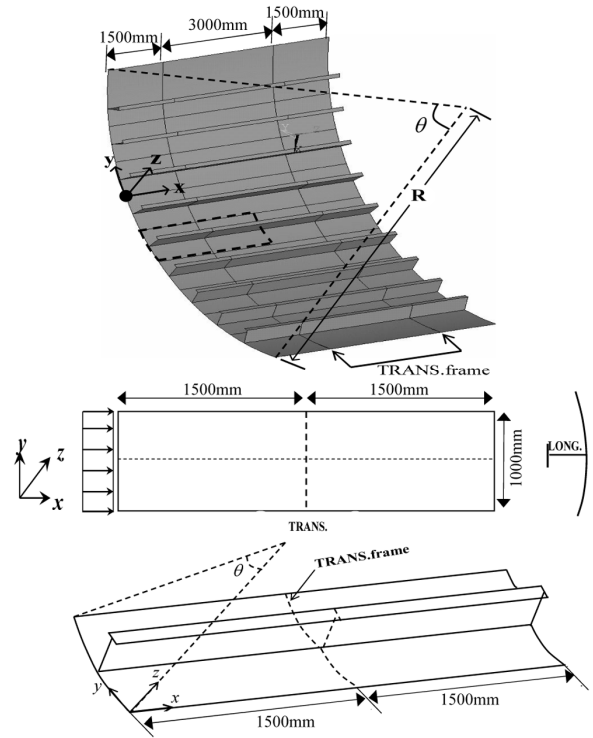


Fig. 2 Double span/double bay model of stiffened curved plate

(stiffeners, large girder) around the stiffened curved plate. The boundary condition for a numerical analysis is assumed to be simply supported, and the boundary condition in which the loading edge and the non-loading edge are kept straight in the in-plane direction while the stiffened curved plate is buckled by a compressive load is applied. In addition, for the large girder effect, a one-bay (1/2 + 1/2 bay) finite element analysis model was selected by implementing symmetrical conditions at both ends.

Three shapes, as discussed above, were examined (Fig. 3). The stiffener web height (h_w) ranged from 50 to 400 mm, and the web (t_w) and flange (t_f) thicknesses were fixed at 12 and 15 mm, respectively, and the collapse characteristics for the web height of the stiffener were examined. The plate thickness (t_p) of the curved plate was determined as a variable of between 12 to 26 mm, and the collapse characteristics

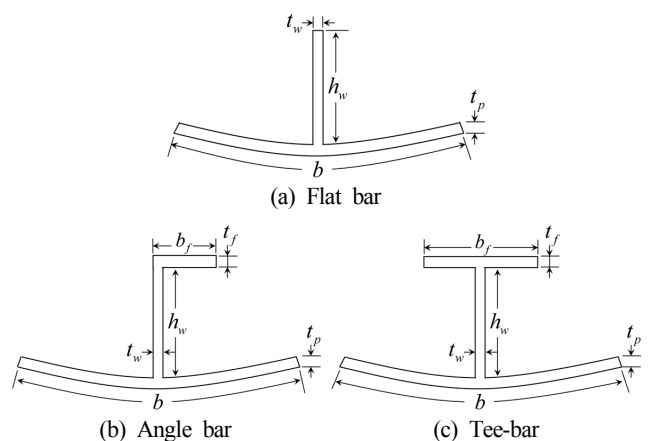


Fig. 3 Typical shapes of curved plate and stiffener

Table 1 Number of elements in circumferential/radial direction

Part	Number of elements
Plate	10
Stiffener web	6
Stiffener flange	4

Table 2 Material properties for stiffened curved plate

Material	High tensile steel
Elastic modulus (E)	205.8 GPa
Poisson ratio (ν)	0.3
Yield stress (σ_Y)	352.8 MPa

of the slenderness ratio of the plate were examined. The width (b) and length (a) of the curved plate were fixed at 1,000 and 3,000 mm, respectively, and the flank angle corresponding to the curvature was varied from 5° to 45° .

The finite element model of the plate consists of ten elements with a finite element longitudinal aspect ratio of 1.0 (a/b) in the circumferential direction. The web height and flange width of the stiffener used to describe the local buckling phenomenon are 6 and 4, respectively (Table 1).

A nonlinear analysis was conducted by considering the material and geometric nonlinearities. In an analysis of a large deflection, which is a geometric nonlinearity, the arc-length method for describing the secondary buckling phenomena is used. For the nonlinearity of the material, a perfect plastic model was assumed, and a bilinear isotropic hardening model was considered. The material properties are as shown in Table 2.

2.2 Initial imperfection

A fillet welding is commonly used to fabricate stiffened curved plates used in ship and offshore structures. Consequently, a residual stress and an initial deflection are inevitably generated from the welding. In particular, an initial deflection is known to be a major cause of a geometrically nonlinear behavior.

In an existing flat stiffened plate, Eq. (1), which is a deflection equation of a plate, and Eq. (2) applied for a stiffener, are assumed for application to a buckling mode shape.

However, the deflection equation for the curvature of a curved plate differs from that of a flat plate. Therefore, the eigenvalue characteristics need to be examined, and in this regard, the initial deflection shape is applied through a mode analysis using an eigenvalue analysis.

$$w_{opl} = \sum_m \sum_n A_{omn} \sin \frac{m\pi x}{a} \sin \frac{n\pi y}{b} \quad (1)$$

$$w_{os} = 0.00025a \sin \frac{\pi x}{a} \quad (2)$$

The size of the initial deflection comes from the welding, as shown

in Eqs. (3) and (4), using the size of the initial deflection proposed by Smith (1988), when applying a flat stiffened plate and stiffener in the structure.

$$Plate: \frac{w_{opl}}{t} = \begin{cases} 0.025\beta^2 & \text{for slight level} \\ 0.1\beta^2 & \text{for average level} \\ 0.3\beta^2 & \text{for severe level} \end{cases} \quad (3)$$

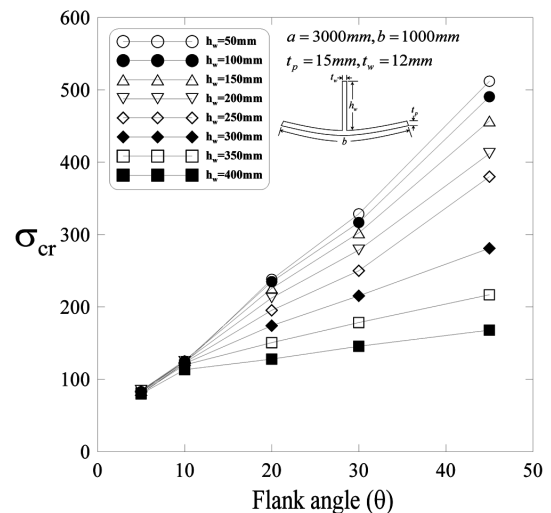
$$Stiffener: \frac{w_{osx}}{a} = \begin{cases} 0.00025 & \text{for slight level} \\ 0.0015 & \text{for average level} \\ 0.0046 & \text{for severe level} \end{cases} \quad (4)$$

Here, w_{opl} represents the initial deflection of the plate, w_{oc} is the deflection of a column-type stiffener, w_{os} is the deflection of a sideways-type stiffener, and m and n represent the buckling half wave number in the x -(length) and y -directions (width). The initial deflection size was applied using the mean value of the stiffened curved plates as a function of the plate slenderness ratio and thickness (ISO, 2007). In this study, the welding residual stress arising from the welding was not considered.

2.3 Eigenvalue Mode

To analyze the buckling mode, an eigenvalue analysis was conducted using the general-purpose finite element analysis program (ANSYS, 2015). The eigenvalue mode can predict the collapse mode through the geometric characteristics and can be used as a numerical deflection equation or analysis of the initial deflection shape according to the geometric characteristics of the stiffened curved plate, as described above.

In the stiffened curved plate model included in most basic flat-bar stiffeners used in ship structures, the elastic buckling strength characteristics according to the curvature are compared, as shown in Fig. 4, based on the change in the web height of the stiffener. As the curvature (flank angle) increases, the buckling strength tends to


Fig. 4 Elastic buckling strength of stiffened curved plates subjected to axial compression (flat-bar stiffener)

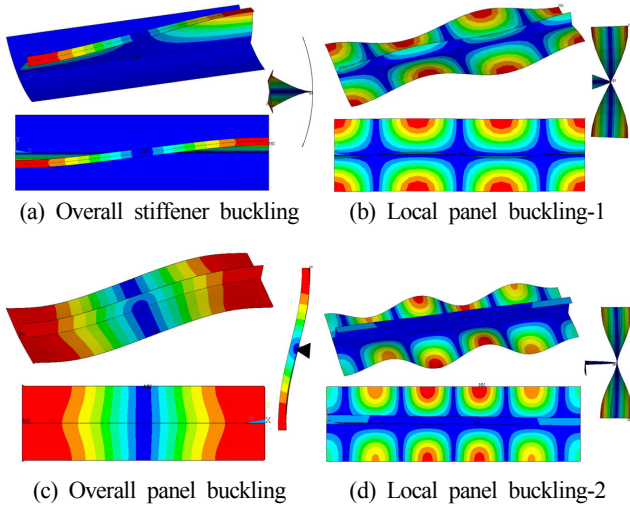


Fig. 5 Typical buckling modes of stiffened curved plates

increase, and when the curvature is lower than 10° at the same elastic buckling strength, it can be seen that the increase in buckling strength with a change in the stiffener height is not large. However, according to the shape characteristics of a flat-bar stiffener, owing to the weak torsional rigidity against a compressive load, the elastic buckling strength is estimated to be lower as the web height of the stiffener is increased. The main reason for this can be explained by the tripping collapse phenomenon in which buckling occurs in the web as the web height increases.

The buckling mode determined through an eigenvalue analysis can be classified into four characteristics, as shown in Fig. 5. (1) As indicated in Fig. 5 (a), an overall stiffener buckling is observed in the longitudinal direction, and this lateral buckling mode occurs when the web height is large. (2) Fig. 5 (b) shows that the typical curved plate and stiffener are in local buckling mode, as in the case of a flat stiffened plate, when subjected to axial compression. (3) When the stiffener is relatively weak compared to the plate, the plate shows the overall column type buckling mode, as indicated in Fig. 5 (c). (4) Finally, as shown in Fig. 5 (d), a local buckling phenomenon occurring

in a curved plate and stiffener was observed when the web height and torsional rigidity were both high.

The existing flat stiffened plate demonstrated six collapse modes (Paik, 2018). Mode I shows the collapse of a stiffener and panel with a small stiffener size, whereas mode II shows a collapse by a plate, and only the panel collapses when a biaxial pressure is applied. Modes III–V indicate a collapse by the stiffener; mode III shows a stiffened plate collapsing in a beam-column shape, mode IV shows a collapse with a buckling in the web of the stiffener, and mode V shows a tripping phenomenon in which the stiffener lies sideways. Finally, mode VI indicates a collapse occurring from the plasticity of the shear surface. Theoretical and numerical solutions for each collapse mode were derived, and the minimum value is defined as the ultimate strength of the flat stiffened plate.

Therefore, the collapse mode of a stiffened curved plate, which is similar to the collapse mode of a conventional flat stiffened plate, can be identified in the eigenvalue analysis. As a follow-up, investigations into the elastic buckling and elasto-plastic buckling behavior are required to identify the ultimate strength collapse mode characteristics when considering the material and geometrical nonlinearities.

2.4 Elastic Buckling Behaviour

Through an investigation into the elastic buckling behavior under the assumption of a stiffened curved plate as an elastic body and considering the geometric nonlinearity, various geometric collapse characteristics can be analyzed according to the curvature effect of the curved plate. Therefore, the buckling behavior of the stiffened curved plate was analyzed through a large deflection analysis for a geometric nonlinearity and under the assumption of an elastic material.

For three types of stiffener, the web height ($h_w = 400$ mm) was fixed to show the dimensionless elastic buckling strength and strain according to the curvature change, as summarized in Fig. 6.

In general, as the curvature increases, the elastic buckling strength increases regardless of the stiffener shape. As shown in Fig. 6 (b), when the flange angle of the angle-bar stiffener is 20° , the elastic

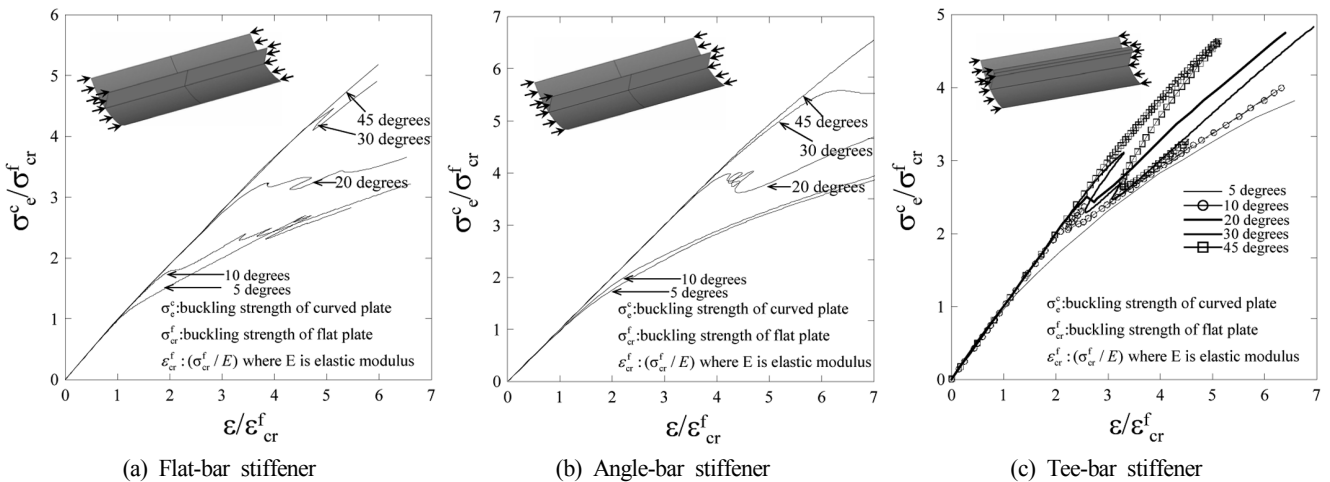


Fig. 6 Average stress-average strain relationships for stiffened curved plates under axial compression ($h_w = 400$ mm)

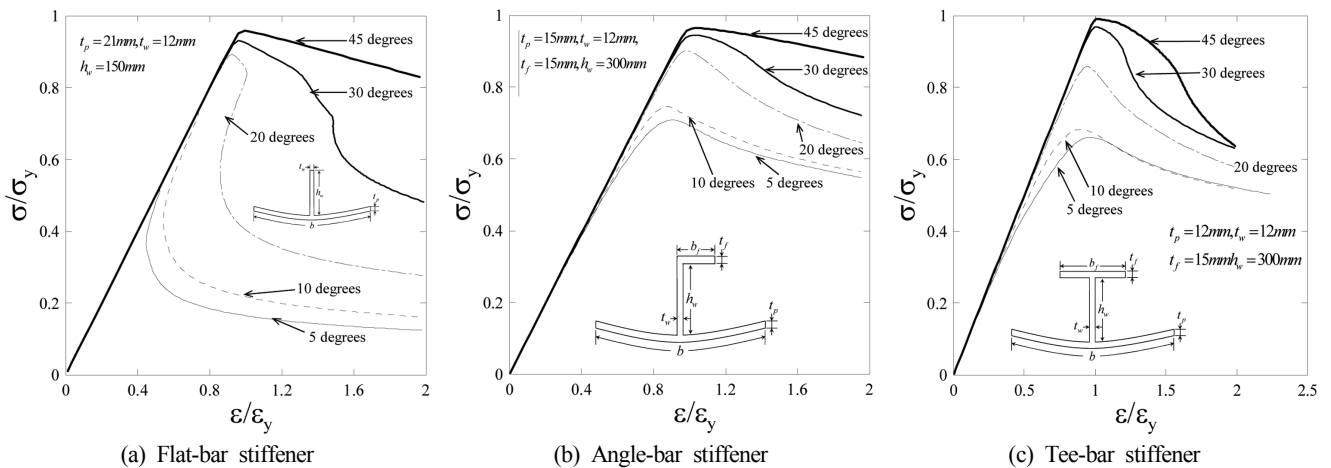


Fig. 7 Buckling/plastic collapse behaviour of curved stiffened plates subjected to axial compression

buckling behavior changes rapidly. This is a secondary buckling phenomenon, which can be explained by the sharp change in deflection mode with an increase in load.

It can be stated that the geometric instability caused by the relationship between the shape of the stiffener and the curvature differs from that of an existing flat plate. The flat- and angle-bar stiffeners did not show a secondary buckling phenomenon within the applicable strain range when the curvature was 45°. This is because a curvature of more than 45° indicates a cylindrical curved shape, and the geometrical characteristics of a cylindrical curved plate dominate over the stiffener characteristics. In addition, in the case of flat stiffened plates, a secondary buckling phenomenon generally occurs when the slenderness ratio is large at a specific aspect ratio, whereas in the case of a curved plate, it is highly likely that such a curvature effect will bring about a secondary buckling phenomenon according to the change in the geometric buckling mode.

2.5 Elastic / plastic Buckling Behaviour

The collapse mode characteristics of a curved stiffened plate were examined through a large elasto-plastic deflection analysis when considering a material nonlinearity. In the same way as in an elastic buckling behavior analysis, the buckling strength and collapse behavior characteristics were investigated based on the slenderness ratio of the plate, curvature, and web height of the stiffener.

Fig. 7 shows the results of the elasto-plastic buckling strength behavior for three different stiffeners. With the use of a perfect elasto-plastic model, which is a bilinear isotropic hardening material model, similar characteristics as in the elastic buckling strength are shown. However, owing to the material plastic effect, a secondary buckling phenomenon did not occur, unlike with the elastic buckling behavior. This can be explained as a yield occurring before a secondary buckling occurs, and the material yield region spreading to surrounding members such that the initial eigenvalue mode is maintained without changing the buckling mode.

In addition, as shown in Table 3, five types of collapse modes were identified through a total of 75 series analyses. This is similar to the

four characteristics derived through an eigenvalue analysis and can be classified as follows.

(A-mode) overall collapse mode: In this mode, a stiffened curved plate with a flat-bar stiffener shows a stiffener collapsing into a column type buckling shape before the local buckling of the curved plate occurs when the stiffener height is low or the flank angle is large. This mode is shown in Fig. 8 (a).

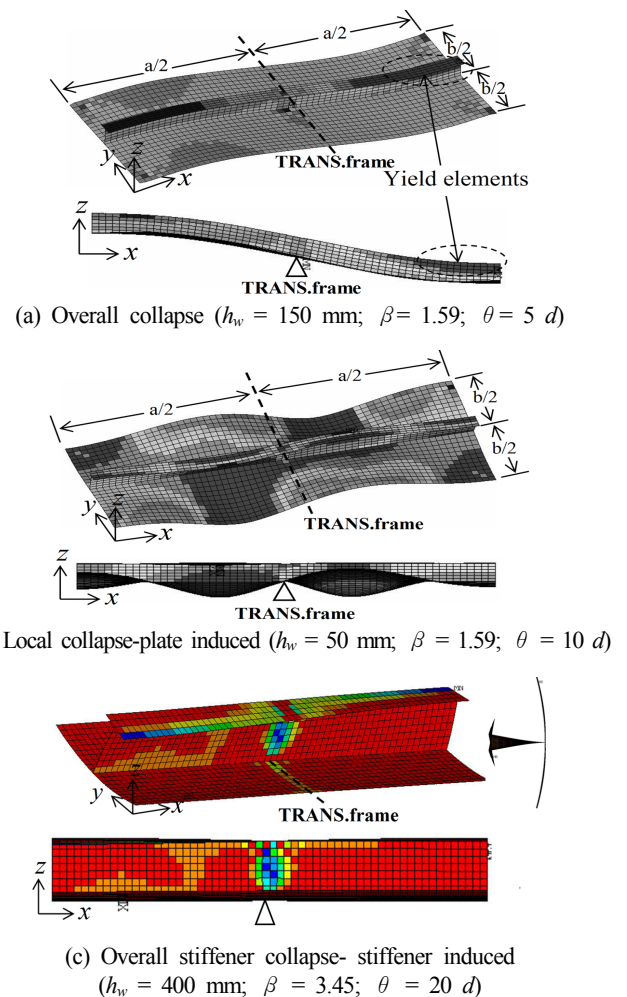


Fig. 8 Typical collapse modes of stiffened curved plates (Continued)

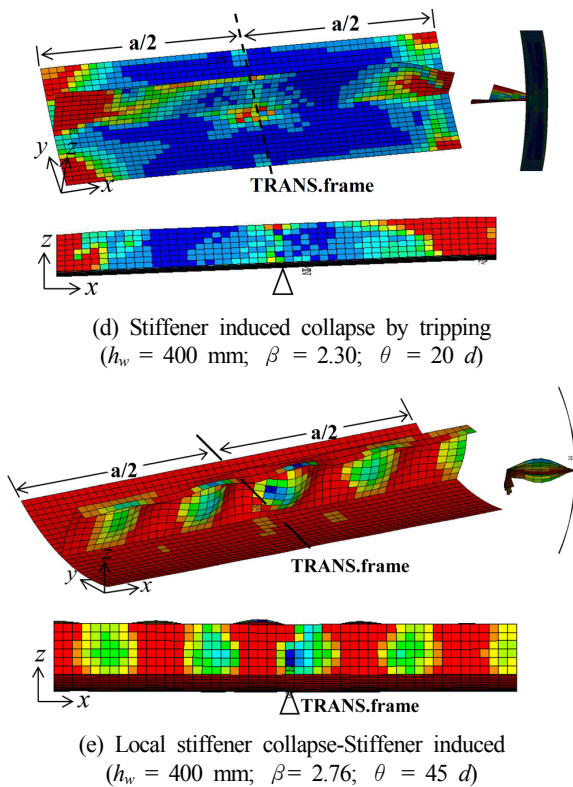


Fig. 8 Typical collapse modes of stiffened curved plates

(B-mode) local collapse-plate induced mode: This is a mode in which a curved plate first collapses locally, and the stiffener then collapses according to the curved plate shape; this collapse mode is dominated by plates, as shown in Fig. 8 (b).

(C-mode) overall stiffener collapse-stiffener induced mode: In this mode, a stiffener has a higher rigidity than the plate, and the stiffener is dominant and collapses sideways in a column type collapse shape, as shown in Fig. 8 (c).

(D-mode) stiffener-induced collapse by tripping mode: This is a collapse mode that occurs when there is no flange in the stiffener or when the web height is high, and shows a tripping phenomenon in which the stiffener lies sideways, as shown in Fig. 8 (d).

(T-mode) stiffener induced collapse by web buckling: In this mode, the stiffener has a high web height, the flange has a high rigidity, and the web collapses locally in the form of a plate, as shown in Fig. 8 (e).

For each collapse mode defined, all series analysis results according to the stiffener type and slenderness ratio of the plate are as summarized in Table 3.

3. Ultimate strength collapse mode

The main collapse modes obtained through a finite element series analysis need to be analyzed to determine the ultimate strength

Table 3 Collapse modes of stiffened curved plates

β	h_w (mm)	Flat-bar					Angle-bar					T-bar				
		5 d	10 d	20 d	30 d	45 d	5 d	10 d	20 d	30 d	45 d	5 d	10 d	20 d	30 d	45 d
1.59	150	D	D	D	D	D	D	D	D	D	D	D	D	D	D	D
	200	D	D	C	C	C	D	D	D	D	D	A	A	A	D	B
	250	D	C	C	C	C	A	A	A	D	D	A	A	A	D	C
	300	C	C	C	C	C	A	A	A	D	D	A	A	C	C	C
	400	C	C	C	C	C	A	A	A	A	D	A	C	C	C	C
1.97	150	D	D	D	D	D	D	D	D	D	D	A	A	A	D	D
	200	A	A	C	C	C	A	A	A	D	B	A	A	A	A	C
	250	A	A	C	C	C	A	A	D	D	D	A	A	A	A	C
	300	A	C	C	C	C	A	A	A	A	C	A	A	A	A	C
	400	C	C	C	C	C	A	A	A	C	C	A	A	A	C	C
2.30	150	D	D	D	D	D	A	D	D	B	B	A	A	A	A	D
	200	A	T	A	C	C	A	A	A	A	B	A	A	A	A	B
	250	A	A	C	C	C	A	A	A	A	C	A	A	A	A	C
	300	A	A	C	C	C	A	A	A	A	A	A	A	C	C	C
	400	A	C	T	C	C	A	A	C	C	C	A	A	A	C	C
2.76	150	A	A	A	D	D	A	A	A	D	D	A	A	A	A	B
	200	A	A	A	C	C	A	A	A	A	D	A	A	A	A	A
	250	A	A	C	C	C	A	A	A	A	B	A	A	A	A	A
	300	A	A	C	C	C	A	A	A	A	A	A	A	A	A	A
	400	A	C	C	C	C	A	A	A	C	C	A	A	A	A	C
3.45	150	A	A	A	A	A	A	A	A	D	D	A	A	A	A	D
	200	A	A	A	A	A	A	A	A	A	B	A	A	A	A	A
	250	A	A	C	C	C	A	A	A	A	B	A	A	A	A	B
	300	A	T	C	C	C	A	A	A	A	A	A	A	A	B	B
	400	A	C	C	C	C	A	A	A	A	C	A	A	C	C	C

Note: A is Local collapse, B: Local stiffener collapse, C is Overall stiffener collapse, D is overall panel collapse, T is stiffener collapse by tripping

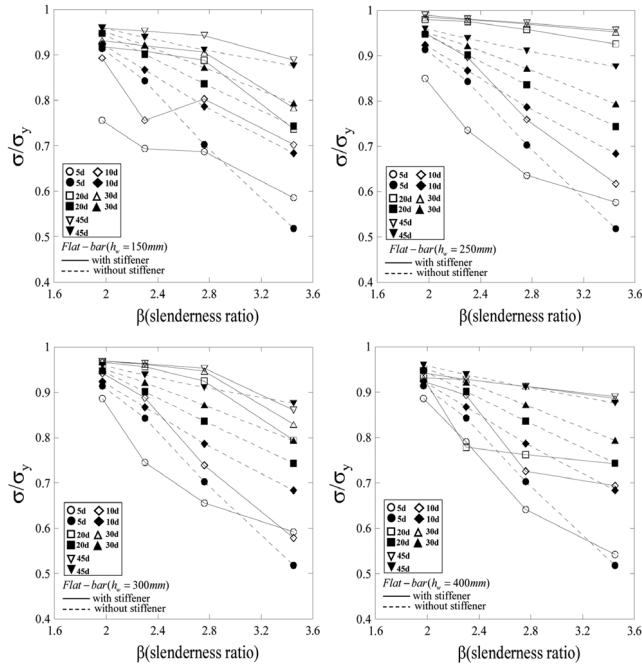


Fig. 9 Ultimate compressive strength of stiffened curved plate with flat-bar stiffener under axial compression

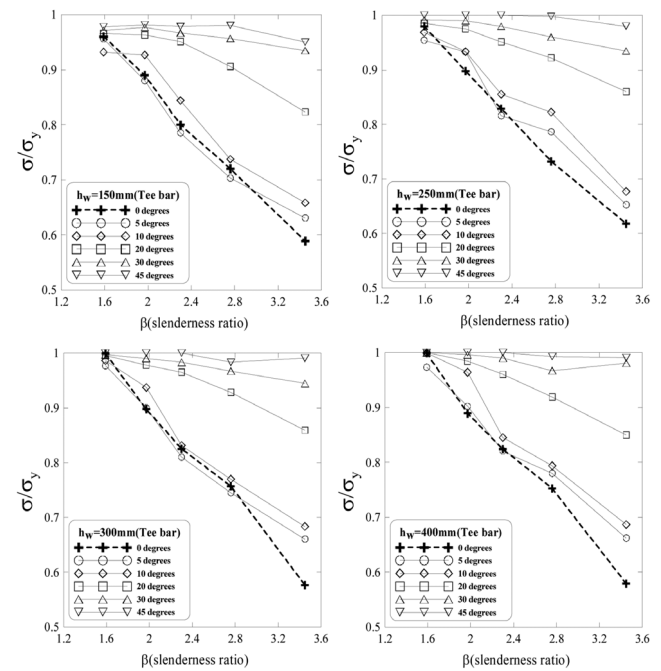


Fig. 11 Ultimate compressive strength of stiffened curved plate with tee-bar stiffener under axial compression

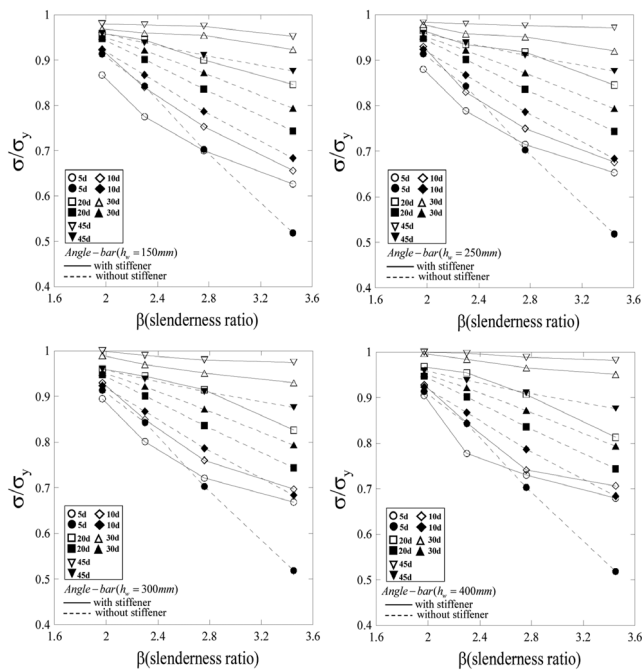


Fig. 10 Ultimate compressive strength of stiffened curved plate with angle-bar stiffener under axial compression

characteristics. The ultimate strength for the in-plane compression of a stiffened curved plate is shown in Figs. 9-11 based on the stiffener type according to the curvature, stiffener height, and slenderness ratio of the plate. In addition, to examine the ultimate strength characteristics under the impact of a stiffener, the ultimate change in strength was comparatively analyzed for a case with a stiffener and for a case with an unstiffened curved plate, which considers a curve plate only.

As in the case of the plate shown in Fig. 9, when the slenderness ratio is low and the curvature is similar to that of a flat plate (less than 10° flank angle), it was found that the ultimate strength of a stiffened curved plate is estimated to be smaller than that of an unstiffened curved plate. This can be explained through the collapse mode (A: overall collapse mode) of the overall buckling of the stiffened curved plate in a column shape before the local buckling, as shown in Fig. 8(a).

In the case of a flat-bar stiffened curved plate, the highest ultimate strength was shown in the stiffened curved plate with the same slenderness ratio of the plate at the stiffener height ($h_w = 250$ mm). This suggests that the bending rigidity of stiffeners with a low web height is low and that the stiffener with a high web height has a low torsional rigidity, and thus for a stiffened curved plate under this condition, the ultimate strength is estimated to be rather low even though the effective longitudinal cross section area is large.

In the case of an angle-bar, the web is rotationally restrained owing to the flange effect of the stiffener, as shown in Fig. 10. As a result, in the case of the same curvature and slenderness ratio of the plate, the ultimate strength of the stiffened curved plate increases with an increase in the stiffener height. This can be regarded as the typical difference from a flat-bar stiffener. However, the ultimate strength of a flat-bar stiffened curved plate shows the reverse behavior. This can be explained based on the collapse mode (C: overall stiffener collapse-stiffener induced mode) characteristics in which the stiffener shows columnar buckling before a local buckling of the plate occurs.

In Figs. 10 and 11, the ultimate strengths of the angle- and T-bar stiffeners show similar strengths. However, under the same collapse mode, the angle-bar stiffener shows a low ultimate strength. This difference is caused by the rotationally restrained flange.

4. Conclusion

In this study, the large elastic/plastic deflection behavior, ultimate strength, and collapse characteristics were determined through a precise nonlinear numerical analysis to identify the buckling and collapse modes of stiffened curved plates. For a stiffened curved plate, the following conclusions were drawn for three types of stiffeners applied to a ship bilge according to the curvature, stiffener height, and plate slenderness ratio.

(1) In general, the increases in the stiffener height and curvature increase the elastic and elasto-plastic buckling strengths of the stiffened curved plate, and in the case of elastic buckling, a complex secondary buckling behavior occurs, whereas in the case of elasto-plastic buckling when considering the material plastic effect, the secondary buckling behavior does not occur. This indicates that, because a stiffened curved plate has a geometrically unstable structure compared to a flat stiffened plate, a design based on elasto-plastic buckling when considering the material nonlinearity is required.

(2) A large series elasto-plastic deflection analysis was conducted to derive the collapse mode characteristics. Based on the analysis results, the collapse mode of the stiffened curved plate was categorized into five modes similar to the collapse mode of a conventional flat stiffened plate: the (A) overall collapse mode, (B) local collapse mode-curved plate induced mode, (C) overall stiffener collapse mode-stiffener induced mode, (D) stiffener collapse mode induced by tripping mode, and (T) stiffener collapse mode induced by a stiffener web buckling. In addition, the effects of the collapse characteristics on the ultimate strengths were analyzed, and the characteristics of the stiffened curved plates derived through this analysis were investigated.

(3) The defined stiffened curved plate collapse mode will be used as important information for the development of a theoretical analysis method when considering the respective deflection characteristics of the corresponding collapse characteristics. In the future, this mode can be used as a deflection equation for applying theoretical analysis and numerical methods to each collapse mode derived.

(4) Further study is needed to verify the collapse mode characteristics based on the experimental methods, and a follow-up investigation is needed to develop an equation for predicting the ultimate strength of the stiffened curved plate for each verified collapse mode.

Acknowledgements

This work was supported by a 2-Year Research Grant of Pusan National University.

References

- ANSYS. (2015). Introduction to Material Nonlinearities. ANSYS11.0 User's Manual, ANSYS Inc., USA.
- Cho, S.R., Park, H.Z., Kim, H.S., & Seo, J.S. (2007). Experimental and Numerical Investigations on the Ultimate Strength of Curved Stiffened Plates. Proceedings of the 10th International Symposium on Practical Design of Ships and other Floating Structures, Houston, Texas, USA, 453-60.
- ISO. (2007). Ships and Marine Technology - Ship Structures, Part 1: General Requirements for Their Limit State Assessment. International Standard ISO 18072-1, International Organization for Standardization: Geneva.
- Kim, J.H., Park, J.S., Lee, K.H., Kim, J.H., Kim, M.H., & Lee, J.M. (2014). Computational Analysis and Design Formula Development for the Design of Curved Plates for Ships and Offshore Structures. Structural Engineering Mechanics. 49(6), 705-726. <https://doi.org/10.12989/sem.2014.49.6.705>
- Kwen, Y.W., Park, Y.I., Paik, J.K., & Lee, J.M. (2004). Buckling and Ultimate Strength Characteristics for Ship Curved Plate Structures. Proceedings of the Annual Autumn Meeting, SNAK, Sancheong Korea, 351-356.
- Maeno, Y., Yamaguchi, H., Fujii, Y. & Yao, T. (2004). Buckling/Plastic Collapse Behaviour and Strength of Bilge Circle and Its Contribution to Ultimate Longitudinal Strength of Ship's Hull Girder. Proceedings of International Offshore and Polar Engineering Conference, Toulon, France.
- Oh, Y.C., Kim, K.T., & Ko, J.Y. (2011). Investigation for Collapse Mode of Stiffened Curved Plate with Tee Shaped Stiffeners. Journal of the Korean Society of Marine Environment & Safety. 17(3), 295-300. <https://doi.org/10.7837/kosomes.2011.17.3.295>
- Park, H.J., Cho, S.R., Chung, J.N., & Lee, D.B. (2005). Ultimate Strength Analysis of Curved Stiffened Shell of Container Bilge Strake. Proceedings of The Annual Autumn Meeting, SNAK, Yongjin, 189-195.
- Paik, J.K. (2018). Ultimate Limit State Analysis and Design of Plated Structures. Chichester, UK: John Wiley & Sons.
- Park, J.S., & Seo, J.K. (2019). Development of Design Factor Predicting the Ultimate Strength for Wide Spacing in Container Curved Bilge Structures. Journal of Marine Science and Technology. 24, 526-542. <https://doi.org/10.1007/s00773-018-0572-0>
- Park, J.S., Iijima, K., & Yao, T. (2008). Characteristics of Buckling and Ultimate Strength and Collapse Behaviour of Cylindrically Curved Plates Subjected to Axial Compression. Advanced Materials Research, 33-37, 1195-1200. <https://doi.org/10.4028/www.scientific.net/AMR.33-37.1195>
- Seo, J.K., Song, C.H., Park, J.S., & Paik, J.K. (2016). Nonlinear Structural Behaviour and Design Formulae for Calculating the Ultimate Strength of Stiffened Curved Plates under Axial Compression. Thin-Walled Structures. 107, 1-17. <https://doi.org/10.1016/j.tws.2016.05.003>
- Smith, C.S., Davidson, P.C., Chapman, J.C., & Dowling, P.J. (1988). Strength and Stiffness of Ship's Plating under In-plane Compression and Tension. Royal Institution of Naval Architects Transactions, 130(1988), 227-296.

Author ORCIDs and Contributions

Author name	ORCID	Contributions
Park, Joo Shin	0000-0001-5335-8151	①②③
Ha, Yeon Chul	0000-0003-3591-8471	④
Seo, Jung Kwan	0000-0002-3721-2432	④⑤

- ① Conceived of the presented idea or developed the theory
- ② Carried out the experiment or collected the data
- ③ Performed the analytic calculations or numerical simulations
- ④ Wrote the manuscript
- ⑤ Supervised the findings of this study

Algorithm to Estimate Oil Spill Area Using Digital Properties of Image

Hye-Jin Jang¹ and Jong-Ho Nam²

¹Graduate Student, Department of Naval Architecture and Ocean Systems Engineering, Korea Maritime & Ocean University, Busan, Korea

²Professor, Division of Naval Architecture and Ocean Systems Engineering, Korea Maritime & Ocean University, Busan, Korea

KEY WORDS: Oil spill, Digital image, Image processing, Binarization, Image histogram

ABSTRACT: Oil spill accidents at sea result in a wide range of damages, including the destruction of ocean environments and ecosystems, as well as human illnesses by the generation of harmful gases caused by phase changes in crude oil. When an oil spill occurs, an immediate initial action should be performed to minimize the potential damage. Existing studies have attempted to identify crude oil spillage by calculating the crude oil spill range using synthetic aperture radar (SAR) satellite images. However, SAR cannot capture rapidly evolving events because of its low acquisition frequency. Herein, an algorithm for estimating an oil spill area from an image obtained using a digital camera is proposed. Noise that may occur in the image when it is captured is first eliminated by preprocessing, and then the image is analyzed. After analyzing the characteristics of the digital image, a strategy to binarize an image using the color, saturation, or lightness contained in it is adopted. It is found that the oil spill area can be readily estimated from a digital image, allowing for a faster analysis than any conventional method. The usefulness of the oil spill area measurement was confirmed by applying the developed algorithm to various oil spill images.

1. Introduction

Ocean accidents typically result in environmental pollution. Among the various causes of environmental pollution, such as ship wastewater or unauthorized oil discharge, oil spill accidents cause damage on the largest scale. Because the oil begins to diffuse instantly when it is spill, the contaminated area increases with time. Therefore, a quick response is necessary.

Typically, when an incident is reported, aerial surveying is conducted over the incident area to prepare an initial report. The oil spill area can be calculated using a global positioning system (GPS), side-looking airborne radar, and infrared or ultraviolet scanners (IPIECA, 2016). According to the International Tanker Owners Pollution Federation (ITOPF), oil-contaminated areas are currently estimated using GPS measurements.

The US national weather service uses satellites to not only estimate the range of an oil spill, but also to predict its spread. It is known that remote sensing technology can be used to collect information regarding the wind, ocean currents and tides, sea level heights, and other estimates, including the damage from oil spills (NOAA, 2016). Synthetic aperture radar (SAR) technology has been continuously used

as a powerful tool for providing various types of information regarding sea conditions. An example of an oil spill region shown in a SAR image is depicted in Fig. 1 (Fiscella et al., 2000).

A study was performed to distinguish between pixels with and without oil using the histogram shape of SAR images (Kim et al., 2013). A special model, called the thresholding-guided stochastic fully connected conditional random field model, was introduced to infer binary labels from SAR images (Xu et al., 2015). Machine learning techniques have been applied to find oil spill areas. Topouzelis (2008)



Fig. 1 SAR image of oil spill area

Received 19 November 2019, revised 24 December 2019, accepted 14 February 2020

Corresponding author Jong-Ho Nam: +82-51-410-4301, jhnam@kmou.ac.kr

© 2020, The Korean Society of Ocean Engineers

This is an open access article distributed under the terms of the creative commons attribution non-commercial license (<http://creativecommons.org/licenses/by-nc/4.0>) which permits unrestricted non-commercial use, distribution, and reproduction in any medium, provided the original work is properly cited.

introduced a method for distinguishing oil films using the phenomenon where an oil film appears to be darker than its surroundings by reducing the backscatter of the sea level in SAR images. Subsequently, an automatic detection algorithm using nonlinear spatial filters was proposed. This algorithm scans the region that appears darker than its surroundings (Schvartzman et al., 2016). Unlike previous studies that approached SAR images visually, images were analyzed based on various types of data in this study.

By analyzing SAR images, a relatively accurate oil spill area can be estimated. However, to obtain SAR images at an accident location, a satellite should be orbiting above the location, or SAR equipment should be installed on an aircraft performing reconnaissance. Given that an immediate action is essential to control oil spills at sea, an effective method that does not require the abovementioned preconditions is strongly recommended.

Herein, to identify oil spill regions promptly, a method for estimating an oil spill area from a digital image is proposed. Such digital images are normally obtained from drones or an aircraft flying around the accident area. Image processing is required to automatically digitize and process information such as the size or direction of the contamination. An algorithm that automatically calculates the oil spill area in the digital domain was developed based on the assumption that the oil spill images captured with a digital camera are similar to those confirmed visually. The general image processing techniques needed for the algorithm are explained, and the theory and practical application of filtering and thresholding are discussed. This paper analyzes numerous oil spilled images currently available and classifies them according to their characteristics; subsequently, an appropriate analysis method is proposed for each classification.

2. Image Processing Preliminaries

2.1 Digital Image

A digital image is generated by sampling and quantizing a portion of light reflected by an object into a camera sensor. The process of converting an analog value sensed by a sensor to a digital value is defined as sampling, while quantization is the process of “integerizing” an infinite sequence of sampled digital values. An image can be mathematically defined by a two-dimensional function $f(x, y)$, where x and y are the two-dimensional coordinates of the image.

Image processing techniques are typically used to extract the desired pieces of information from images (Petrou and Petrou, 2010). After an image is represented digitally, an appropriate image processing technique is used for each image analysis. Image processing refers to comprehensive technology that uses a computer to process images and acquire the desired results. Image processing includes both low-level processing to reduce noise or improve contrast and high-level processing to analyze and recognize images. An image may be characterized by observing its changing period in the frequency domain and detecting specific objects or textures in the image using the pixel value distribution. These techniques were actively used in this study.

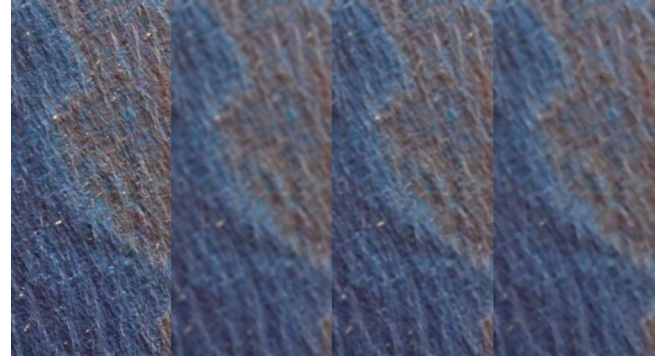


Fig. 2 Various filtering effects: source, blur, Gaussian blur, and median (from left to right)

2.2. Filtering

Image processing can yield improved results by appropriately utilizing the relevant techniques involved. Among these, the role of a filter is essential. Filtering removes noise in an image and extracts visual features, thus enabling resampling functions such as image scaling and pixel value conversion, among others.

Most digital images are accompanied by unwanted noise. Photographs of the sea taken from an aircraft or other flying object are no exception; in particular, noise such as that caused by reflected ambient light is inevitable. An image typically includes other noise components that can be removed or reduced using ultraviolet and polarizing filters (ITOPF, 2014). Nevertheless, the noise caused by the remaining light must be treated using other filters.

Filters are used according to their principles and characteristics (Gonzalez and Woods, 2017). A linear filter typically represents an entire image smoothly. A blur filter, as a representative linear filter, blurs an image by replacing each pixel with an average pixel value calculated over a rectangular neighborhood. Similar to the blur filter, a Gaussian filter imposes the weights of neighboring pixels by applying the Gaussian function. A median filter uses the median of a set calculated by converting a pixel and its surrounding pixels into a set of median values. The ripples appearing in images captured from the sea produce noise by reflecting the sunlight. This noise is similar to the salt-and-pepper noise that can be effectively removed or reduced by applying a median filter. The median filter tends to outshine the original colors, as shown in Fig. 2.

2.3. Binarization

Spilled oil diffuses over the sea surface over time. If the shape of the diffused oil can be defined geometrically, it is possible to calculate its area mathematically. Unfortunately, because the shape is typically random and irregular, it is complex to define a mathematical representation of the shape, which renders it difficult to calculate its area analytically. Herein, a binarization technique is proposed that uses the digital characteristics of an image to classify the area according to the pixel information.

Binarization represents all of the pixel values as either black or white. When the number of bits of one pixel representing the color is N , the

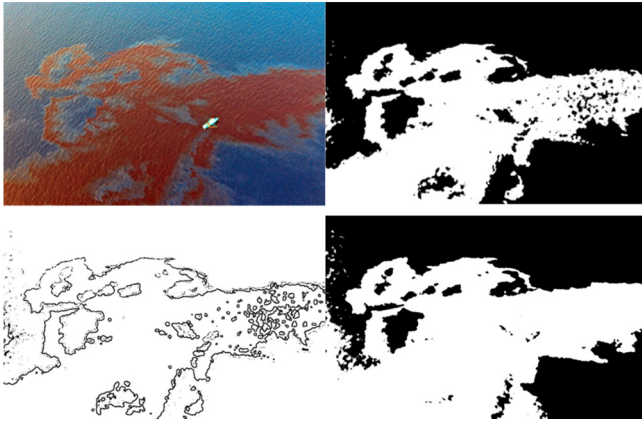


Fig. 3 Comparison of binarized images from original image (top-left): Otsu algorithm (top-right), adaptive binarization (bottom-left), and our algorithm (bottom-right)

range of the color representation becomes $[0, 2^{N-1}]$. For example, the color range of an 8-bit image primarily used in image processing is $[0, 255]$. Because binarization uses only two extreme values in this color range, it can theoretically split two other objects in the image, such as water and oil.

To binarize an image, the threshold must be calculated in advance. Representative methods for calculating the threshold value include global fixed binarization using the brightness values of the entire image and local variable binarization using the neighboring pixel values of each pixel.

Among the global fixed binarization methods, the Otsu (1979) algorithm has been widely used. It calculates the threshold value using the brightness distribution of an entire image. However, when determining the threshold value for a wide range of color information, all of the areas are not readily distinguished by the Otsu method because it only uses a single threshold value. The adaptive thresholding method, which is categorized as a local variable binarization method, uses a weighted average calculated by setting the size of a block to determine neighboring pixels at a selected pixel position (Bradley and Roth, 2007). When adaptive thresholding is applied, pixels with a large difference from their neighboring pixels are binarized to obtain an edge-highlighted result.

Fig. 3 compares the results obtained by the Otsu method and adaptive thresholding, as well as those by the algorithm developed in this study. The developed algorithm synthesizes binarized images using multiple thresholds. Details regarding the algorithm are presented in the upcoming section.

3. Calculation of Oil Spill Area

3.1 First Step: Analysis by Hue Property

To estimate the extent of spilled oil at sea, it is necessary to separate the fraction of oil from seawater. In this study, histograms of 20 images, as shown in Fig. 4, of distinct oil-spilled patterns were collected and analyzed for a clear separation. The images used in the analysis were

color-expressed scenes in a digital format and were regarded as a population of various oil patterns appearing at the accident site.

To obtain the desired characteristics from an image, it is necessary to extract the distinct feature included in the image. It is clear that most viewers can intuitively identify an oil spill from seawater using their eyes. Because human intuition is influenced by the color difference shown in the image, the first step is to select a method that distinguishes the areas using this color difference.

A digital image is a medium that expresses an entire image as a mathematical model, called a color model, by combining the specific colors of each pixel of an image. The typical color models used in image processing include red, green, blue (RGB); hue, saturation, value (HSV); and hue, saturation, lightness (HSL). The RGB model is a numerical representation of the changes in the three major colors, which allows it to be easily understood. However, when the three colors are combined, the results are difficult to predict. Meanwhile, the HSV and HSL models have structures that make it easy for humans to perceive color; thus, they are widely used in image processing. When only the desired color information from the RGB model must be extracted, RGB is converted to either HSV or HSL.

The OpenCV library is used for the computational treatment of image processing techniques. OpenCV is an open-source library for developing computer vision applications (OpenCV, 2019). It provides numerous functions necessary for image processing; furthermore, it can be seamlessly executed on multiple platforms.

An OpenCV function is utilized to convert the color space read in RGB into the HSV color space. General equations for changing the color space are easily found in the literature or online, as in Eq. (1).

$$\begin{aligned}
 V &\leftarrow \max(R, G, B) \\
 S &\leftarrow \begin{cases} \frac{v - \min(R, G, B)}{v} & \text{if } V \neq 0 \\ 0 & \text{otherwise} \end{cases} \\
 H &\leftarrow \begin{cases} 60(G - B) / (V - \min(R, G, B)) & \text{if } V = R \\ 120 + 60(B - R) / (V - \min(R, G, B)) & \text{if } V = G \\ 240 + 60(R - G) / (V - \min(R, G, B)) & \text{if } V = B \end{cases}
 \end{aligned} \quad (1)$$

After the color space conversion, when processing for a single color is required, a three-channel (HSV) image is separated into single channels (H/S/V). Subsequently, the histogram of the separated channel image is obtained, and binarization is performed.

An example of changing the RGB color space to HSV is shown in Fig. 5, followed by three images after separation into individual channels in Fig. 6. The histogram for the left hue image of Fig. 6 is depicted in Fig. 7. After the minimum and maximum values are obtained from the histogram, the peaks and valleys are determined using the slopes of the neighboring values. To find the peaks or valleys, the histogram is first blurred and curved. To distinguish neighboring peaks, certain parameters are used as criteria. The parameters are determined in the image analysis step according to the image size, that is, the total number of pixels of the image, and the determined parameters are applied in the image processing step.



Fig. 4 Twenty sample images of oil spill. The images were labeled from 1 to 20

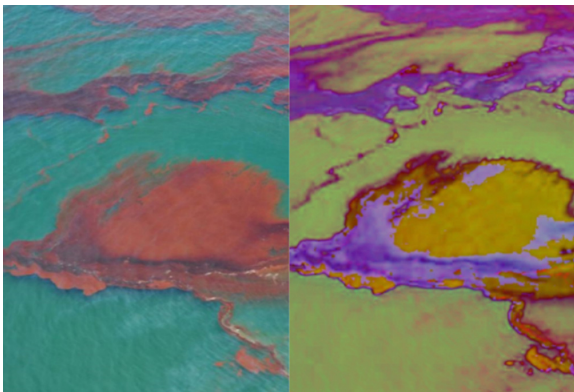


Fig. 5 Conversion of image from RGB (left) to HSV (right)

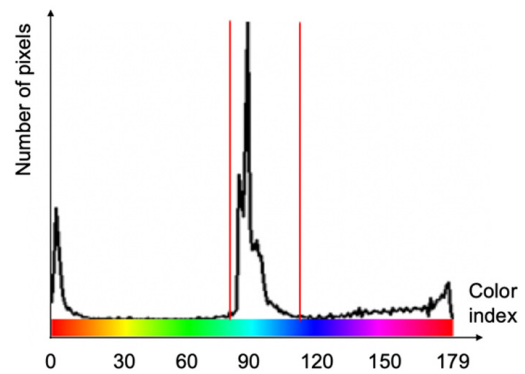


Fig. 7 Histogram of hue image in Fig. 6

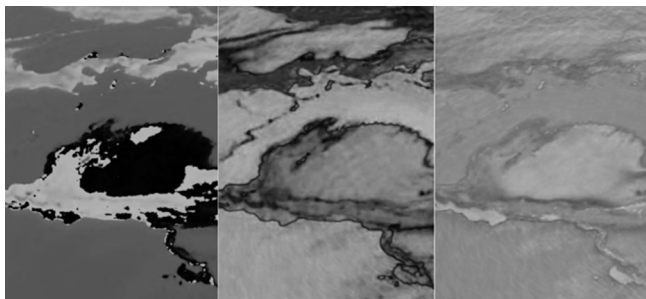


Fig. 6 Separated channels: hue, saturation, and value (from left to right)

Table 1 lists the number of peaks in the hue histograms of the 20 sample images.

Even though multiple peaks appear in the color range of seawater, not all of these peaks represent meaningful values. Thus, it is plausible to discard peaks other than the peak with the lowest value within the range. The number of valid peaks adjusted from the number of peaks in Table 1 is rewritten in Table 2.

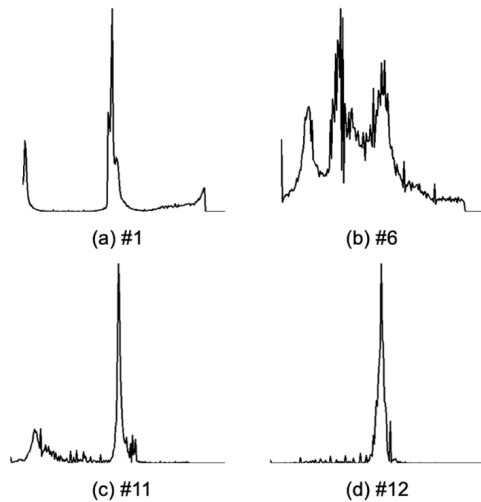
The spilled crude oil initially appears black (#9 in Fig. 4; the image index is denoted by a mark (#) followed by its number, hereinafter) and becomes emulsified to a reddish color over time. By analysis, the color histogram of the black or red image shows two peaks near both ends and one peak in between. With three peaks, the two valleys between the peaks can be used as the thresholds. Images with two peaks, e.g., #2 and #11, do not show red or black colors, but the seawater and oil can easily be distinguished by different colors when confirmed visually.

Table 1 Number of peaks in hue image histograms of 20 sample images

Index	1	2	3	4	5	6	7	8	9	10	11	12	13	14	15	16	17	18	19	20
H_{PEAKS}	3	2	3	4	5	5	3	3	4	3	3	1	1	4	3	3	3	1	4	3

Table 2 Number of valid peaks in hue image histogram

Index	1	2	3	4	5	6	7	8	9	10	11	12	13	14	15	16	17	18	19	20
H_{PEAKS}	3	2	3	3	4	5	3	3	3	3	2	1	1	3	3	3	3	1	3	3

**Fig. 8** Four distinct histograms: (a) #1 with three peaks, (b) #6 with multiple peaks, (c) #11 with two peaks, and (d) #12 with one peak

Histograms with silver or iridescent oil films such as #5, #6, #12, #13, and #18 have either one, four, or more than four peaks, which make the analysis more complicated. The histograms for the selected sample images are illustrated in Fig. 8.

When the images were binarized using the threshold value obtained by the histogram analysis, the separation between water and oil was possible in the 13 three-peak images (#1, #3, #4, #7, #8, #9, #10, #14, #15, #16, #17, #19, and #20) through two binarizations. However, in the images with other peak numbers, the separation was not successful in whole or in part. The separation failure could be attributed to several reasons, but it can be deduced that an important factor was the fact that

the hue characteristic considered in this step was limited to chromatic colors. This implies that other separation methods are needed.

3.2 Second Step: Analysis by Saturation Property

Saturation is used for images whose hue histogram has either a single threshold value or when a valid threshold value cannot be obtained. This is a strategy to separate different regions by utilizing the level of sharpness, which the hue itself cannot express. In other words, through saturation, some achromatic information can be utilized, which can provide a clue for additionally processing regions not separated by the hue.

Saturation histograms were created and analyzed for the seven sample images that did not have valid threshold values in the hue analysis. The results are summarized in Table 3.

If the saturation histogram is bimodal, then one effective threshold is obtained. In this case, two binary images obtained by the hue and saturation analyses, separately, are synthesized to generate a combined image that attempts to complement the two results. Consequently, valid threshold values could be obtained for images #2, #5, #6, and #11.

Fig. 9, for instance, illustrates the synthesis process for sample #2, which combines the hue image (left) and saturation image (middle) to yield the synthesized result shown on the right.

If a binarized result is obtained from the hue images such as #2 or #11, the oil spill area can be obtained by additionally considering the result of the saturation image. However, when three or more valleys are obtained from the hue images, such as #5 or #6, some regions are still not detected, as shown in Fig. 10.

In some cases (#5, #6, #12, #13, and #18), hue and saturation analyses were not applicable. Hence, the regions had to be separated using a feature other than the hue or saturation.

Table 3 Number of peaks in saturation image histogram

Index	1	2	3	4	5	6	7	8	9	10	11	12	13	14	15	16	17	18	19	20
H_{PEAKS}	3	2	3	3	4	5	3	3	3	3	2	1	1	3	3	3	3	1	3	3
S_{PEAKS}	-	2	-	-	2	2	-	-	-	-	2	1	1	-	-	-	-	1	-	-

**Fig. 9** Combination of two binarized images for sample #2: by hue (left), by saturation (middle), and combined (right)

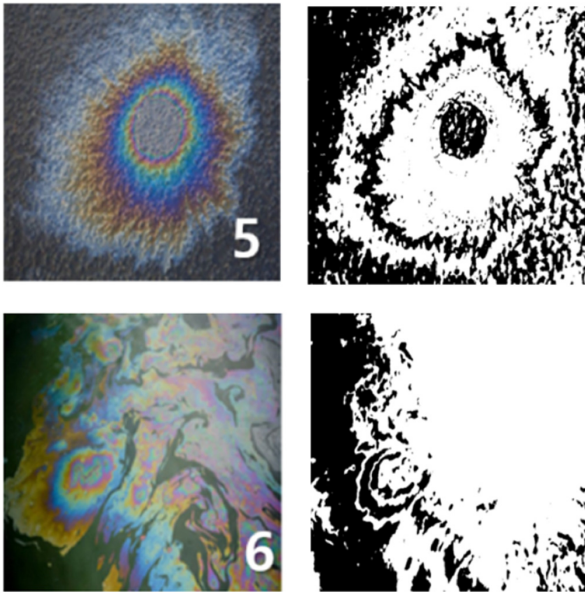


Fig. 10 Unsuccessful binarization results for samples #5 and #6

3.3 Third Step: Analysis by Lightness Property

A smaller spill or already decomposed oil appears as a thin film that shows silvery or iridescent colors. The silvery film shows little difference from the sea in terms of color, while the rainbow colors produce many different colors simultaneously, rendering it difficult to calculate a valid threshold value with hue and saturation analyses.

In this case, it will be effective to use the lightness information as a new characteristic by focusing on the fact that the oil film reflects more light than the seawater. This is due to the nature of the oil film floating on the water surface. In this study, the separation was performed using the grayscale lightness after the original image was converted to grayscale.

Table 4 lists the number of peaks obtained from the lightness histogram. Because the lightness histogram indicates the increase or decrease in lightness, even if two or more peaks occur, only one binarization is performed using the value located at the lowest valley as a threshold. For example, sample image #6 shows three peaks, that is, two valleys, after the lightness histogram analysis. In this case, one binarization is performed using the lowest threshold value.

Fig. 11 shows the results of binarization using the lightness valley as a threshold. The three-step binarization reveals a reasonable separation. Nevertheless, all of the results are far from ideal. In some regions, water and oil are reversed. The fact that the oil and water areas in #13 are difficult to distinguish even with the naked eye is also a cause of incomplete results.

Because the #12 and #18 images with one peak could not be

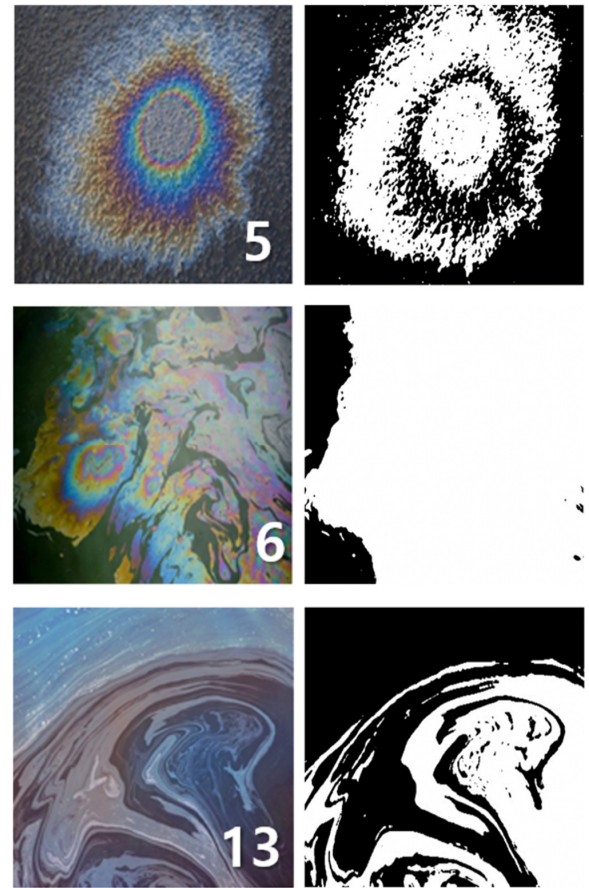


Fig. 11 Binarized images for sample images #5, #6, and # 13

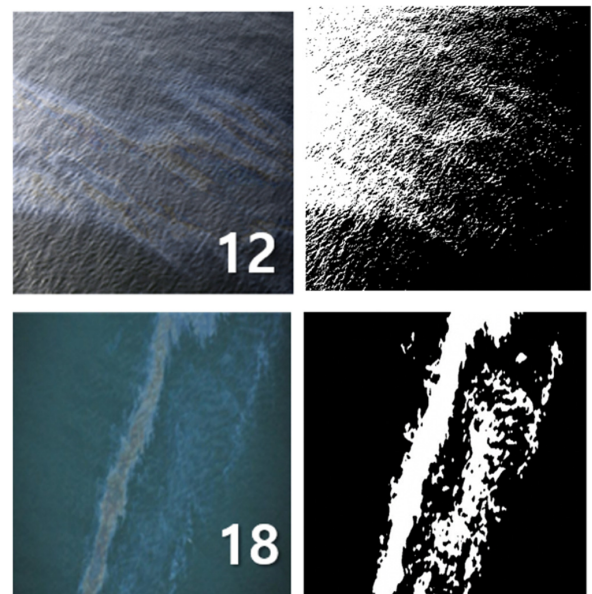


Fig. 12 Binarization results for sample images #12 and #18

Table 4 Number of peaks in lightness histogram

Index	1	2	3	4	5	6	7	8	9	10	11	12	13	14	15	16	17	18	19	20
H_{PEAKS}	3	2	3	3	4	5	3	3	3	3	2	1	1	3	3	3	3	1	3	3
S_{PEAKS}	-	2	-	-	2	2	-	-	-	-	2	1	1	-	-	-	-	1	-	-
L_{PEAKS}	-	-	-	-	2	3	-	-	-	-	-	1	2	-	-	-	-	1	-	-

determined because no valley existed, the binarization was performed using the Otsu (1979) method. The results are shown in Fig. 12, and it is difficult to infer the oil spill area from the binarization result. In the #12 image, the binarization result becomes meaningless because the spilled

oil and highlight of the reflected light are mixed for the binarization. In this study, it was considered impossible to automatically separate images such as #12 and #18. It is more logical for the user to perform the separation semi-automatically or manually.

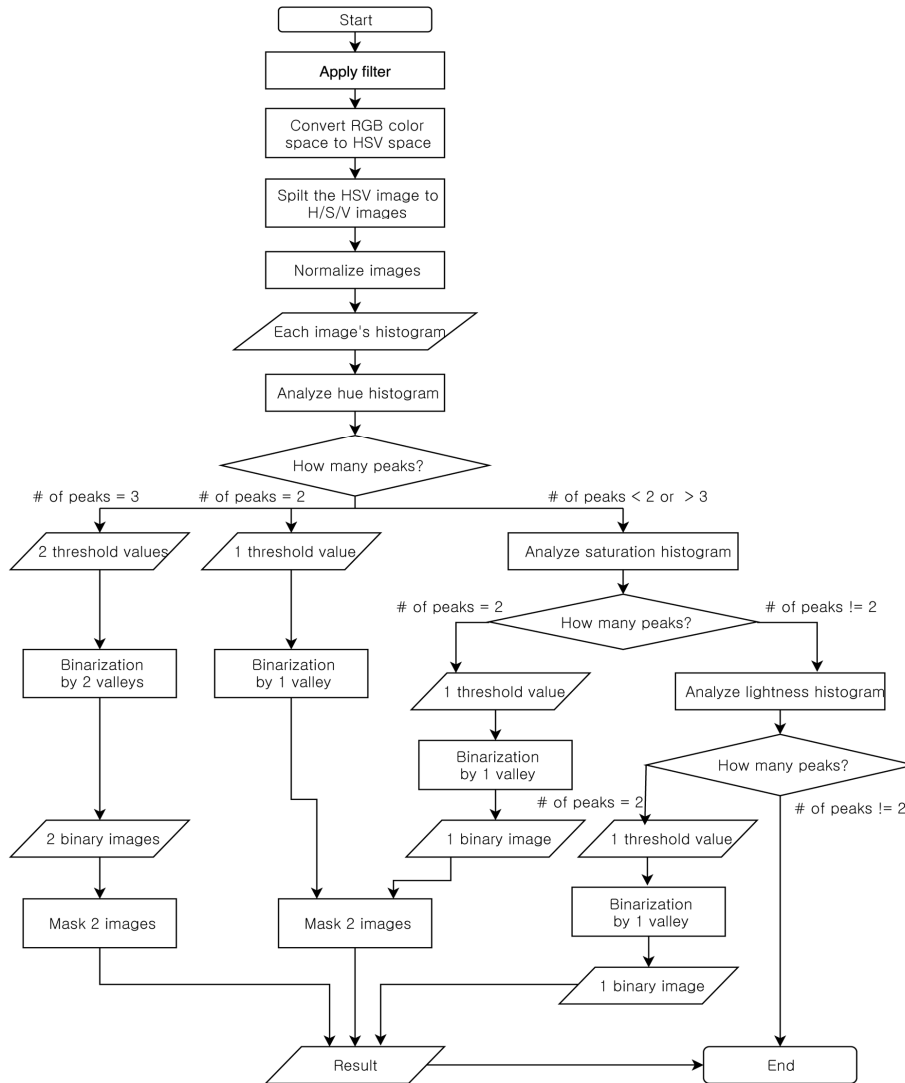


Fig. 13 Flowchart of algorithm for oil spill image classification

Table 5 Comparison of analysis results for 20 sample images

	Step #1: Hue analysis	Step #2: Saturation analysis, with hue	Step #3: Lightness analysis	Undefined
Image index	1, 3, 4, 7, 8, 9, 10, 14, 15, 16, 17, 19, 20	2, 11	5, 6, 13	12, 18
Number of peaks in hue histogram	3	2	-	-
Number of peaks in saturation histogram	-	2	-	-
Number of peaks in lightness histogram	-	-	2 or more	-
Strategy	Binarization with two threshold values obtained from hue histogram. Combination of two binarized images	Combination of a binarized image from saturation histogram and another image from hue histogram	Binarization with the lowest valley obtained from lightness histogram	The user must manually estimate the oil spill area

3.4 Summary of Proposed Algorithm and Binarization Results

The flowchart of the developed oil spill separation algorithm is summarized in Fig. 13.

After preprocessing, the resulting histograms are classified into three different cases, depending on the number of peaks in a histogram. The first case includes three-peak histograms that possess two valid thresholds. In this case, the oil area can be inferred by synthesizing two binarized images obtained using those threshold values from an image converted into the hue. If the number of peaks obtained from the hue histogram is either one or more than three, a further analysis is required. The saturation histogram is further analyzed in this case. With two peaks, binarization by saturation is first performed, and the result is combined with that of the hue histogram. Otherwise, the lightness histogram should also be analyzed. If two peaks occur in the lightness histogram, the oil area can be estimated as a result of binarization. Table 5 lists the binarized results for all of the oil spill images analyzed in this study.

3.5. GUI Design

The initial screen of the GUI system for implementing the developed algorithm is shown in Fig. 14. The area ratio of the image extracted from the binarized result is recorded below the original image. If the user knows the scale of an input image, then the actual area of the image can be computed. The area calculation is based on a pixel-millimeter conversion, and the scale can be calculated using the aerial altitude where the camera is positioned.

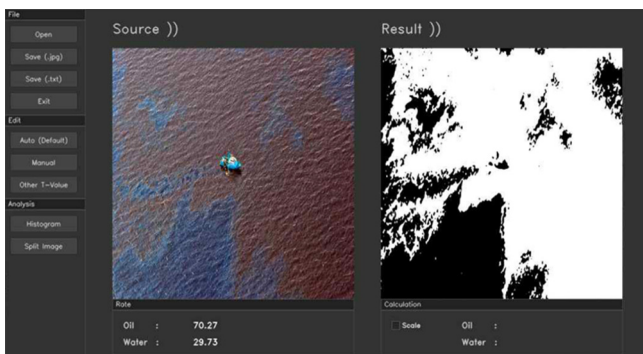


Fig. 14 Initial screen of developed system

4. Conclusions

An algorithm for rapidly estimating oil spills at sea was introduced. SAR images, which have been widely used, can be used to produce accurate data; however, the difficulty in promptly accessing an accident site is disadvantageous. The purpose of this study was to suggest a method to analyze an oil spill site quickly using a digital image.

Binarization was performed by sequentially considering the hue, saturation, and lightness of an oil spill image. Color is an important factor that indicates the thickness of the spilled oil. Because an oil film is typically black, brown, or orange, the color can be used to differentiate an oil spill area from the surrounding seawater. If

separation by color is difficult or not applicable, additional image binarizations are performed by examining other characteristics of the image, such as the saturation or lightness.

Using the algorithm proposed in this paper, oil spill areas could be estimated quickly, and oil accident sites could be controlled.

Acknowledgments

The authors would like to thank the Ministry of Trade, Industry, and Energy of Korea for their financial support through the projects, “Education program in design and regulation experts in autonomous ships (KITECH 2019-0259-01)” and “Development of master data system of lead time for precision enhancement of shipbuilding production management (project ID: 20000208).”

References

- Bradley, D., & Roth, G. (2007). Adaptive Thresholding Using the Integral Image. *Journal of Graphic Tools*, 12(2), 13-21. <https://doi.org/10.1080/2151237X.2007.10129236>
- Fiscella, B., Giancaspro, A., Nirchi, F., Pavese, P., & Trivero, P. (2000). Oil Spill Detection Using Marine SAR Images. *International Journal of Remote Sensing*, 21(18), 3561-3566. <https://doi.org/10.1080/014311600750037589>
- International Petroleum Industry Environmental Conservation Association (IPIECA). (2016). Aerial Observation of Oil Spills at Sea. Retrieved 25 August 2019 from <http://www.ipieca.org/resources/good-practice/aerial-observation-of-oil-spills-at-sea>
- International Tanker Owners Pollution Federation Limited (ITOPF). (2014). Documents & Guides. Retrieved 12 March 2019 from <https://www.itopf.org/kr/knowledge-resources/documents-guides>
- Kim, T., Park, K., Lee, M., Park, J., Hong, S., Kim, K., & Chang, E. (2013). Application of Bimodal Histogram Method to Oil Spill Detection from a Satellite Synthetic Aperture Radar Image. *Korean Journal of Remote Sensing*, 29(6), 645-655. <https://doi.org/10.7780/kjrs.2013.29.6.7>
- National Oceanic and Atmospheric Administration (NOAA). (2016). How Do We Use Satellite Data During Oil Spills? Retrieved 27 February 2019 from <https://response.restoration.noaa.gov/about/media/how-do-we-use-satellite-data-during-oil-spills.html>
- Open Source Computer Vision (OpenCV). (2019). Online Documentation. Retrieved 18 September 2019 from <https://docs.opencv.org>
- Otsu, N. (1979). A Threshold Selection Method from Gray-level Histograms. *IEEE Transactions on Systems, Man, and Cybernetics*, 9(1), 62-66. <https://doi.org/10.1109/tsmc.1979.4310076>
- Gonzalez, R., & Woods, R. (2017). *Digital Image Processing*. 4th Edition, Pearson.

Petrou, M., & Petrou, C. (2010). *Image Processing: the Fundamentals*. John Wiley and Sons.

Schvartzman, I., Havivi, S., Maman, S., Rotman, S., & Blumberg, D. (2016). Large Oil Spill Classification Using SAR Images Based on Spatial Histogram. *The International Archives of the Photogrammetry, Remote Sensing and Spatial Information Sciences*, XLI-B8, 1183-1186. <https://doi.org/10.5194/isprsarchives-XLI-B8-1183-2016>

Topouzelis, K.N. (2008). Oil Spill Detection by SAR Images: Dark Formation Detection, Feature Extraction and Classification Algorithms. *Sensors*, 8(10), 6642-6659. <https://doi.org/10.3390/s8106642>

Xu, L., Shafiee, M., Wong, A., Li, F., Wang, L., & Clausi, D. (2015). Oil Spill Candidate Detection from SAR Imagery Using a Thresholding-Guided Stochastic Fully Connected Conditional Random Field Model. *Proceedings of IEEE*

Conference on Computer Vision and Pattern Recognition Workshops, 79-86.

Author ORCIDs and Contributions

Author name	ORCID	Contributions
Jang, Hye-Jin	0000-0003-1822-0100	②③
Nam, Jong-Ho	0000-0002-9613-477X	①④⑤

- ① Conceived of the presented idea or developed the theory
- ② Carried out the experiment or collected the data
- ③ Performed the analytic calculations or numerical simulations
- ④ Wrote the manuscript
- ⑤ Supervised the findings of this study



Title of Article

Firstname Lastname¹, Firstname Lastname² and Firstname Lastname³

¹Professor, Department of OO, OO School, OO University, Busan, Korea

²Graduate Student, Department of OO, OO University, Seoul, Korea

³Senior Researcher, Department of OO, OO Engineering. Corp., Seoul, Korea

KEY WORDS: Lumped mass line model, Explicit method, Steel lazy wave riser (Immediately after the abstract, provide a maximum of 5 or 6 keywords.)

ABSTRACT: A concise and factual abstract is required. The abstract should state briefly the purpose of the research, the principal results and major conclusions. An abstract should be written in around 300 words and is often presented separately from the article, so it must be able to stand alone. For this reason, References should be avoided, but if essential, then cite the author(s) and year(s). Also, non-standard or uncommon abbreviations should be avoided, but if essential they must be defined at their first mention in the abstract itself.

Nomenclature

<i>I</i> TOC	Increment of total operating cost (\$/yr)
<i>L</i> HV	Lower heating value (kJ/kg)
<i>P</i> w	Power (kW)
<i>T</i>	Temperature (K)
<i>V</i>	Volume (m ³)
ρ	Density (kg/m ³)

1. Introduction

The introduction should briefly place the study in a broad context and highlight why it is important. It should define the purpose of the work and its significance. The current state of the research field should be reviewed carefully and key publications cited. Please highlight controversial and diverging hypotheses when necessary. Finally, briefly mention the main aim of the work and highlight the principal conclusions. As far as possible, please keep the introduction comprehensible to scientists outside your particular field of research.

2. General Information for Authors

2.1 Requirement for Membership

One of the authors who submits a paper or papers should be member of

The Korea Society of Ocean Engineers (KSOE), except a case that editorial board provides special admission of submission.

2.2 Publication type

Manuscript is made up of scholarly monographs, technical reports and data. The paper should have not been submitted to other academic journal. Conference papers, research reports, dissertations and review articles can be submitted to Journal Of Ocean Engineering and Technology (JOET). When part or whole of a paper was already published to conference papers, research reports, dissertations, and review articles, then corresponding author should note it clearly in the manuscript. After published to JOET, the copyright of manuscript belongs to KSOE.

(example) It is noted that this paper is revised edition based on proceedings of KAOST 2100 in Jeju.

2.3 Manuscript submission

Manuscript should be submitted through the on-line manuscript website (<http://www.joet.org>). The date that corresponding author submits a paper through on-line website is official date of submission. Other correspondences can be sent by an email to the Editor in Chief. The manuscript must be accompanied by a signed statement that it has been neither published nor currently submitted for publication elsewhere. The manuscript should be written in English or Korean and a

Received 00 February 2100, revised 00 October 2100, accepted 00 October 2100

Corresponding author Firstname Lastname: +82-51-759-0656, e-mail@e-mail.com

It is a recommended paper from the proceedings of 2019 spring symposium of the Korea Marine Robot Technology (KMRTS).

© 2100, The Korean Society of Ocean Engineers

This is an open access article distributed under the terms of the creative commons attribution non-commercial license (<http://creativecommons.org/licenses/by-nc/4.0>) which permits unrestricted non-commercial use, distribution, and reproduction in any medium, provided the original work is properly cited.

minimum standard of the proficiency in the English or Korean language should be met before submission to the editorial office.

Ensure that online submission or submission by e-mail text files are in a standard word processing format (Hangul or MS Word are preferred). Ensure that graphics are high-resolution. Be sure all necessary files have been uploaded/attached.

2.3.1 Author's checklist and Transfer of copyright

Author's checklist and Transfer of copyright can be found in submission homepage (<http://www.joet.org>).

2.4 Research and Publication Ethics

Authorship should be limited to those who have made a significant contribution to the conception, design, execution, or interpretation of the reported study. All those who have made significant contributions should be listed as co-authors. Where there are others who have participated in certain substantive aspects of the research project, they should be acknowledged or listed as contributors.

The corresponding author should ensure that all appropriate co-authors and no inappropriate co-authors are included on the paper, and that all co-authors have seen and approved the final version of the paper and have agreed to its submission for publication.

If the work involves chemicals, procedures or equipment that have any unusual hazards inherent in their use, the author must clearly identify these in the manuscript. If the work involves the use of animal or human subjects, the author should ensure that the manuscript contains a statement that all procedures were performed in compliance with relevant laws and institutional guidelines and that the appropriate institutional committee(s) has approved them. Authors should include a statement in the manuscript that informed consent was obtained for experimentation with human subjects. The privacy rights of human subjects must always be observed.

When an author discovers a significant error or inaccuracy in his/her own published work, it is the author's obligation to promptly notify the journal editor or publisher and cooperate with the editor to retract or correct the paper. If the editor or the publisher learns from a third party that a published work contains a significant error, it is the obligation of the author to promptly retract or correct the paper or provide evidence to the editor of the correctness of the original paper.

3. Manuscript

Manuscript must consist of as follow: (1) Title, (2) Author's information (include title), (3) Key word, (4) Abstract, (5) Nomenclature description, (6) Introduction, (7) Body (analysis, test, results and discussion), (8) Conclusion, (9) Acknowledgements, (10) Reference, (11) Appendix, etc.

3.1 Unit

Use the international system units(SI). If other units are mentioned, please give their equivalent in SI.

3.2 Equations

All mathematical equations should be clearly printed/typed using well accepted explanation. Superscripts and subscripts should be typed clearly above or below the base line. Equation numbers should be given in Arabic numerals enclosed in parentheses on the right-hand margin. They should be cited in the text as, for example, Eq. (1), or Eqs. (1)-(3).

$$G_{GEV}(x;\mu,\sigma,\xi) = \begin{cases} \exp[-(1+\xi(x-\mu)/\sigma)^{-1/\xi}] & \xi \neq 0 \\ \exp[-\exp(-(x-\mu)/\sigma)] & \xi = 0 \end{cases} \quad (1)$$

in which μ , σ , and ξ represent the location ("Shift" in figures), scale, and shape parameters, respectively.

3.3 Tables

Tables should be numbered consecutively with Arabic numerals. Each table should be typed on a separate sheet of paper and be fully titled. All tables should be referred to in the text.

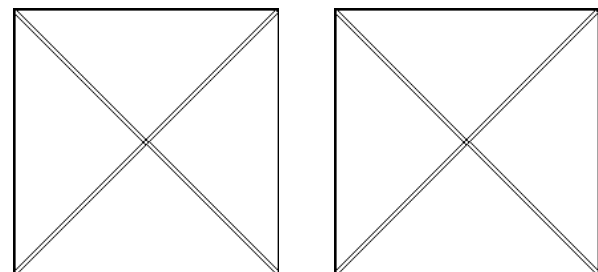
Table 1 Tables should be placed in the main text near to the first time they are cited

Item	Buoyancy riser
Segment length ¹ (m)	370
Outer diameter (m)	1.137
Inner diameter (m)	0.406
Dry weight (kg/m)	697
Bending rigidity (N·m ²)	1.66E8
Axial stiffness (N)	7.098E9
Inner flow density (kg·m ³)	881
Seabed stiffness (N/m ²)	6,000

¹Tables may have a footer.

3.4 Figures

All the illustrations should be of high quality meeting with the publishing requirement with legible symbols and legends. In preparing the illustrations, authors should consider a size reduction during the



(a) Description of what is contained in the first panel

(b) Description of what is contained in the first panel

Fig. 1 Schemes follow the same formatting. If there are multiple panels, they should be listed as: (a) Description of what is contained in the first panel; (b) Description of what is contained in the second panel. Figures should be placed in the main text near to the first time they are cited

printing process to have acceptable line clarity and character sizes. All figures should have captions which should be supplied on a separate sheet. They should be referred to in the text as, for example, Fig. 1, or Figs. 1-3.

3.5 How to describe the references in main texts

All references should be listed at the end of the manuscripts, arranged in order of Alphabet. The exemplary form of listed references is as follows:

- Single author: (Kim, 1998) or Kim (1998)
- Two authors: (Kim and Lee, 2000) or Kim and Lee (2000)
- Three or more authors: (Kim et al., 1997) or Kim et al. (1997)
- Two or more papers: (Lee, 1995a; Lee, 1995b; Ryu et al., 1998)
- Year unknown: (Kim, n.d.) or Kim (n.d.)

4. Conclusions

.....

Acknowledgments

Please add: "This research was funded by Name of Funder, grant number XXX" and "The OOO was funded by XXX". Check carefully that the details given are accurate and use the standard spelling of funding agency names at <https://search.crossref.org/funding>

In this section you can acknowledge any support given which is not covered by the author contribution or funding sections. This may include administrative and technical support, or donations in kind (e.g., materials used for experiments).

References

- Journal name should not be abbreviated.
- A private report with limited access or download availability can not be a reference.
- Include the digital object identifier DOI or URL for all references where available.

Referring to journal publications:

- Author, A.A., Author, B.B., & Author, C.C. (Year). Title of Article. Journal Title, vol(no), pp-pp. <https://doi.org/xx.xxxx/xxxxxx>
- Author, A.A., Author, B.B., Author, C.C. (accepted; in press). Title of Article. Title of Periodical. Retrieved from <http://xx.xxx/x.pdf>
- Lee, T.K., Kim, T.W., Rim, C.W., & Kim, S.C. (2013). A Study on Calculation of Local Ice Pressures for ARAON Based on Data Measured at Arctic Sea. Journal of Ocean Engineering and Technology, 27(5), 88-92. <https://doi.org/10.5574/KSOE.2013.27.5.088>
- Lee, T.K., Kim, T.W., Rim, C.W., & Kim, S.C. (accepted; in press). A Study on Calculation of Local Ice Pressures for ARAON Based on Data Measured at Arctic Sea. Journal of Ocean Engineering and Technology, Retrieved from <http://xxx.xxx/xxx.pdf>

Referring to conference proceedings:

- Author, A.A., Author, B.B., & Author, C.C. (Year). Title of Article. Proceeding Title, City, Country, pp-pp. <https://doi.org/xx.xxxx>
- Aoki, S., Liu, H., & Sawaragi, T. (1994). Wave Transformation and Wave Forces on Submerged Vertical Membrane. Proceedings of International Symposium Waves - Physical and Numerical Modeling, Vancouver, Canada, 1287-1296.
- Tsukamoto, C.L., Lee, W., Yuh, J., Choi, S.K., & Lorentz, J. (1997). Comparison Study on Advanced Thruster Control of Underwater Robots. Proceedings of International Conference on Robotics and Automation, 1845-1850. <https://doi.org/110.1109/ROBOT.1997.619056>

Referring to books:

- Author, A.A. (Year). Title of Book (xx ed.). Location: Publisher.
- Strunk, W., & White, E.B. (2000). The Elements of Style (4th ed.). New York, USA: Longman.
- Schlichting, H. (1968). Boundary Layer Theory (6th ed.). New York, USA: McGraw-Hill.

Referring to theses or dissertations:

- Author, A.A. (Year). Title of Doctoral Dissertation or Master's thesis (Doctoral Dissertation or Master's thesis). Name of Institution, City, Country.
- Giovanni, I. (1998). Modelling and Identification of Underwater Robotic Systems (Ph.D. Thesis). University of Genova, Genova, Italy.

Referring to technical reports, rules, or guidelines:

- Author, A.A. (Year). Title of report (Reprot No. xxx), Location: Publisher.
- Likhomanov, V. (2010). Full-Scale Ice Trials of the Korean Research Icebreaker ARAON. Daejeon, Korea: Arctic and Antarctic Research Institute (AARI).
- ABS. (2011). Guide for Ice Loads Monitoring Systems. Houston, USA: American Bureau of Shipping.
- Lloyd's Register. (2011). FDA ICE Fatigue Induced by Ice Loading, ShipRight Design and construction - Fatigue Design Assesment. London, United Kingdom: Lloyd's Register.
- Larson, M., & Kraus, N.C. (1989). SBEACH: Numerical Model for Simulating Storm-Induced Beach Change - Report 1 Empirical Foundation and Model Development (Technicla Report CERC-89-9). Coastal Engineering research center Vicksburg Ms.

Referring to patents:

- Righsholder, A.A. (Year). Title of Patent. Patent number, Patent office with country.
- Dawoo Shipbulding & Maringe Engineering (DSME). (2013). Distance Length Standardization Method for Preventing Interference at the time of Uploading Cell Guide of Container Ship. Unexamined Patent Publication 1020130044635, Korean Interlllectual Property Office.

Referring to websites:

- Righsholder, A.A. (Year). Title of webpage. Retrieved Month Year from <http://xxxx>
- International Association of Classification Societies (IACS). (2010a).

Common Structural Rules for Bulk Carriers. Retrieved July 2010 from <http://www.iacs-data.org.uk>

US Congressional Hearing. (2009). Strategic Importance of the Arctic in Us Policy. Retrieved June 2019 from <https://fas.org/irp/arctic.pdf>

Dawoo Shipbuilding & Maringe Engineering (DSME). (2013). Distance Length Standardization Method for Preventing Interference at the time of Uploading Cell Guide of Container Ship. Retrieved June 2019 from <https://patentimages.storage./pdfs/792.pdf>

Referring to software:

Righsholder, A.A. (Year). Title of Software. Downloaded Month Year from <http://xxxx>

Referring to some exceptional cases:

- when authors are missing, institution can replace authors

National Oceanic and Atmospheric Administration (NOAA). (2015). Deep-ocean Assessment and Reporting of Tsunamis (DART). Retrieved December 2019 from <https://nctr.pmel.noaa.gov/Dart/>

- when dates or years are missing, it is replaced with "n.d."

National Oceanic and Atmospheric Administration (NOAA). (n.d.). Deep-ocean Assessment and Reporting of Tsunamis (DART).

- when more than seven authors, first 6 authors ... last author.

Yeu, T., Choi, H.T., Lee, Y., Chae, J., Lee, Y., Kim, S.S., ... Lee, T.H. (2019). Development of Robot Platform for Autonomous Underwater Intervention. *Journal of Ocean Engineering and Technology*, 33(2), 168-177. <https://doi.org/10.26748/KSOE.2019.021>

Appendix

The appendix is an optional section that can contain details and data supplemental to the main text. For example, explanations of experimental details that would disrupt the flow of the main text, but nonetheless remain crucial to understanding and reproducing the research shown; figures of replicates for experiments of which representative data is shown in the main text can be added here if brief, or as Supplementary data. Mathematical proofs of results not central to the paper can be added as an appendix.

All appendix sections must be cited in the main text. In the appendixes, Figures, Tables, etc. should be labeled starting with 'A', e.g., Fig. A1, Fig. A2, etc.

Examples:

<https://doi.org/10.26748/KSOE.2019.022>

<https://doi.org/10.26748/KSOE.2018.4.32.2.095>

Author ORCIDs and Contributions

Author name	ORCID	Contributions
So, Hee	0000-0000-000-00X	①②③
Park, Hye-Il	0000-0000-000-00X	④
Yoo, All	0000-0000-000-00X	⑤
Jung, Jewelry	0000-0000-000-00X	⑤

① Conceived of the presented idea or developed the theory

② Carried out the experiment or collected the data

③ Performed the analytic calculations or numerical simulations

④ Wrote the manuscript

⑤ Supervised the findings of this study

General Information for Authors

Requirement for Membership

One of the authors who submits a paper or papers should be member of KSOE, except a case that editorial board provides special admission of submission.

Publication type

Manuscript is made up of scholarly monographs, technical reports and data. The paper should have not been submitted to other academic journal. Conference papers, research reports, dissertations and review articles can be submitted to JOET. When part or whole of a paper was already published to conference papers, research reports, dissertations, and review articles, then corresponding author should note it clearly in the manuscript. After published to JOET, the copyright of manuscript belongs to KSOE. (example) It is noted that this paper is revised edition based on proceedings of KAOST 2010 in Jeju.

Manuscript submission

Manuscript should be submitted through the on-line manuscript website (<http://www.joet.org>). The date that corresponding author submits a paper through on-line website is official date of submission. Other correspondences can be sent by an email to the Editor in Chief. The manuscript must be accompanied by a signed statement that it has been neither published nor currently submitted for publication elsewhere. The manuscript should be written in English or Korean and a minimum standard of the proficiency in the English or Korean language should be met before submission to the editorial office.

Ensure that online submission or submission by e-mail text files are in a standard word processing format (Hangul or MS Word are preferred). Ensure that graphics are high-resolution. Be sure all necessary files have been uploaded/attached.

Submission checklist

See 'Authors' checklist' for details.

Research and Publication Ethics

Authorship of the paper

Authorship should be limited to those who have made a significant contribution to the conception, design, execution, or interpretation of the reported study. All those who have made significant contributions should be listed as co-authors. Where there are others who have participated in certain substantive aspects of the research project, they should be acknowledged or listed as contributors.

The corresponding author should ensure that all appropriate co-authors and no inappropriate co-authors are included on the paper, and that all co-authors have seen and approved the final version of the paper and have agreed to its submission for publication.

Hazards and human or animal subjects

If the work involves chemicals, procedures or equipment that have any

unusual hazards inherent in their use, the author must clearly identify these in the manuscript. If the work involves the use of animal or human subjects, the author should ensure that the manuscript contains a statement that all procedures were performed in compliance with relevant laws and institutional guidelines and that the appropriate institutional committee(s) has approved them. Authors should include a statement in the manuscript that informed consent was obtained for experimentation with human subjects. The privacy rights of human subjects must always be observed.

Fundamental errors in published works

When an author discovers a significant error or inaccuracy in his/her own published work, it is the author's obligation to promptly notify the journal editor or publisher and cooperate with the editor to retract or correct the paper. If the editor or the publisher learns from a third party that a published work contains a significant error, it is the obligation of the author to promptly retract or correct the paper or provide evidence to the editor of the correctness of the original paper.

Article structure

Manuscript must consist of as follow : (1)Title, (2)Author's name, (3)Key word, (4)Abstract, (5)Nomenclature description, (6)Introduction, (7)Body (analysis, test, results and discussion, (8)Conclusion, (9)Acknowledgements, (10)Reference, (11)Appendix, etc.

Abstract

A concise and factual abstract is required. The abstract should state briefly the purpose of the research, the principal results and major conclusions. An abstract should be written in around 300 words and is often presented separately from the article, so it must be able to stand alone. For this reason, References should be avoided, but if essential, then cite the author(s) and year(s). Also, non-standard or uncommon abbreviations should be avoided, but if essential they must be defined at their first mention in the abstract itself.

Keywords

Immediately after the abstract, provide a maximum of 5 or 6 keywords.

Unit

Use the international system units(SI). If other units are mentioned, please give their equivalent in SI.

Equations

All mathematical equations should be clearly printed/typed using well accepted explanation. Superscripts and subscripts should be typed clearly above or below the base line. Equation numbers should be given in Arabic numerals enclosed in parentheses on the right-hand margin. They should be cited in the text as, for example, Eq. (1), or Eqs. (1)-(3).

Tables

Tables should be numbered consecutively with Arabic numerals. Each table should be typed on a separate sheet of paper and be fully titled. All tables should be referred to in the text.

Figures

All the illustrations should be of high quality meeting with the publishing requirement with legible symbols and legends. In preparing the illustrations, authors should consider a size reduction during the printing process to have acceptable line clarity and character sizes. All figures should have captions which should be supplied on a separate sheet. They should be referred to in the text as, for example, Fig. 1, or Figs. 1-3.

Reference

All references should be listed at the end of the manuscripts, arranged in order. The exemplary form of listed references is as follows :

- 1) Single author : (Kim, 1998)
- 2)Two authors: (Kim and Lee, 2000)
- 3) Three or more authors: (Kim et al., 1997)
- 4) Two or more paper: (Lee, 1995; Ryu et al., 1998)

References, including those pending publications in well-known journals or pertaining to private communications, not readily available to referees and readers will not be acceptable if the understanding of any part of any part of the submitted paper is dependent upon them. Single or two authors can be referred in the text; three or more authors should be shortened to the last name of the first author, like smith et al.

Examples:

Reference to a journal publication:

Cho, I.H. and Kim, M.H., 1998. Interactions of a Horizontal Flexible Membrane with Oblique Waves. *Journal of Fluid Mechanics*, 356(4), 139-161.

Van der Geer, J., Hanraads, J.A.J., and Lupton, R.A., 2010. The Art of Writing a Scientific Article. *Journal of Science Communication*. 163, 51-59.

Reference to a book:

Strunk, W. and White, E.B., 2000. *The Elements of Style*, 4th Edition, Longman, New York.

Schlichting, H., 1968. *Boundary Layer Theory*. 6th Edition, McGraw-Hill, New York.

Reference to a proceeding:

Aoki, S., Liu, H. and Sawaragi, T., 1994. Wave Transformation and Wave Forces on Submerged Vertical Membrane. *Proceedings of International Symposium Waves - Physical and Numerical Modeling*, Vancouver Canada, 1287-1296.

Reference to a website:

International Association of Classification Societies (IACS), 2010a. Common Structural Rules for Bulk Carriers. [Online] (Updated July 2010) Available at: <http://www.iacs-data.org.uk/> [Accessed August 2010].

Journal abbreviations

Journal names should not be abbreviated.

Revised manuscripts

Manuscripts reviewed that require revision should be revised and uploaded with a response to the reviewer's comment at JOET editorial manger within two months. Otherwise, the manuscript will be considered as a new manuscript when and if it is resubmitted.

Proofs and reprints

Galley proofs will be provided as a PDF file to the author with reprint order and copyright transfer form. The author should return the corrected galley proofs within a week with the signed reprint order and copyright transfer form. Attention of the authors is directed to the instructions which accompany the proof, especially the requirement that all corrections, revisions, and additions be entered on the proofs and not on the manuscripts. Proofs should be carefully checked and returned to the JOET editorial office by e-mail if the changes are minimal. If the changes are extensive, proofs should be returned by fax only. Substantial changes in an article at this stage may be made at the author's expense. The reprint request form must be returned with the proof. Reprints should be made at the author's expense.

Peer review

Every manuscript received is circulated to three peer reviewers. The author's name and affiliation is disclosed during review process to reviewers. The review process can be repeated till three times if the request of revision is suggested by reviewers. If the re-review is repeated more than three times, it may not be considered for publication. If two reviewers do not agree to accept the journal, it may not be also considered for publication. Usually the first review process ends within one month. Statistical Review: If there are any complicated statistical analyses in the manuscript, it may be reviewed by statistical editor.

Manuscript Editing: The finally accepted manuscript will be reviewed by manuscript editor for the consistency of the format and the completeness of references. The manuscript may be revised according to the opinion of the manuscript editor.

Page charge

The charge per a paper for the publication is 150,000KRW (Express review service : 300,000KRW) up to 6 pages. Extra rate, 30,000KRW per page, will be charged for more than 6 pages. Page charge include forty copies of offprints. Offprints in color pages or extra copies of offprints will require actual expenses. The charge per a paper for the paper review is 40,000KRW. Rate for the express review service is 240,000KRW.

Editing checklist

See 'Authors' checklist' for details.

Transfer of copyright

Transfer of copyright can be found in submission homepage (<http://www.joet.org>).

Authors' Checklist

The following list will be useful during the final checking of an article prior to sending it to the journal for review. Please submit this checklist to the KSOE when you submit your article.

< Editing checklist >

- I checked my manuscript has been 'spell-checked' and 'grammar-checked'.
나의 원고에 오타 및 문법적 오류가 있는지 확인하였습니다.

One author has been designated as the corresponding author with contact details such as

- E-mail address
 - Phone numbers
- 최소한 한명의 저자는 교신저자로 지정되었으며, 다음의 연락처가 표기되었습니다.
- 이메일 주소
 - 전화 번호

I checked abstract 1) stated briefly the purpose of the research, the principal results and major conclusions, 2) was written in around 300 words, and 3) did not contain references (but if essential, then cite the author(s) and year(s)).

- 나는 초록이 1) 간결하게 연구의 목적, 주요 결과 및 결론을 포함하고 있음을 확인하였으며, 2) 300단어 내외의 단어로 구성되었음을 확인하였으며, 3) 참고문헌을 포함하고 있지 않음을 확인하였습니다 (꼭 필요시 참고문헌 삽입 가능).

- I provided 5 or 6 keywords.
나는 5-6개의 키워드를 사용하였습니다.

I checked manuscript consisted of as follow: 1) Title, 2) Author's name, 3) Key word, 4) Abstract, 5) Nomenclature description, 6) Introduction, 7) Body (analysis, test, results and discussion), 8) Conclusion, 9) Acknowledgements,

- 10) Reference, 11) Appendix, etc.
나는 원고가 다음의 순서로 구성되었음을 확인하였습니다: 1) 제목, 2) 저자명, 3) 키워드, 4) 초록, 5) 기호, 6) 서론, 7) 본문 (해석, 실험, 결과, 검토), 8) 결론, 9) 후기(사사), 10) 참고문헌, 11) 부록, 등.

I checked color figures were clearly marked as being intended for color reproduction on the Web and in print, or to be reproduced in color on the Web and in black-and-white in print.

- 나는 모든 컬러 그림이 컬러 웹이 또는 컬러(또는 흑백) 인쇄물에 잘 나타날 수 있도록 선명한 그림을 사용하였음을 확인하였습니다.

- I checked all table and figure captions were written in English.
나는 원고의 모든 표 제목과 그림 제목은 영문으로 작성되었음을 확인하였습니다.

- I checked all table and figure numbered consecutively in accordance with their appearance in the text.
나는 본문에서 나타나는 순서대로 표 번호 및 그림 번호가 지정되었음을 확인하였습니다.

I checked abbreviations were defined at their first mention there and used with consistency throughout the article.

- 나는 영문 약자를 원고의 첫 번째 사용에서 정의하였으며, 이후 원고에서는 동일한 약자를 사용하였음을 확인하였습니다.

- I checked that references were in the correct format for the journal (See 'Guide for Authors' for details).
나는 모든 참고문헌이 본 저널의 참고문헌 표기법(저자 가이드 참조)에 따라서 작성되었음을 확인하였습니다.

I checked all references mentioned in the Reference list were cited in the text, and vice versa.

- 나는 'References'에 존재하는 모든 참고문헌은 원고 본문에서 언급되었으며, 반대로 원고 본문에 언급된 모든 참고문헌은 'References'에 표기되었음을 확인하였습니다.

- I checked I used the international system units (SI) or SI-equivalent engineering units.
나는 SI 단위계 또는 공학적으로 인정되어지는 단위계를 사용하였음을 확인하였습니다.

< **Submission checklist** >

- I checked the work described has not been published previously (except in the form of an abstract or as part of a published lecture or academic thesis).
나는 본 원고의 내용이 초록, 단행본, 학위논문 등을 제외한 타 저널 등에 게재된 사실이 없음을 확인하였습니다.

- I checked when the work described has been published previously in other proceedings without copyright, it has clearly noted in the text.
나는 본 원고의 내용이 판권이 없는 프로시딩에 게재되었던 경우 이를 원고에서 명시하였음을 확인하였습니다.

- I checked permission has been obtained for use of copyrighted material from other sources (including the Web)
나는 웹을 포함하여 판권이 있는 자료의 사용 허가를 득했습니다.

- I have processed Plagiarism Prevention Check through reliable web sites such as www.kci.go.kr, <http://www.ithenticate.com/>, or <https://www.copykiller.org/> for my submission.
나는 논문 표절 유사도 검사를 마친 후 투고하였습니다.

- I agree that final decision for my final manuscript can be changed according to results of Plagiarism Prevention Check by JOET administrator.
나의 최종본 논문에 대한 JOET 자체적인 논문 표절 유사도 검토 결과에 따라 최종 판정이 변경될 수 있다는 사실에 동의합니다.

- I checked minimum one author is member of the Korean Society of Ocean Engineers.
나는 저자 중 1인 이상이 한국해양공학회 회원임을 확인하였습니다.

- I agreed all policies related to 'Ethical Code of Research' and 'Research and Publication Ethics' of the Korean Society of Ocean Engineers.
나는 연구출판정책과 연구윤리규정을 확인했으며, 준수할 것을 서약합니다.

- I agreed to transfer copyright to the publisher as part of a journal publishing agreement and this article will not be published elsewhere including electronically in the same form, in English or in any other language, without the written consent of the copyright-holder.
나는 한국해양공학회지의 저작권 정책에 동의하며, 저작권 위임동의서를 제출하겠습니다.

- I made a payment for reviewing of the manuscript, and I will make a payment for publication on acceptance of the article.
나는 심사료를 납부하였으며, 논문 게재 확정 후 게재료를 납부하겠습니다.

- I have read and agree to the terms of Author's Checklist.
나는 저자 체크리스트 모든 조항을 검토하였으며, 모든 조항에 동의합니다.

Title of article :

Date of submission : DD/MM/YYYY

Corresponding author : signature

Email address :

※ Print and sign completed form. Fax(+82 51 759 0657) or E-mail scanned file to ksoehj@ksoe.or.kr

Research and Publication Ethics

Authorship of the paper

Authorship should be limited to those who have made a significant contribution to the conception, design, execution, or interpretation of the reported study. All those who have made significant contributions should be listed as co-authors. Where there are others who have participated in certain substantive aspects of the research project, they should be acknowledged or listed as contributors.

The corresponding author should ensure that all appropriate co-authors and no inappropriate co-authors are included on the paper, and that all co-authors have seen and approved the final version of the paper and have agreed to its submission for publication.

Hazards and human or animal subjects

If the work involves chemicals, procedures or equipment that have any unusual hazards inherent in their use, the author must clearly identify these in the manuscript. If the work involves the use of animal or human subjects, the author should ensure that the manuscript contains a statement that all procedures were performed in compliance with relevant laws and institutional guidelines and that the appropriate institutional committee(s) has approved them. Authors should include a statement in the manuscript that informed consent was obtained for experimentation with human subjects. The privacy rights of human subjects must always be observed.

Fundamental errors in published works

When an author discovers a significant error or inaccuracy in his/her own published work, it is the author's obligation to promptly notify the journal editor or publisher and cooperate with the editor to retract or correct the paper. If the editor or the publisher learns from a third party that a published work contains a significant error, it is the obligation of the author to promptly retract or correct the paper or provide evidence to the editor of the correctness of the original paper.

Ethical Codes of Research

for The Korean Society of Ocean Engineers [1, Nov. 2008 amended]

All members of The Korean Society of Ocean Engineers, by observing the following codes of conduct and regulations regarding research in the field, will contribute to the development of ocean engineering and the security and prosperity of the society and the nation, thus holding our honesty, reputation and authority in the highest standards.

A. Foundational Spirit

1. We make a contribution to mutual prosperity of mankind through ocean development, using the knowledge and technique in the field of ocean engineering.
2. We contribute to fostering the good spirit of citizenship by conducting responsible research.
3. We make efforts to enhance our authority and competitiveness as experts in ocean engineering.

B. Fundamental Canons

1. We consider the public security and welfare as a top priority and conform to the principle of sustainable use of ocean in conducting our research.
2. We promote professional development through performing proper research and provide young researchers with the opportunities to develop professionally.

3. We respect the public values such as honesty, accuracy, efficiency and objectivity in offering services such as providing expertise or disclosing research results.
4. We do not have unfair competitions with others and solve problems with objective information and processes when there is a clash of interests.
5. We raise common issues only through objective and fair methods.

C. Practical Platforms

1. We consider the public security and welfare as a top priority and conform to the principle of sustainable use of ocean in conducting our research.
 - (a) We must acknowledge the fact that the life, security, health and welfare of the public have an absolute reliance over our products such as structures, equipments and machines that are given thought to and made into decision by engineers.
 - (b) We must not propose or approve research plans which cause harm to the public health and welfare.
 - (c) We must conform to the principle of sustainable use of ocean to enhance the quality of the public life and endeavor to improve the ocean environment.
2. We promote professional development through performing proper research and provide young researchers with the opportunities to develop professionally.
 - (a) As we build our career, we must continue to acquire new knowledge and promote intellectual development by keeping track of research results, organizing research methods and raising necessary issues voluntarily.
 - (b) We must be thoroughly honest to the contributions from cooperators, competitors and predecessors and utilize them for our professional development.
 - (c) We, as administrators, must supervise young researchers in a fair manner and, as their advisors, must assist them sincerely to grow into socially recognized members.
3. We respect the public values such as honesty, accuracy, efficiency and objectivity in offering services such as providing expertise or disclosing research results.
 - (a) When we offer service under our responsibility that involves providing professional knowledge, we must act according to professionalism as a commissioner, trying to prevent waste of resources and reporting objective facts, trustworthy data and accurate research results.
 - (b) We prohibit any fraudulent acts in conducting research such as fabrications, forgeries and plagiarism.
 - (c) We must admit our mistakes or errors when they are verified and must not try to justify them by distorting facts or data.
4. We do not have unfair competitions with others and solve problems with objective information and processes when there is a clash of interests.
 - (a) We must not distort the professional, academical qualifications of ourselves and coworkers. We must not fabricate or exaggerate our positions or authorities of the past achievements.
 - (b) Our papers must contain facts and no exaggeration that are contributed to media sources. When publishing a paper or a report which involves multiple researchers, we must allocate authors based on their levels of contributions and mention every person and institution that is concerned and provided assistance.
 - (c) We must not criticise others' achievements in an irresponsible manner by intentionally distorting their professional reputation, prospects and character in both direct and indirect ways.
 - (d) When a clash of interests occur, we must organize a committee composed of authoritative experts in the field and fairly solve the problem based on objective facts and data.
5. We raise common issues only through objective and fair methods.
 - (a) We must be thoroughly objective and honest when submitting expert reports or policy proposals and include relevant, sufficient and appropriate information.

- (b) When addressing public issues through open debates or forums, we must provide opinions based on objective facts and data and must not cause harm to the public interest by making groundless argument or being involved in private interests with others.
 - (c) We must be honest when explaining our business and its advantages, and must not try to meet our interests by damaging professional honor and coordination with coworkers.
6. All members of The Korean Society of Ocean Engineers must abide by the ethical codes of research stated above.

D. The Scope of Manuscript

1. Manuscripts include papers, technical reports and commentaries, and papers must be the ones that are not released in other journals.
2. "Journals" are the ones that have an appropriate screening of submitted theses and that are published on a regular basis.
3. All manuscripts other than the ones stated in the previous clause can be submitted such as conference papers, research reports, diploma papers and academic articles, provided that their sources are stated according to the 3rd clause of The Regulations on Paper Submission in The Journal of the Korean Society of Ocean Engineers.

E. The Definitions and Types of Fraudulent Acts in Research

1. "Fraudulent acts in research" include all affairs that violates ethical codes of research: fabrications, forgeries, plagiarism, overlapping publications and unfair marking of writers which may occur in every phase of research process, such as in a proposal, conducting, a report or presentation of research results.
2. "Fabrication and forgeries" refers to an act of distorting the content or outcome of research by making up false data or results.
3. "Plagiarism" refers to an act of unfairly employing all research results, such as others' publications, research proposals, ideas, hypotheses and theories, without a fair approval or quotation.
4. "Overlapping publications" refers to two writings published in different media sources that are totally identical in their contents or share the major contents. It is also the case of overlapping publication where the paper published later contains a slightly different viewpoint, yet contains the same or slightly different analysis on the same data from the previous paper.
5. "Unfair marking of writers" refers to an act of unfairly gaining reputation by pretending to be a real author of a paper without any participation in research.
6. Fraudulent acts also include a behavior of intentionally disturbing investigations regarding assumed misconducts in research or inflicting an injury on an informant.
7. "Other fraudulent acts in research" refers to all affairs that are generally accepted as the violations to ethical codes of research in the academia.

F. Screening System, Processing Criteria and Procedure

1. Screening System
 - (a) Authors must submit a "consent form of delegation of copyright" which necessitates an author's confirmation on any violations to ethical codes of research.
 - (b) When inspectors raise question on any violations to ethical codes of research, The Committee of Ethical Codes of Research determines its/their compliance to the regulations after examining all materials concerned and giving the contributor a chance to defend him/herself.
 - (c) When any violations to ethical codes of research are found while screening or editing (after the insertion of a paper in an academic magazine), The Committee of Ethical Codes of Research determines its/their compliance to the regulations after giving the contributor a chance to defend him/herself.
 - (d) When any violations to ethical codes of research are called into question after a paper is published, The Committee of Ethical Codes of Research determines its/their compliance to the regulations after giving the

contributor a chance to defend him/herself.

2. Processing Criteria

- (a) All processing criteria regarding fraudulent acts in research follow the regulations and detailed rules for operation of The Committee of Ethical Codes of Research of this society.

3. Processing Procedure

- (a) When any affair is determined as a violation to the ethical codes of research in the phase of submission or screening, The Editing Commission should report it to The Committee of Ethical Codes of Research.
- (b) When any affair is determined as a violation to the ethical codes of research after the insertions of a paper in an academic magazine, The Committee of Ethical Codes of Research should immediately cancel its publication and notify the cancellation to the author/s

G. Ethical codes of Editing

1. The editor must a strong sense of ethics regarding the codes of conduct in research and in publication. Also, he/she must not have any personal interests with others in the process of edition.
2. The editor must thoroughly keep security in all matters related to the contribution of manuscripts, screening and publication.
3. The editor must be well-informed about the violations to ethical codes of research and make a neutral and impersonal judgement when he/she found any violations.

Supplementary Provisions

1. Regulations stated above are enacted after 1 Nov. 2008. For the manuscripts contributed in academic magazines before 1, Nov. 2008, the 3rd clause in “D” is not applied. Also, they are not interpreted as violations to the ethical codes of research even if they did not stated their source in the journal of this society.
2. Also, for the papers applicable to the clause “D” or “E”, the writer/s can take measures such as “cancellation of a paper” based on their judgement, or “rejection of screening” if the paper is under screening.

1, Nov. 2008

The Korean Society of Ocean Engineers

[31, May 2007 enacted]

[1, Nov. 2008 amended]

Publishing Agreement

Article details

Article :
Corresponding author :
E-mail address :
DOI :

YOUR STATUS

I am one author signing on behalf of all co-authors of the manuscript.

ASSIGNMENT OF COPYRIGHT

I hereby assign to Korean Society of Ocean Engineers, the copyright in the manuscript identified above and any tables, illustrations or other material submitted for publication as part of the manuscript (the "Article"). This assignment of rights means that I have granted to Korean Society of Ocean Engineers the exclusive right to publish and reproduce the Article, or any part of the Article, in print, electronic and all other media (whether now known or later developed), in any form, in all languages, throughout the world, for the full term of copyright, and the right to license others to do the same, effective when the Article is accepted for publication. This includes the right to enforce the rights granted hereunder against third parties.

SCHOLARLY COMMUNICATION RIGHTS

I understand that no rights in patents, trademarks or other intellectual property rights are transferred to the Journal owner. As the author of the Article, I understand that I shall have: (i) the same rights to reuse the Article as those allowed to third party users of the Article under the CC-BY-NC License, as well as (ii) the right to use the Article in a subsequent compilation of my works or to extend the Article to book length form, to include

I have read and agree to the terms of the Journal Publishing Agreement.

Corresponding author :

name

signature

Print and sign completed form. Fax(+82 51 759 0657) or E-mail scanned file to : ksoehj@ksoe.or.kr
(Papers will not be published unless this form is signed and returned)

the Article in a thesis or dissertation, or otherwise to use or re-use portions or excerpts in other works, for both commercial and non-commercial purposes. Except for such uses, I understand that the assignment of copyright to the Journal owner gives the Journal owner the exclusive right to make or sub-license commercial use.

USER RIGHTS

The publisher will apply the Creative Commons Attribution-Noncommercial Works 4.0 International License (CC-BY-NC) to the Article where it publishes the Article in the journal on its online platforms on an Open Access basis.

The CC-BY-NC license allows users to copy and distribute the Article, provided this is not done for commercial purposes and further does not permit distribution of the Article if it is changed or edited in any way, and provided the user gives appropriate credit (with a link to the formal publication through the relevant DOI), provides a link to the license, and that the licensor is not represented as endorsing the use made of the work. The full details of the license are available at <http://creativecommons.org/licenses/by-nc/3.0/legalcode>.

REVERSION OF RIGHTS

Articles may sometimes be accepted for publication but later rejected in the publication process, even in some cases after public posting in "Articles in Press" form, in which case all rights will revert to the author.

한국해양공학회지(JOET) 논문투고규정 (2016. 10. 20 개정)

1. 본 학회지에 투고하고자 하는 사람은 한국해양공학회 회원임을 원칙으로 하며 공저인 경우에는 적어도 1인 이상이 회원이어야 한다. 단, 본 학회의 편집위원회가 특별히 인정한 사람은 예외로 한다.
2. 원고는 학술논문, 기술보고 및 자료를 포함하고, 학술논문의 경우 다른 학술지에 게재되지 않은 것이라야 한다. 학술지라 함은 투고 논문에 대한 적절한 심사체계와 주기적 발간이 이루어지는 저널(Journal) 등을 의미한다. 학술지 이외의 학술대회 논문, 연구 보고서, 학위논문, 학술기사 등 모든 원고는 투고가 가능하다. 또한 본 학회지에 게재되면 본 학회 편집위원회의 서면승인 없이 타학술지에 전부 또는 일부가 동일형식으로 발표되어서는 안되며, 저작권은 학회에 귀속된다.
3. 투고논문 중 학술지 이외의 학술대회 논문, 연구보고서, 학위논문, 학술기사 등의 경우는 각주를 통해서 아래 예와 같이 원고 전체 혹은 부분이 출판되었음을 명시하여야 한다.
예) 본 논문은 2008년 제주도에서 개최된 한국해양과학기술협의회 공동학술대회에서 발표된 논문을 근간으로 하고 있음을 밝힙니다.
4. 원고는 인터넷 상에서 WebReview 시스템을 이용하여 제출하여야 하며 이때 본 학회의 논문투고양식(template)에 맞도록 한글(Hangul) 또는 MS 워드(MS Word) 파일을 첨부로 제출하여야 한다. 원고접수 시 소정의 심사료를 납부하여야 한다. 또한 저작권 위임동의서를 학회 사무국으로 제출하여야 한다.
5. 원고가 인터넷 상에서 접수된 날을 접수일자로 한다.
6. 원고의 채택여부는 논문심사규정에 따라 정한다.
7. 학회지에 게재될 원고의 규정면수는 6면 이내이고, 규정면수를 초과할 때 저자는 소정의 게재료 이외에 초과분에 대한 게재료를 납부하여야 한다.
8. 논문원고의 체제는 다음을 원칙으로 한다. (1)제목, (2)저자명, (3)주요기술용어(Key Words), (4)영문초록, (5)기호설명, (6)서론, (7)본론(이론해석, 실험방법, 결과, 결과의 해석, 고찰), (8)결론, (9)후기, (10)참고문헌, (11)부록, 기타
9. 상세한 편집 방법은 한국해양공학회지(JOET) 템플릿을 따른다.
10. 원고에 포함될 도표 및 사진은 한글 또는 MS워드에서 처리가 가능하여야 하며 그 선명도에 대한 책임은 저자가 진다.
11. 원고 내용 및 탈오자의 책임은 저자가 진다.
12. 편집위원회는 본 학회의 논문투고규정을 따르지 않는 원고에 대하여 심사 및 게재를 거부할 수 있다.
13. 기타 본 규정에 명시되지 않은 사항(투고분야 포함)은 본 학회 편집위원회의 결정에 따른다.
14. 학회는 저자에게 별쇄본을 제공하지 않는 것을 원칙으로 하나, 필요한 경우는 저자가 실비를 부담하여야 한다.

한국해양공학회지

제34권 제1호(통권 제152호)

인쇄: 2020년 2월 26일

발행: 2020년 2월 29일

발행인: 조철희

편집인: 정준모

발행소: 사단법인 한국해양공학회

부산광역시 동구 중앙대로 180번길 13, 1302호 (초량동 프레지던트오피스텔)

전화: (051)759-0656 FAX: (051)759-0657

담당: 사무국장 이희진

E-mail: ksoehj@ksoe.or.kr

Homepage: www.ksoe.or.kr

인쇄소: 한림원(주)

서울특별시 중구 퇴계로51길 20 1303(오장동, 넥서스타워)

전화: (02)2273-4201 FAX: (02)2179-9083

E-mail: hanrim@hanrimwon.co.kr



사단법인 **한국해양공학회**

The Korean Society of Ocean Engineers